Numerical convergence of finite difference approximations for state based peridynamic fracture models☆

Prashant K. Jha[a,1,*], Robert Lipton[a,b,2]

[a] *Department of Mathematics, Louisiana State University, Baton Rouge, LA*
[b] *Center for Computation and Technology, Louisiana State University, Baton Rouge, LA*

Abstract

In this work, we study the finite difference approximation for a class of nonlocal fracture models. The nonlocal model is initially elastic but beyond a critical strain the material softens with increasing strain. This model is formulated as a state-based peridynamic model using two potentials: one associated with hydrostatic strain and the other associated with tensile strain. We show that the dynamic evolution is well-posed in the space of Hölder continuous functions $C^{0,\gamma}$ with Hölder exponent $\gamma \in (0, 1]$. Here the length scale of nonlocality is ϵ, the size of time step is Δt and the mesh size is h. The finite difference approximations are seen to converge to the Hölder solution at the rate $C_t\Delta t + C_s h^\gamma/\epsilon^2$ where the constants C_t and C_s are independent of the discretization. The semi-discrete approximations are found to be stable with time. We present numerical simulations for crack propagation that computationally verify the theoretically predicted convergence rate. We also present numerical simulations for crack propagation in pre-cracked samples subject to a bending load.

Keywords: Nonlocal fracture models, state based peridynamics, numerical analysis, finite difference approximation
AMS Subject 34A34, 34B10, 74H55, 74S20

1. Introduction

In Silling (2000) and Silling et al. (2007) a self consistent non-local continuum mechanics is proposed. This formulation known as peridynamics has been employed in the computational reproduction of dynamic fracture as well as offering dynamically based explanations for features observed in fracture, see e.g.,Silling et al. (2010); Foster et al. (2011); Lipton et al. (2016); Bobaru and Hu (2012); Ha and Bobaru (2010); Silling and Bobaru (2005); Agwai et al. (2011); Ghajari et al. (2014). These references are by no means complete and a recent review of this approach together with further references to the literature can be found in Bobaru et al. (2016).

The peridynamic formulation expresses internal forces as functions of displacement differences as opposed to displacement gradients. This generalization allows for an extended kinematics and provides a unified treatment of differentiable and non-differentiable displacements. The motion of a point $\boldsymbol{x}$ is influenced by its neighbors through non-local forces. In its simplest formulation forces act within a horizon and only neighbors confined to a ball of radius ϵ surrounding $\boldsymbol{x}$ can influence the motion of $\boldsymbol{x}$. The radius ϵ is referred to as the peridynamic horizon. When the forces are linear in the strain and when length scale of nonlocality

☆**Funding:** This material is based upon work supported by the U. S. Army Research Laboratory and the U. S. Army Research Office under contract/grant number W911NF1610456.
*Corresponding author (pjha4@lsu.edu)
Email addresses: prashant.j16o@gmail.com, pjha4@lsu.edu (Prashant K. Jha), lipton@lsu.edu (Robert Lipton)
[1]Orcid: https://orcid.org/0000-0003-2158-364X
[2]Orcid: https://orcid.org/0000-0002-1382-3204

ϵ tends to zero the peridynamic models converge to the linear elastic model Emmrich et al. (2013); Silling and Lehoucq (2008); Aksoylu and Unlu (2014); Mengesha and Du (2015). If one considers non-linear forces associated with two point interactions that are initially elastic and then soften after a critical strain, then the dynamic evolutions are found to converge to a different "limiting" dynamics associated with a crack set and a displacement that satisfies the balance of linear momentum away from the crack set and has bounded elastic energy and Griffith surface energy, see Lipton (2016, 2014) and Jha and Lipton (2018a). A numerical analysis of this two-point interaction or bond based peridynamic model is carried out in Jha and Lipton (2018a, 2017). In these works the a-priori convergence rates for finite difference and finite element methods together with different time stepping schemes are reported.

This article focuses on the numerical analysis of a state based peridynamic fracture model governed by forces that are initially elastic and then soften for sufficiently large tensile and hydrostatic strains. Attention is given to the prototypical state-based peridynamic model proposed in Lipton et al. (2018). The analysis performed here provides a-priori upper bounds on the convergence rate for a numerical scheme that applies the finite difference approximation in space and the forward Euler discretization scheme in time. The state based peridynamic model treated here has two components of non-local force acting on a point. The first force is due to tensile strains acting on $\boldsymbol{x}$ by its neighbors $\boldsymbol{y}$, while the second force is due to the net hydrostatic strain on $\boldsymbol{x}$ associated with the change in volume about $\boldsymbol{x}$. In this article we analyze the convergence of the numerical scheme for two different cases of constitutive law relating non-local force to strain. For the first case we take both tensile and hydrostatic forces to be initially linear and increasing with the strain and then after reaching critical values of tensile and hydrostatic strain respectively the forces decrease to zero with strain, see Figure 1b and Figure 2b. For the second case we choose the hydrostatic force to be a linear function of the hydrostatic strain (see dashed line Figure 2b) while the tensile force is initially linear and then decreases to zero after a critical tensile strain is reached, see Figure 1b. The choice of the two constitutive models studied here is motivated by the prospect of simulating materials that exhibit failure due to extreme local tensile stress or strain or materials that fail due to extreme local hydrostatic stress or strain. Here the quadratic potential function for the dilatational strain can be associated with materials that fail under extreme local tensile loads while the convex-concave dilatational potential function can be associated with materials in which fail under extreme local hydrostatic loads.

The primary new contribution of this paper is that a-priori convergence rates are established for numerical schemes used for simulation using these prototypical state based peridynamic models. As mentioned earlier the constitutive behavior is non-linear, non-convex and material properties can degrade during the course of the evolution. We consider the class of Hölder continuous displacement fields and show the existence of a unique Hölder continuous evolution for a prescribed Hölder continuous initial condition and body force, see Theorem 1. To obtain a-priori bounds on the error, we develop an L^2 approximation theory for the finite difference approximation in the spatial variables and the forward Euler approximation in time, see Section 4. We show that discrete approximations converge to the exact Hölder continuous solution uniformly over finite time intervals with respect to the L^2 norm. The a-priori rate of convergence in the L^2 norm is given by $(C_t\Delta t + C_s h^\gamma/\epsilon^2)$, where Δt is the size of the time step, h is the size of spatial mesh discretization, $\gamma \in (0, 1]$ is the Hölder exponent, and ϵ is the length scale of nonlocal interaction relative to the size of the domain, see Theorem 3. The constant C_t depends on the L^2 norm of the time derivatives of the solution, C_s depends on the Hölder norm of the solution and the Lipschitz constant of peridynamic force. We point out that the convergence results derived here can be extended to general single step time discretization using arguments provided in Jha and Lipton (2018a). Although the constitutive law relating force to strain is nonlinear we are still able to establish stability for the semi-discrete approximation and it is shown that the energy at any given time t is bounded above by the energy of the initial conditions and the total work done by the body force up to time t, see Theorem 2. We provide the connection between the non-dimensionalized dynamics used in the a-priori convergence analysis and the simulated dynamics using dimensional quantities, see Section 5. The numerics are carried out for Plexiglass. Our numerical simulations are consistent with the theoretical studies, see Section 6. In the simulations we introduce a straight crack and it propagates in response to applied boundary conditions. For these simulations we use piecewise constant interpolants and record the rate of convergence with respect to mesh size while keeping the horizon fixed. Our results show that convergence rate remains above the a-priori estimated rate of 1 during the simulation. For illustration

we also present numerical simulations for a pre-cracked samples subject to a bending load.

It is pointed out that there is now a significant number of investigations examining the numerical approximation of singular kernels for non-local problems with applications to nonlocal diffusion, advection, and continuum mechanics. Numerical formulations and convergence theory for nonlocal p-Laplacian formulations are developed in D'Elia and Gunzburger (2013), Nochetto et al. (2015). Numerical analysis of nonlocal steady state diffusion is presented in Tian and Du (2013) and Mengesha and Du (2013), and Chen and Gunzburger (2011). The use of fractional Sobolev spaces for nonlocal problems is investigated and developed in Du et al. (2012). Quadrature approximations and stability conditions for linear peridynamics are analyzed in Weckner and Emmrich (2005) and Silling and Askari (2005). The interplay between nonlocal interaction length and grid refinement for linear peridynamic models is presented in Bobaru et al. (2009). Analysis of adaptive refinement and domain decomposition for the linearized peridynamics are provided in Aksoylu and Parks (2011), Lindsay et al. (2016), and Aksoylu and Mengesha (2010). This list is by no means complete and the literature continues to grow rapidly.

The paper is organized as follows. In Section 2, we describe the nonlocal model and state the peridynamic equation of motion. The Lipschitz continuity of the peridynamic force and global existence of unique solutions are presented in Section 3. The finite difference discretization is introduced in Section 4. We demonstrate the energy stability of the semi-discrete approximation in Section 4.1. In Section 4.2 we give the a-priori bound on the error for the fully discrete approximation, see Theorem 3. The equivalence between the dynamics formulated in terms of quantities with dimensions and the non dimensional dynamics is established in Section 5. The numerical simulations are described and presented in Section 6. In Section 7 we summarize our results.

2. Nonlocal Dynamics

We now formulate the nonlocal dynamics. Here all quantities are non-dimensional. In Section 5 we illustrate how to take the equations of dynamics formulated in terms of dimensional quantities and recover the equivalent nonlocal dynamics in dimensionless form. Let $D \subset \mathbb{R}^d$ denote the material domain of dimension $d = 2, 3$ and let the horizon be given by $\epsilon > 0$. We make the assumption of small (infinitesimal) deformations so that the displacement field $\boldsymbol{u} : D \times [0, T] \to \mathbb{R}^d$ is small compared to the size of D and the deformed configuration is the same as the reference configuration. We have $\boldsymbol{u} = \boldsymbol{u}(\boldsymbol{x}, t)$ as a function of space and time but will suppress the $\boldsymbol{x}$ dependence when convenient and write $\boldsymbol{u}(t)$. The tensile strain S between two points $\boldsymbol{x}, \boldsymbol{y} \in D$ along the direction $\boldsymbol{e}_{\boldsymbol{y}-\boldsymbol{x}}$ is defined as

$$S(\boldsymbol{y}, \boldsymbol{x}, \boldsymbol{u}(t)) = \frac{\boldsymbol{u}(\boldsymbol{y}, t) - \boldsymbol{u}(\boldsymbol{x}, t)}{|\boldsymbol{y} - \boldsymbol{x}|} \cdot \boldsymbol{e}_{\boldsymbol{y}-\boldsymbol{x}}, \tag{1}$$

where $\boldsymbol{e}_{\boldsymbol{y}-\boldsymbol{x}} = \frac{\boldsymbol{y}-\boldsymbol{x}}{|\boldsymbol{y}-\boldsymbol{x}|}$ is a unit vector and "$\cdot$" is the dot product. Let $H_\epsilon(\boldsymbol{x})$ be the ball of radius ϵ centered at $\boldsymbol{x}$ in dimension d and let $\omega_d = |H_1(\boldsymbol{0})|$ be the volume (area) of unit ball (circle). It follows that $|H_\epsilon(\boldsymbol{x})| = \epsilon^d \omega_d$.

The spherical or hydrostatic strain at $\boldsymbol{x}$ is a measure of the volume change about $\boldsymbol{x}$ and is given by

$$\theta(\boldsymbol{x}, \boldsymbol{u}(t)) = \frac{1}{\epsilon^d \omega_d} \int_{H_\epsilon(\boldsymbol{x})} \omega(\boldsymbol{y}) J^\epsilon(|\boldsymbol{y} - \boldsymbol{x}|) S(\boldsymbol{y}, \boldsymbol{x}, \boldsymbol{u}(t)) |\boldsymbol{y} - \boldsymbol{x}| \, d\boldsymbol{y}, \tag{2}$$

where $J^\epsilon(|\boldsymbol{y} - \boldsymbol{x}|)$ is a influence function and it measures the influence of point $\boldsymbol{y}$ on $\boldsymbol{x}$. Only points inside the horizon can influence $\boldsymbol{x}$ so $J^\epsilon(|\boldsymbol{y} - \boldsymbol{x}|)$ is nonzero for $|\boldsymbol{y} - \boldsymbol{x}| < \epsilon$ and zero otherwise. We take J^ϵ to be of the form: $J^\epsilon(|\boldsymbol{y} - \boldsymbol{x}|) = J(\frac{|\boldsymbol{y}-\boldsymbol{x}|}{\epsilon})$ with $J(r) = 0$ for $r \geq 1$ and $0 \leq J(r) \leq M < \infty$ for $r < 1$.

In Equation 2, we have introduced the boundary function $\omega(\boldsymbol{x})$ providing the influence of the boundary on the non-local force. In the interior, all the point in $\boldsymbol{x} \in D$ atleast ϵ away from boundary ∂D, $\omega(\boldsymbol{x})$ takes the value 1. As $\boldsymbol{x}$ approaches ∂D from the interior, $\omega(\boldsymbol{x})$ smoothly decays from 1 to 0 on ∂D and is extended by zero outside D. The boundary function $\omega : D \to [0, 1]$ is introduced to make the initial boundary value problem well posed. We point this out in Section 3 where existence of solution is presented.

2.1. The class of nonlocal potentials

Motivated by potentials of Lennard-Jones type, the force potential for tensile strain is defined by

$$\mathcal{W}^\epsilon(S(\boldsymbol{y},\boldsymbol{x},\boldsymbol{u}(t))) = \omega(\boldsymbol{x})\omega(\boldsymbol{y})J^\epsilon(|\boldsymbol{y}-\boldsymbol{x}|)\frac{1}{\epsilon|\boldsymbol{y}-\boldsymbol{x}|}f(\sqrt{|\boldsymbol{y}-\boldsymbol{x}|}S(\boldsymbol{y},\boldsymbol{x},\boldsymbol{u}(t))) \tag{3}$$

and the potential for hydrostatic strain is defined as

$$\mathcal{V}^\epsilon(\theta(\boldsymbol{x},\boldsymbol{u}(t))) = \omega(\boldsymbol{x})\frac{g(\theta(\boldsymbol{x},\boldsymbol{u}(t)))}{\epsilon^2} \tag{4}$$

where $\mathcal{W}^\epsilon(S(\boldsymbol{y},\boldsymbol{x},\boldsymbol{u}(t)))$ is the pairwise force potential per unit length between two points $\boldsymbol{x}$ and $\boldsymbol{y}$ and $\mathcal{V}^\epsilon(\theta(\boldsymbol{x},\boldsymbol{u}(t)))$ is the hydrostatic force potential density at $\boldsymbol{x}$. They are described in terms of their potential functions f and g, see Figure 1 and Figure 2.

The potential function f represents a convex-concave potential such that the associated force acting between material points $\boldsymbol{x}$ and $\boldsymbol{y}$ are initially elastic and then soften and decay to zero as the strain between points increases, see Figure 1. The first well for $\mathcal{W}^\epsilon(S(\boldsymbol{y},\boldsymbol{x},\boldsymbol{u}(t)))$ is at zero tensile strain and the potential function satisfies

$$f(0) = f'(0) = 0. \tag{5}$$

The behavior for infinite tensile strain is characterized by the horizontal asymptotes $\lim_{S\to\infty} f(S) = C^+$ and $\lim_{S\to-\infty} f(S) = C^-$ respectively, see Figure 1. The critical tensile strain $S_c^+ > 0$ for which the force begins to soften is given by the inflection point $r^+ > 0$ of f and is

$$S_c^+ = \frac{r^+}{\sqrt{|\boldsymbol{y}-\boldsymbol{x}|}}. \tag{6}$$

The critical negative tensile strain is chosen much larger in magnitude than S_c^+ and is

$$S_c^- = \frac{r^-}{\sqrt{|\boldsymbol{y}-\boldsymbol{x}|}}, \tag{7}$$

with $r^- < 0$ and $r^+ << |r^-|$.

We assume here that all the potential functions are bounded and have bounded derivatives up to order 3. We denote the i^{th} derivative of the function f by $f^{(i)}$, $i = 1,2,3$. Let C_i^f for $i = 0,1,2,3$ denote the bounds on the functions and derivatives given by

$$C_0^f := \sup_r |f(r)|, \qquad C_i^f := \sup_r |f^{(i)}(r)| \quad \text{for } i = 1,2,3, \tag{8}$$

and $C_i^f < \infty$ for $i = 0,1,2,3$.

We will consider two types of potentials associated with hydrostatic strain. The first potential we consider is a quadratic potential characterized by a quadratic potential function g with a minimum at zero strain. The second potential we consider is characterized by a convex-concave potential function g, see Figure 2. If g is assumed to be quadratic then the force due to spherical strain is linear and there is no softening of the material. However, if g is convex-concave the force internal to the material is initially linear and increasing but then becomes decreasing with strain as the hydrostatic strain exceeds a critical value. For the convex-concave g, the critical values $0 < \theta_c^+$ and $\theta_c^- < 0$ beyond which the force begins to soften is related to the inflection point r_*^+ and r_*^- of g as follows

$$\theta_c^+ = r_*^+, \qquad \theta_c^- = r_*^-. \tag{9}$$

The critical compressive hydrostatic strain where the force begins to soften for negative hydrostatic strain is chosen much larger in magnitude than θ_c^+, i.e. $\theta_c^+ << |\theta_c^-|$. When g is convex-concave we assume it is bounded and has bounded derivatives up to order three. These bounds are denoted by $C_i^g < \infty$ for $i = 0,1,2,3$ and,

$$C_0^g := \sup_r |g(r)|, \qquad C_i^g := \sup_r |g^{(i)}(r)| \quad \text{for } i = 1,2,3. \tag{10}$$

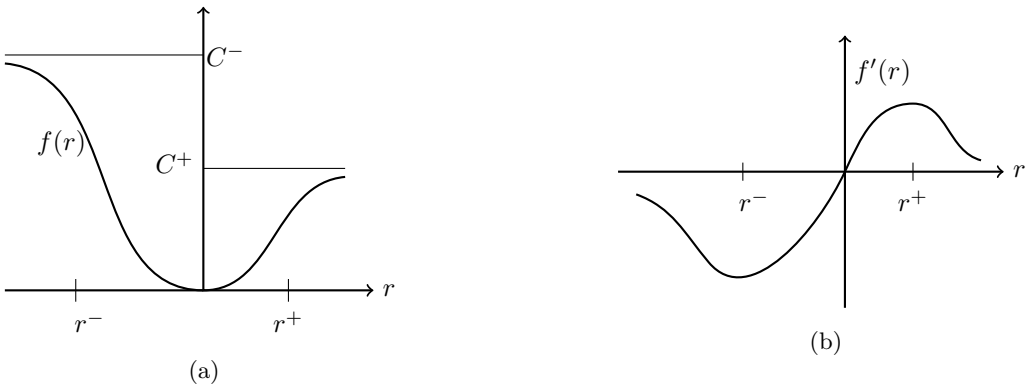

Figure 1: (a) The potential function $f(r)$ for tensile force. Here C^+ and C^- are the two asymptotic values of f. (b) Cohesive tensile force.

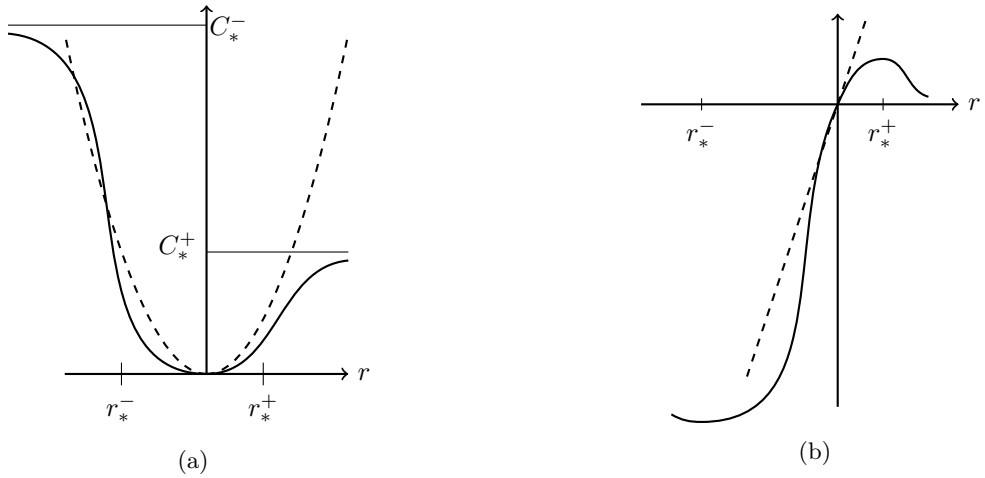

Figure 2: (a) Two types of potential function $g(r)$ for hydrostatic force. The dashed line corresponds to the quadratic potential $g(r) = \beta r^2/2$. The solid line corresponds to the convex-concave type potential $g(r)$. For the convex-concave type potential, there are two special points r_*^- and r_*^+ at which material points start to soften. C_*^+ and C_*^- are two extreme values. (b) Hydrostatic forces. The dashed line corresponds to the quadratic potential and solid line corresponds to the convex-concave potential.

2.2. Peridynamic equation of motion

The potential energy of the motion is given by

$$PD^\epsilon(\boldsymbol{u}) = \frac{1}{\epsilon^d \omega_d} \int_D \int_{H_\epsilon(\boldsymbol{x})} |\boldsymbol{y}-\boldsymbol{x}| \mathcal{W}^\epsilon(S(\boldsymbol{y},\boldsymbol{x},\boldsymbol{u}(t)))\, d\boldsymbol{y} d\boldsymbol{x} + \int_D \mathcal{V}^\epsilon(\theta(\boldsymbol{x},\boldsymbol{u}(t)))\, d\boldsymbol{x}. \tag{11}$$

In this treatment the material is assumed homogeneous and the density ρ is constant. We denote the body force by $\boldsymbol{b}(\boldsymbol{x},t)$ and define the Lagrangian

$$\mathrm{L}(\boldsymbol{u}, \partial_t \boldsymbol{u}, t) = \frac{\rho}{2} ||\dot{\boldsymbol{u}}||^2_{L^2(D;\mathbb{R}^d)} - PD^\epsilon(\boldsymbol{u}) + \int_D \boldsymbol{b}\cdot\boldsymbol{u} d\boldsymbol{x},$$

where $\dot{\boldsymbol{u}} = \frac{\partial \boldsymbol{u}}{\partial t}$ is the velocity and $\|\dot{\boldsymbol{u}}\|_{L^2(D;\mathbb{R}^d)}$ denotes the L^2 norm of the vector field $\dot{\boldsymbol{u}} : D \to \mathbb{R}^d$. Applying the principal of least action gives the nonlocal dynamics

$$\rho \ddot{\boldsymbol{u}}(\boldsymbol{x},t) = \mathcal{L}^\epsilon(\boldsymbol{u})(\boldsymbol{x},t) + \boldsymbol{b}(\boldsymbol{x},t), \text{ for } \boldsymbol{x} \in D, \tag{12}$$

where

$$\mathcal{L}^\epsilon(\boldsymbol{u})(\boldsymbol{x},t) = \mathcal{L}^\epsilon_T(\boldsymbol{u})(\boldsymbol{x},t) + \mathcal{L}^\epsilon_D(\boldsymbol{u})(\boldsymbol{x},t). \tag{13}$$

Here $\mathcal{L}^\epsilon_T(\boldsymbol{u})$ is the peridynamic force due to the tensile strain and is given by

$$\mathcal{L}^\epsilon_T(\boldsymbol{u})(\boldsymbol{x},t) = \frac{2}{\epsilon^d \omega_d} \int_{H_\epsilon(\boldsymbol{x})} \omega(\boldsymbol{x})\omega(\boldsymbol{y}) \frac{J^\epsilon(|\boldsymbol{y}-\boldsymbol{x}|)}{\epsilon|\boldsymbol{y}-\boldsymbol{x}|} \partial_S f(\sqrt{|\boldsymbol{y}-\boldsymbol{x}|} S(\boldsymbol{y},\boldsymbol{x},\boldsymbol{u}(t))) \boldsymbol{e}_{\boldsymbol{y}-\boldsymbol{x}}\, d\boldsymbol{y}, \tag{14}$$

and $\mathcal{L}^\epsilon_D(\boldsymbol{u})$ is the peridynamic force due to the hydrostatic strain and is given by

$$\mathcal{L}^\epsilon_D(\boldsymbol{u})(\boldsymbol{x},t) = \frac{1}{\epsilon^d \omega_d} \int_{H_\epsilon(\boldsymbol{x})} \omega(\boldsymbol{x})\omega(\boldsymbol{y}) \frac{J^\epsilon(|\boldsymbol{y}-\boldsymbol{x}|)}{\epsilon^2} \left[\partial_\theta g(\theta(\boldsymbol{y},\boldsymbol{u}(t))) + \partial_\theta g(\theta(\boldsymbol{x},\boldsymbol{u}(t)))\right] \boldsymbol{e}_{\boldsymbol{y}-\boldsymbol{x}}\, d\boldsymbol{y}. \tag{15}$$

The dynamics is complemented with the initial data

$$\boldsymbol{u}(\boldsymbol{x},0) = \boldsymbol{u}_0(\boldsymbol{x}), \qquad \partial_t \boldsymbol{u}(\boldsymbol{x},0) = \boldsymbol{v}_0(\boldsymbol{x}), \tag{16}$$

and we prescribe zero Dirichlet boundary condition on the boundary ∂D

$$\boldsymbol{u}(\boldsymbol{x}) = \boldsymbol{0} \qquad \forall \boldsymbol{x} \in \partial D. \tag{17}$$

The zero boundary value is extended outside D by zero to $\mathbb{R}^d$. Last we note that since the material is homogeneous we will divide both sides of the equation of motion by ρ and assume, without loss of generality, that $\rho = 1$.

3. Existence of solutions

Let $C^{0,\gamma}(D;\mathbb{R}^d)$ be the Hölder space with exponent $\gamma \in (0,1]$. We introduce $C^{0,\gamma}_0(D) = C^{0,\gamma}(D) \cap C_0(D)$ where $C_0(D)$ is the closure of continuous functions with compact support on D in the supremum norm. Functions in $C_0(D)$ are uniquely extended to $\overline{D}$ and take zero values on ∂D, see Driver (2003). In this paper we extend all functions in $C^{0,\gamma}_0(D)$ by zero outside D. The norm of $\boldsymbol{u} \in C^{0,\gamma}_0(D;\mathbb{R}^d)$ is given by

$$\|\boldsymbol{u}\|_{C^{0,\gamma}(D;\mathbb{R}^d)} := \sup_{\boldsymbol{x}\in D} |\boldsymbol{u}(\boldsymbol{x})| + [\boldsymbol{u}]_{C^{0,\gamma}(D;\mathbb{R}^d)},$$

where $[\boldsymbol{u}]_{C^{0,\gamma}(D;\mathbb{R}^d)}$ is the Hölder semi norm and given by

$$[\boldsymbol{u}]_{C^{0,\gamma}(D;\mathbb{R}^d)} := \sup_{\substack{\boldsymbol{x}\neq\boldsymbol{y},\\ \boldsymbol{x},\boldsymbol{y}\in D}} \frac{|\boldsymbol{u}(\boldsymbol{x})-\boldsymbol{u}(\boldsymbol{y})|}{|\boldsymbol{x}-\boldsymbol{y}|^{\gamma}},$$

and $C_0^{0,\gamma}(D;\mathbb{R}^d)$ is a Banach space with this norm. Here we make the hypothesis that the domain function ω belongs to $C_0^{0,\gamma}(D;[0,1])$.

We consider the first order system of equations equivalent to Equation 12. Let $y_1(t)=\boldsymbol{u}(t)$, $y_2(t)=\boldsymbol{v}(t)$ with $\boldsymbol{v}(t)=\dot{\boldsymbol{u}}(t)$. We form the vector $y=(y_1,y_2)^T$ where $y_1,y_2\in C_0^{0,\gamma}(D;\mathbb{R}^d)$ and let $F^\epsilon(y,t)=(F_1^\epsilon(y,t),F_2^\epsilon(y,t))^T$ with

$$F_1^\epsilon(y,t) := y_2 \tag{18}$$
$$F_2^\epsilon(y,t) := \mathcal{L}^\epsilon(y_1(t))+\boldsymbol{b}(t). \tag{19}$$

We point out here that the domain function ω insures that $F^\epsilon(y,t)$ maps into $C_0^{0,\gamma}(D;\mathbb{R}^d)\times C_0^{0,\gamma}(D;\mathbb{R}^d)$. The initial boundary value associated with the evolution Equation 12 is equivalent to the initial boundary value problem for the first order system given by

$$\frac{d}{dt}y = F^\epsilon(y,t), \tag{20}$$

with initial condition given by $y(0)=(\boldsymbol{u}_0,\boldsymbol{v}_0)^T\in C_0^{0,\gamma}(D;\mathbb{R}^d)\times C_0^{0,\gamma}(D;\mathbb{R}^d)$.

We next show that $F^\epsilon(y,t)$ is Lipschitz continuous.

Proposition 1. ***Lipschitz continuity and bound***
Let $X=C_0^{0,\gamma}(D;\mathbb{R}^d)\times C_0^{0,\gamma}(D;\mathbb{R}^d)$. We suppose that the boundary function ω belongs to $C_0^{0,\gamma}(D;[0,1])$. Let f be a convex-concave potential function satisfying Equation 8 and let the potential function g either be a quadratic function or be a convex-concave function satisfying Equation 10, then the function $F^\epsilon(y,t)=(F_1^\epsilon,F_2^\epsilon)^T$, as defined in Equation 18 and Equation 19, is Lipschitz continuous in any bounded subset of X. We have, for any $y,z\in X$ and $t>0$,

$$\begin{aligned}&\|F^\epsilon(y,t)-F^\epsilon(z,t)\|_X\\ &\leq \frac{L_1(1+||\omega||_{C^{0,\gamma}})(1+||y||_X+||z||_X)}{\epsilon^{2+\alpha(\gamma)}}||y-z||_X.\end{aligned} \tag{21}$$

where L_1 is independent of $\boldsymbol{u},\boldsymbol{v}$ and ϵ, and depends on f, J, and g. The exponent $\alpha(\gamma)$ is 0 if $\gamma\geq 1/2$ and is $1/2-\gamma$ if $\gamma\leq 1/2$. Furthermore, for any $y\in X$ and any $t\in[0,T]$, we have the bound

$$\|F^\epsilon(y,t)\|_X \leq \frac{L_2(1+||\omega||_{C^{0,\gamma}})(1+||y||_X)}{\epsilon^2}+b, \tag{22}$$

where $b=\sup_t\|\boldsymbol{b}(t)\|_{C^{0,\gamma}(D;\mathbb{R}^d)}$ and L_2 is independent of y.

We easily see that on choosing $z=0$ in Equation 21 that $\mathcal{L}^\epsilon(\boldsymbol{u})$ is in $C^{0,\gamma}(D;\mathbb{R}^d)$ provided that $\boldsymbol{u}$ belongs to $C^{0,\gamma}(D;\mathbb{R}^3)$. Moreover since $\mathcal{L}^\epsilon(\boldsymbol{u})$ takes the value $\mathbf{0}$ on ∂D we can conclude that $\mathcal{L}^\epsilon(\boldsymbol{u})$ also belongs to $C_0^{0,\gamma}(D;\mathbb{R}^d)$.

The following theorem gives the existence and uniqueness of solution in any given time domain $I_0=(-T,T)$.

Theorem 1. ***Existence and uniqueness of Hölder solutions over finite time intervals***
Let f be a convex-concave function satisfying Equation 8 and let g either be a quadratic function or a convex-concave function satisfying Equation 10. For any initial condition $x_0\in X=C_0^{0,\gamma}(D;\mathbb{R}^d)\times C_0^{0,\gamma}(D;\mathbb{R}^d)$,

time interval $I_0 = (-T, T)$, *and right hand side* $\boldsymbol{b}(t)$ *continuous in time for* $t \in I_0$ *such that* $\boldsymbol{b}(t)$ *satisfies* $\sup_{t\in I_0} ||\boldsymbol{b}(t)||_{C^{0,\gamma}} < \infty$, *there is a unique solution* $y(t) \in C^1(I_0; X)$ *of*

$$y(t) = x_0 + \int_0^t F^\epsilon(y(\tau), \tau)\, d\tau, \tag{23}$$

or equivalently

$$y'(t) = F^\epsilon(y(t), t), \text{ with } y(0) = x_0, \tag{24}$$

where $y(t)$ *and* $y'(t)$ *are Lipschitz continuous in time for* $t \in I_0$.

The proof of this theorem follows directly from Proposition 1 and is established along the same lines as the existence proof for Hölder continuous solutions of bond based peridynamics given in [Theorem 2, Jha and Lipton (2018a)].

We conclude this section by stating the following result which shows the Lipschitz bound of peridynamic force in L^2 norm for functions in $L^2_0(D; \mathbb{R}^d)$. Here $L^2_0(D; \mathbb{R}^d)$ denotes the space of functions $\boldsymbol{u} \in L^2(D; \mathbb{R}^d)$ such that $\boldsymbol{u} = \boldsymbol{0}$ on ∂D. We assume that functions in $L^2_0(D; \mathbb{R}^d)$ are extended to $\mathbb{R}^d$ by zero.

Proposition 2. ***Lipschitz continuity of peridynamic force in*** L^2
Let f *and* g *satisfy the hypothesis of Proposition Proposition 1, then for any* $\boldsymbol{u}, \boldsymbol{v} \in L^2_0(D; \mathbb{R}^d)$ *we have*

$$||\mathcal{L}^\epsilon(\boldsymbol{u}) - \mathcal{L}^\epsilon(\boldsymbol{v})||_{L^2(D;\mathbb{R}^d)} \leq \frac{L_3}{\epsilon^2} ||\boldsymbol{u} - \boldsymbol{v}||_{L^2(D;\mathbb{R}^d)}, \tag{25}$$

where the constants L_3 *and* L_4 *are independent of* ϵ, $\boldsymbol{u}$ *and* $\boldsymbol{v}$. *Here* $L_3 = 4(C_1^f \bar{J}_1 + C_2^g \bar{J}_0^2)$, *for convex-concave* g, *and* $L_3 = 4(C_1^f \bar{J}_1 + g''(0)\bar{J}_0^2)$, *for quadratic* g. *Here* $\bar{J}_\alpha = \frac{1}{\omega_d} \int_{H_1(\mathbf{0})} J(|\boldsymbol{\xi}|)|\boldsymbol{\xi}|^{-\alpha} d\boldsymbol{\xi}$.

The proofs of Proposition 1 and Proposition 2 are provided in Appendix A. We now describe the finite difference scheme and analyze the rate of convergence to Hölder continuous solutions of the peridynamic equation of motion.

4. Finite difference approximation

In this section we consider the discrete approximation to the dynamics given by finite differences in space and the forward Euler discretization in time. Let h denote the mesh size and $D_h = D \cap (h\mathbb{Z})^d$ be the

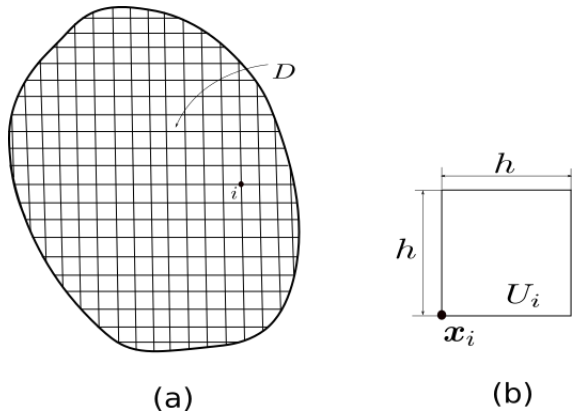

Figure 3: (a) Typical mesh of size h. (b) Unit cell U_i corresponding to material point $\boldsymbol{x}_i$.

associated discretization of the material domain D. In this paper we will keep the horizon length scale ϵ

fixed and assume that the spatial discretization length satisfies $h < \epsilon < 1$. Let $i \in \mathbb{Z}^d$ be the index such that $\boldsymbol{x}_i = hi \in D$, see Figure 3. Let U_i be a the cell of volume h^d corresponding to the grid point $\boldsymbol{x}_i$. The exact solution evaluated at grid points is denoted by $(\boldsymbol{u}_i(t), \boldsymbol{v}_i(t))$. Given any discrete set $\{\hat{\boldsymbol{u}}_i\}_{i,\boldsymbol{x}_i \in D}$, where i is index representing grid point of mesh, we define its piecewise constant extension as

$$\hat{\boldsymbol{u}}(\boldsymbol{x}) := \sum_{i,\boldsymbol{x}_i \in D} \hat{\boldsymbol{u}}_i \chi_{U_i}(\boldsymbol{x}). \tag{26}$$

In this way we have representation of the discrete set as a piecewise constant function.

We now describe the L^2-projection of the function $\boldsymbol{u} : D \to \mathbb{R}^d$ onto the space of piecewise constant functions defined over the cells U_i. We denote the average of $\boldsymbol{u}$ over the unit cell U_i as $\tilde{\boldsymbol{u}}_i$ and

$$\tilde{\boldsymbol{u}}_i := \frac{1}{h^d} \int_{U_i} \boldsymbol{u}(\boldsymbol{x}) d\boldsymbol{x} \tag{27}$$

and the L^2 projection of $\boldsymbol{u}$ onto piecewise constant functions is $\tilde{\boldsymbol{u}}$ given by

$$\tilde{\boldsymbol{u}}(\boldsymbol{x}) := \sum_{i,\boldsymbol{x}_i \in D} \tilde{\boldsymbol{u}}_i \chi_{U_i}(\boldsymbol{x}). \tag{28}$$

Lemma 1. *Let $\boldsymbol{u} \in C_0^{0,\gamma}(D; \mathbb{R}^d)$ and let $\tilde{\boldsymbol{u}}$ be its L^2 projection defined in Equation 28, then we have*

$$\begin{aligned} |\tilde{\boldsymbol{u}}(\boldsymbol{x}) - \boldsymbol{u}(\boldsymbol{x})| &\leq [c^\gamma ||\boldsymbol{u}||_{C^{0,\gamma}}]\, h^\gamma, \qquad \forall \boldsymbol{x} \in D, \\ ||\tilde{\boldsymbol{u}}(\boldsymbol{x}) - \boldsymbol{u}(\boldsymbol{x})||_{L^2} &\leq \left[c^\gamma \sqrt{|D|}\, ||\boldsymbol{u}||_{C^{0,\gamma}}\right] h^\gamma, \end{aligned} \tag{29}$$

where $c = \sqrt{2}$ for $d = 2$ and $c = \sqrt{3}$ for $d = 3$.

This lemma can be demonstrated easily by substituting Equation 28 for $\tilde{\boldsymbol{u}}$ and using the fact that $\boldsymbol{u} \in C_0^{0,\gamma}(D; \mathbb{R}^d)$. We also note that first line of Equation 29 remains valid of $\boldsymbol{x}$ in a layer of thickness 2ϵ surrounding D.

4.1. Stability of the semi-discrete approximation

We first introduce the semi-discrete boundary condition by setting $\hat{\boldsymbol{u}}_i(t) = \boldsymbol{0}$ for all t and for all $\boldsymbol{x}_i \notin D$. Let $\{\hat{\boldsymbol{u}}_i(t)\}_{i,\boldsymbol{x}_i \in D}$ denote the semi-discrete approximate solution which satisfies the following, for all $t \in [0, T]$ and i such that $\boldsymbol{x}_i \in D$,

$$\ddot{\hat{\boldsymbol{u}}}_i(t) = \mathcal{L}^\epsilon(\hat{\boldsymbol{u}}(t))(\boldsymbol{x}_i) + \boldsymbol{b}(\boldsymbol{x}_i, t), \tag{30}$$

where $\hat{\boldsymbol{u}}(t)$ is the piecewise constant extension of discrete set $\{\hat{\boldsymbol{u}}_i(t)\}_i$ and is defined as

$$\hat{\boldsymbol{u}}(\boldsymbol{x}, t) = \begin{cases} \sum_{i,\boldsymbol{x}_i \in D} \hat{\boldsymbol{u}}_i(t) \chi_{U_i}(\boldsymbol{x}), \\ \boldsymbol{0}, \quad \text{for } \boldsymbol{x} \notin \cup_{i,\boldsymbol{x}_i \in D} U_i. \end{cases} \tag{31}$$

The scheme is complemented with the discretized initial conditions $\hat{\boldsymbol{u}}_i(0) = \boldsymbol{u}_0(\boldsymbol{x}_i)$ and $\hat{\boldsymbol{v}}_i(0) = \boldsymbol{v}_0(\boldsymbol{x}_i)$.

The total kinetic and potential energy is given by

$$\mathcal{E}^\epsilon(\boldsymbol{u})(t) = \frac{1}{2} ||\dot{\boldsymbol{u}}(t)||_{L^2}^2 + PD^\epsilon(\boldsymbol{u}(t)),$$

and we introduce the augmented energy given by

$$\bar{\mathcal{E}}^\epsilon(\boldsymbol{u})(t) := \mathcal{E}^\epsilon(\boldsymbol{u})(t) + \frac{1}{2} ||\boldsymbol{u}(t)||_{L^2}^2. \tag{32}$$

We have the stability of the semi-discrete evolution.

Theorem 2. ***Energy stability of the semi-discrete approximation***
Let $\{\hat{\boldsymbol{u}}_i(t)\}_{i,\boldsymbol{x}_i\in D}$ be the solution to the semidiscrete initial boundary value problem Equation 30 and $\hat{\boldsymbol{u}}(t)$ denote its piecewise constant extension. Similarly let $\hat{\boldsymbol{b}}(\boldsymbol{x},t)$ denote the piecewise constant extension of $\{\boldsymbol{b}(\boldsymbol{x}_i,t)\}_{i,\boldsymbol{x}_i\in D}$. If f and g are convex-concave type functions satisfying Equation 8 and Equation 10, then the total energy $\mathcal{E}^\epsilon(\hat{\boldsymbol{u}})(t)$ satisfies,

$$\mathcal{E}^\epsilon(\hat{\boldsymbol{u}})(t) \leq \left(\sqrt{\mathcal{E}^\epsilon(\hat{\boldsymbol{u}})(0)} + \frac{tC}{\epsilon^2} + \int_0^t ||\hat{\boldsymbol{b}}(s)||_{L^2} ds\right)^2, \ \forall t \in [0,T], \tag{33}$$

and the constant C is independent of ϵ and h.

If f is a convex-concave type function satisfying Equation 8 and g is quadratic then the augmented energy $\bar{\mathcal{E}}^\epsilon(\hat{\boldsymbol{u}})(t)$ satisfies,

$$\begin{aligned}\bar{\mathcal{E}}^\epsilon(\hat{\boldsymbol{u}})(t) \leq \exp[3(C_2/\epsilon^2+1)t]\Bigg(&\bar{\mathcal{E}}^\epsilon(\hat{\boldsymbol{u}})(0) \\ &+ \int_0^T \left(\frac{C_1^2}{\epsilon^4} + ||\hat{\boldsymbol{b}}(s)||_{L^2}^2\right)\exp[-3(C_2/\epsilon^2+1)s]ds\Bigg), \ \forall t \in [0,T],\end{aligned} \tag{34}$$

where the constants C_1 and C_2 are independent of ϵ and h.

We provide proof of Theorem 2 in Appendix B. We now discuss the fully discrete scheme.

4.2. Time discretization

Let Δt be the size of the time step and $[0,T]\cap(\Delta t\mathbb{Z})$ be the discretization of the time domain. We denote the fully discrete solution at $(t^k = k\Delta t, \boldsymbol{x}_i = ih)$ as $(\hat{\boldsymbol{u}}_i^k, \hat{\boldsymbol{v}}_i^k)$ and the exact solution as $(\boldsymbol{u}_i^k, \boldsymbol{v}_i^k)$. We enforce the boundary condition $\hat{\boldsymbol{u}}_i^k = \boldsymbol{0}$ for all $\boldsymbol{x}_i \notin D$ and for all k. The piecewise constant extension of $\{\hat{\boldsymbol{u}}_i^k\}_{i\in\mathbb{Z}^d}$ and $\{\hat{\boldsymbol{v}}_i^k\}_{i\in\mathbb{Z}^d}$ are denoted by $\hat{\boldsymbol{u}}^k$ and $\hat{\boldsymbol{v}}^k$ respectively. The L^2-projection of $\boldsymbol{u}^k$ and $\boldsymbol{v}^k$ onto piecewise constant functions are denoted by $\tilde{\boldsymbol{u}}^k$ and $\tilde{\boldsymbol{v}}^k$ respectively.

The forward Euler time discretization, with respect to velocity, and the finite difference scheme for $(\hat{\boldsymbol{u}}_i^k, \hat{\boldsymbol{v}}_i^k)$ is written

$$\frac{\hat{\boldsymbol{u}}_i^{k+1} - \hat{\boldsymbol{u}}_i^k}{\Delta t} = \hat{\boldsymbol{v}}_i^{k+1} \tag{35}$$

$$\frac{\hat{\boldsymbol{v}}_i^{k+1} - \hat{\boldsymbol{v}}_i^k}{\Delta t} = \mathcal{L}^\epsilon(\hat{\boldsymbol{u}}^k)(\boldsymbol{x}_i) + \boldsymbol{b}_i^k. \tag{36}$$

The initial condition is enforced by setting $\hat{\boldsymbol{u}}_i^0 = (\hat{\boldsymbol{u}}_0)_i$ and $\hat{\boldsymbol{v}}_i^0 = (\hat{\boldsymbol{v}}_0)_i$. We note that the forward difference scheme for the system reduces to the central difference scheme for the second order differential equation Equation 12 on substitution of Equation 35 into Equation 36.

4.2.1. Convergence of approximation

In this section we provide an upper bound on the convergence rate of the fully discrete approximation to the Hölder continuous solution as measured by the L^2 norm. The L^2 approximation error E^k at time t^k, for $0 < t^k \leq T$, is given by

$$E^k := \left\|\hat{\boldsymbol{u}}^k - \boldsymbol{u}^k\right\|_{L^2(D;\mathbb{R}^d)} + \left\|\hat{\boldsymbol{v}}^k - \boldsymbol{v}^k\right\|_{L^2(D;\mathbb{R}^d)}.$$

The following theorem gives an explicit a-priori upper bound on the convergence rate.

Theorem 3. ***Convergence of finite difference approximation (forward Euler time discretization)***

Let $\epsilon > 0$ be fixed. Let $(\boldsymbol{u}, \boldsymbol{v})$ be the solution of peridynamic equation Equation 20. We assume $\boldsymbol{u}, \boldsymbol{v} \in C^2([0,T]; C_0^{0,\gamma}(D;\mathbb{R}^d))$. Then the finite difference scheme given by Equation 35 and Equation 36 is consistent in both time and spatial discretization and converges to the exact solution uniformly in time with respect to the $L^2(D;\mathbb{R}^d)$ norm. If we assume the error at the initial step is zero then the error E^k at time t^k is bounded and satisfies

$$\sup_{0\le k\le T/\Delta t} E^k \le O\left(C_t\Delta t + C_s\frac{h^\gamma}{\epsilon^2}\right), \tag{37}$$

where constant C_s and C_t are independent of h and Δt and C_s depends on the Hölder norm of the solution and C_t depends on the L^2 norms of time derivatives of the solution.

Here we have assumed the initial error is zero for ease of exposition only.

We remark that the explicit constants leading to Equation 37 can be large. The inequality that delivers Equation 37 is given by

$$\sup_{0\le k\le T/\Delta t} E^k \le \exp\left[T(1+L_3/\epsilon^2)\right] T\left[C_t\Delta t + (C_s/\epsilon^2)h^\gamma\right], \tag{38}$$

where the constants L_3, C_t and C_s are given by Equation 60, Equation 63, and Equation 64. The explicit constant C_t depends on the spatial L^2 norm of the time derivatives of the solution and C_s depends on the spatial Hölder continuity of the solution and the constant L_3. The constant L_3 is bounded independently of horizon ϵ. Although the constants are necessarily pessimistic they deliver a-priori error estimates. We provide the connection between the non-dimensionalized dynamics used in the a-priori convergence analysis and the simulated dynamics using dimensional quantities in Section 5. We carry out numerical simulations for different values of the horizon ϵ in Section 6. We find that the convergence rate for piecewise constant finite difference interpolation functions is greater than or equal to $\gamma = 1$ for simulations lasting in the tens of microseconds. These results are seen to be consistent with the a-priori estimates given in Theorem 3 above.

4.2.2. Error analysis

We split the error between $(\hat{\boldsymbol{u}}^k, \hat{\boldsymbol{v}}^k)^T$ and $(\boldsymbol{u}^k, \boldsymbol{v}^k)^T$ in two parts as follows

$$\begin{aligned} E^k &= ||\hat{\boldsymbol{u}}^k - \boldsymbol{u}^k||_{L^2} + ||\hat{\boldsymbol{v}}^k - \boldsymbol{v}^k||_{L^2} \\ &\le \left[||\tilde{\boldsymbol{u}}^k - \boldsymbol{u}^k||_{L^2} + ||\tilde{\boldsymbol{v}}^k - \boldsymbol{v}^k||_{L^2}\right] + \left[||\hat{\boldsymbol{u}}^k - \tilde{\boldsymbol{u}}^k||_{L^2} + ||\hat{\boldsymbol{v}}^k - \tilde{\boldsymbol{v}}^k||_{L^2}\right]. \end{aligned} \tag{39}$$

In Section 4.2.3 we will show that the error between the L^2 projections of the actual solution and the discrete approximation for both forward Euler and implicit one step methods decay according to

$$\sup_{0\le k\le T/\Delta t}\left(||\hat{\boldsymbol{u}}^k - \tilde{\boldsymbol{u}}^k||_{L^2} + ||\hat{\boldsymbol{v}}^k - \tilde{\boldsymbol{v}}^k||_{L^2}\right) = O\left(\Delta t + \frac{h^\gamma}{\epsilon^2}\right). \tag{40}$$

And using Lemma 1 we have

$$\begin{aligned} &\sup_k\left(||\tilde{\boldsymbol{u}}^k - \boldsymbol{u}^k||_{L^2} + ||\tilde{\boldsymbol{v}}^k - \boldsymbol{v}^k||_{L^2}\right) \\ &= c^\gamma\sqrt{|D|}\left[\sup_{t\in[0,T]}||\boldsymbol{u}(t)||_{C^{0,\gamma}} + \sup_{t\in[0,T]}||\boldsymbol{v}(t)||_{C^{0,\gamma}}\right]h^\gamma. \end{aligned}$$

We now study the difference $\hat{\boldsymbol{u}}^k - \tilde{\boldsymbol{u}}^k$ and $\hat{\boldsymbol{v}}^k - \tilde{\boldsymbol{v}}^k$.

4.2.3. Error analysis for approximation of L^2 projection of the exact solution

Let the differences be denoted by $\boldsymbol{e}^k(u) := \hat{\boldsymbol{u}}^k - \tilde{\boldsymbol{u}}^k$ and $\boldsymbol{e}^k(v) := \hat{\boldsymbol{v}}^k - \tilde{\boldsymbol{v}}^k$ and their evaluation at grid points are $\boldsymbol{e}_i^k(u) := \hat{\boldsymbol{u}}_i^k - \tilde{\boldsymbol{u}}_i^k$ and $\boldsymbol{e}_i^k(v) := \hat{\boldsymbol{v}}_i^k - \tilde{\boldsymbol{v}}_i^k$. We have the following lemma for the evolution of the differences in the discrete dynamics.

Lemma 2. *The differences $\boldsymbol{e}_i^k(u)$ and $\boldsymbol{e}_i^k(v)$ discretely evolve according to the equations:*

$$\boldsymbol{e}_i^{k+1}(u) = \boldsymbol{e}_i^k(u) + \Delta t \boldsymbol{e}_i^{k+1}(v) + \Delta t \tau_i^k(u) \tag{41}$$

and

$$\begin{aligned}\boldsymbol{e}_i^{k+1}(v) = \boldsymbol{e}_i^k(v) &+ \Delta t \left(\tau_i^k(v) + \sigma_i^k(u) + \sigma_i^k(v)\right) \\ &+ \Delta t \left(\mathcal{L}^\epsilon(\hat{\boldsymbol{u}}^k)(\boldsymbol{x}_i) - \mathcal{L}^\epsilon(\tilde{\boldsymbol{u}}^k)(\boldsymbol{x}_i)\right).\end{aligned} \tag{42}$$

Here $\tau_i^k(u), \tau_i^k(v)$ and $\sigma_i^k(u), \sigma_i^k(v)$ are consistency error terms and are defined as

$$\begin{aligned}\tau_i^k(u) &:= \frac{\partial \tilde{\boldsymbol{u}}_i^{k+1}}{\partial t} - \frac{\tilde{\boldsymbol{u}}_i^{k+1} - \tilde{\boldsymbol{u}}_i^k}{\Delta t}, \\ \tau_i^k(v) &:= \frac{\partial \tilde{\boldsymbol{v}}_i^k}{\partial t} - \frac{\tilde{\boldsymbol{v}}_i^{k+1} - \tilde{\boldsymbol{v}}_i^k}{\Delta t}, \\ \sigma_i^k(u) &:= \left(\mathcal{L}^\epsilon(\tilde{\boldsymbol{u}}^k)(\boldsymbol{x}_i) - \mathcal{L}^\epsilon(\boldsymbol{u}^k)(\boldsymbol{x}_i)\right) \\ \sigma_i^k(v) &:= \frac{\partial \boldsymbol{v}_i^k}{\partial t} - \frac{\partial \tilde{\boldsymbol{v}}_i^k}{\partial t}.\end{aligned} \tag{43}$$

To prove this we start by subtracting $(\tilde{\boldsymbol{u}}_i^{k+1} - \tilde{\boldsymbol{u}}_i^k)/\Delta t$ from Equation 35 to get

$$\begin{aligned}&\frac{\hat{\boldsymbol{u}}_i^{k+1} - \hat{\boldsymbol{u}}_i^k}{\Delta t} - \frac{\tilde{\boldsymbol{u}}_i^{k+1} - \tilde{\boldsymbol{u}}_i^k}{\Delta t} \\ &= \hat{\boldsymbol{v}}_i^{k+1} - \frac{\tilde{\boldsymbol{u}}_i^{k+1} - \tilde{\boldsymbol{u}}_i^k}{\Delta t} \\ &= \hat{\boldsymbol{v}}_i^{k+1} - \tilde{\boldsymbol{v}}_i^{k+1} + \left(\tilde{\boldsymbol{v}}_i^{k+1} - \frac{\partial \tilde{\boldsymbol{u}}_i^{k+1}}{\partial t}\right) + \left(\frac{\partial \tilde{\boldsymbol{u}}_i^{k+1}}{\partial t} - \frac{\tilde{\boldsymbol{u}}_i^{k+1} - \tilde{\boldsymbol{u}}_i^k}{\Delta t}\right).\end{aligned}$$

Taking the average over unit cell U_i of the exact peridynamic equation Equation 20 at time t^k, we will get $\tilde{\boldsymbol{v}}_i^{k+1} - \dfrac{\partial \tilde{\boldsymbol{u}}_i^{k+1}}{\partial t} = 0$ and we recover Equation 41.

Next, we subtract $(\tilde{\boldsymbol{v}}_i^{k+1} - \tilde{\boldsymbol{v}}_i^k)/\Delta t$ from Equation 36 and add and subtract terms to get

$$\begin{aligned}\frac{\hat{\boldsymbol{v}}_i^{k+1} - \hat{\boldsymbol{v}}_i^k}{\Delta t} - \frac{\tilde{\boldsymbol{v}}_i^{k+1} - \tilde{\boldsymbol{v}}_i^k}{\Delta t} &= \mathcal{L}^\epsilon(\hat{\boldsymbol{u}}^k)(\boldsymbol{x}_i) + \boldsymbol{b}_i^k - \frac{\partial \boldsymbol{v}_i^k}{\partial t} + \left(\frac{\partial \boldsymbol{v}_i^k}{\partial t} - \frac{\tilde{\boldsymbol{v}}_i^{k+1} - \tilde{\boldsymbol{v}}_i^k}{\Delta t}\right) \\ &= \mathcal{L}^\epsilon(\hat{\boldsymbol{u}}^k)(\boldsymbol{x}_i) + \boldsymbol{b}_i^k - \frac{\partial \boldsymbol{v}_i^k}{\partial t} \\ &\quad + \left(\frac{\partial \tilde{\boldsymbol{v}}_i^k}{\partial t} - \frac{\tilde{\boldsymbol{v}}_i^{k+1} - \tilde{\boldsymbol{v}}_i^k}{\Delta t}\right) + \left(\frac{\partial \boldsymbol{v}_i^k}{\partial t} - \frac{\partial \tilde{\boldsymbol{v}}_i^k}{\partial t}\right).\end{aligned} \tag{44}$$

Note that from the exact peridynamic equation, we have

$$\boldsymbol{b}_i^k - \frac{\partial \boldsymbol{v}_i^k}{\partial t} = -\mathcal{L}^\epsilon(\boldsymbol{u}^k)(\boldsymbol{x}_i). \tag{45}$$

Combining Equation 44 and Equation 45, gives

$$\begin{aligned}
\boldsymbol{e}_i^{k+1}(v) &= \boldsymbol{e}_i^k(v) + \Delta t\left(\frac{\partial \tilde{\boldsymbol{v}}_i^k}{\partial t} - \frac{\tilde{\boldsymbol{v}}_i^{k+1} - \tilde{\boldsymbol{v}}_i^k}{\Delta t}\right) + \Delta t\left(\frac{\partial \boldsymbol{v}_i^k}{\partial t} - \frac{\partial \tilde{\boldsymbol{v}}_i^k}{\partial t}\right) \\
&\quad + \Delta t\left(\mathcal{L}^\epsilon(\hat{\boldsymbol{u}}^k)(\boldsymbol{x}_i) - \mathcal{L}^\epsilon(\boldsymbol{u}^k)(\boldsymbol{x}_i)\right) \\
&= \boldsymbol{e}_i^k(v) + \Delta t\left(\frac{\partial \tilde{\boldsymbol{v}}_i^k}{\partial t} - \frac{\tilde{\boldsymbol{v}}_i^{k+1} - \tilde{\boldsymbol{v}}_i^k}{\Delta t}\right) + \Delta t\left(\frac{\partial \boldsymbol{v}_i^k}{\partial t} - \frac{\partial \tilde{\boldsymbol{v}}_i^k}{\partial t}\right) \\
&\quad + \Delta t\left(\mathcal{L}^\epsilon(\hat{\boldsymbol{u}}^k)(\boldsymbol{x}_i) - \mathcal{L}^\epsilon(\tilde{\boldsymbol{u}}^k)(\boldsymbol{x}_i)\right) \\
&\quad + \Delta t\left(\mathcal{L}^\epsilon(\tilde{\boldsymbol{u}}^k)(\boldsymbol{x}_i) - \mathcal{L}^\epsilon(\boldsymbol{u}^k)(\boldsymbol{x}_i)\right)
\end{aligned}$$

and the lemma follows on applying the definitions given in Equation 43.

4.2.4. Consistency

In this section we provide upper bounds on the consistency errors. This error is measured in the L^2 norm. Here the upper bound on the consistency error with respect to time follows using Taylor's series expansion. The upper bound on the spatial consistency error is established using the Hölder continuity of nonlocal forces.

Time discretization: We apply a Taylor series expansion in time to estimate $\tau_i^k(u)$ as follows

$$\begin{aligned}
\tau_i^k(u) &= \frac{1}{h^d}\int_{U_i}\left(\frac{\partial \boldsymbol{u}^{k+1}(\boldsymbol{x})}{\partial t} - \frac{\boldsymbol{u}^{k+1}(\boldsymbol{x}) - \boldsymbol{u}^k(\boldsymbol{x})}{\Delta t}\right) d\boldsymbol{x} \\
&= \frac{1}{h^d}\int_{U_i}\left(\frac{1}{2}\frac{\partial^2 \boldsymbol{u}^{k+1}(\boldsymbol{x})}{\partial t^2}\Delta t + O((\Delta t)^2)\right) d\boldsymbol{x}.
\end{aligned}$$

We form the L^2 norm of $\tau_i^k(u)$ and apply Jensen's inequality to get

$$\begin{aligned}
\left\|\tau^k(u)\right\|_{L^2} &\leq \frac{\Delta t}{2}\left\|\frac{\partial^2 \boldsymbol{u}^{k+1}}{\partial t^2}\right\|_{L^2} + O((\Delta t)^2) \\
&\leq \frac{\Delta t}{2}\sup_t\left\|\frac{\partial^2 \boldsymbol{u}(t)}{\partial t^2}\right\|_{L^2} + O((\Delta t)^2).
\end{aligned}$$

A similar argument gives

$$\left\|\tau^k(v)\right\|_{L^2} = \frac{\Delta t}{2}\sup_t\left\|\frac{\partial^2 \boldsymbol{v}(t)}{\partial t^2}\right\|_{L^2} + O((\Delta t)^2).$$

Spatial discretization: From Equation 43 one can write

$$\sigma_i^k(v) = \frac{\partial \boldsymbol{v}_i^k}{\partial t} - \frac{\partial \tilde{\boldsymbol{v}}_i^k}{\partial t} = \frac{\partial \boldsymbol{v}^k(\boldsymbol{x}_i)}{\partial t} - \frac{\partial \tilde{\boldsymbol{v}}^k(\boldsymbol{x}_i)}{\partial t}.$$

Applying Lemma 1 gives

$$|\sigma_i^k(v)| \leq c^\gamma h^\gamma\left\|\frac{\partial \boldsymbol{v}^k}{\partial t}\right\|_{C^{0,\gamma}} \leq c^\gamma h^\gamma \sup_t\left\|\frac{\partial \boldsymbol{v}(t)}{\partial t}\right\|_{C^{0,\gamma}}.$$

Taking the L^2 norm and using the estimates given above yields the inequality

$$\left\|\sigma^k(v)\right\|_{L^2} \leq h^\gamma c^\gamma\sqrt{|D|}\sup_t\left\|\frac{\partial \boldsymbol{v}(t)}{\partial t}\right\|_{C^{0,\gamma}}.$$

We now estimate $\left|\sigma_i^k(u)\right|$. Since $\mathcal{L}^\epsilon = \mathcal{L}_T^\epsilon + \mathcal{L}_D^\epsilon$, we have from Equation 43

$$\begin{aligned}|\sigma_i^k(u)| &\leq |\mathcal{L}_T^\epsilon(\tilde{\boldsymbol{u}}^k)(\boldsymbol{x}_i) - \mathcal{L}_T^\epsilon(\boldsymbol{u}^k)(\boldsymbol{x}_i)| + |\mathcal{L}_D^\epsilon(\tilde{\boldsymbol{u}}^k)(\boldsymbol{x}_i) - \mathcal{L}_D^\epsilon(\boldsymbol{u}^k)(\boldsymbol{x}_i)| \\ &= I_1 + I_2 \end{aligned} \tag{46}$$

To expedite the calculations we employ the following notation for $\boldsymbol{\xi} \in H_1(\mathbf{0})$,

$$\begin{aligned} s_{\boldsymbol{\xi}} &:= \epsilon|\boldsymbol{\xi}|,\ \boldsymbol{e}_{\boldsymbol{\xi}} := \frac{\boldsymbol{\xi}}{|\boldsymbol{\xi}|}, \\ \omega_{\boldsymbol{\xi}}(\boldsymbol{x}) &:= \omega(\boldsymbol{x} + \epsilon\boldsymbol{\xi})\omega(\boldsymbol{x}), \\ \bar{\boldsymbol{u}}_{\boldsymbol{\xi}}(\boldsymbol{x}) &:= \boldsymbol{u}(\boldsymbol{x} + \epsilon\boldsymbol{\xi}) - \boldsymbol{u}(\boldsymbol{x}). \end{aligned} \tag{47}$$

We also write hydrostatic strain (see Equation 2) as follows

$$\theta(\boldsymbol{x}; \boldsymbol{u}) = \frac{1}{\omega_d} \int_{H_1(\mathbf{0})} \omega(\boldsymbol{x} + \epsilon\boldsymbol{\xi}) J(|\boldsymbol{\xi}|) \bar{\boldsymbol{u}}_{\boldsymbol{\xi}}(\boldsymbol{x}) \cdot \boldsymbol{e}_{\boldsymbol{\xi}} d\boldsymbol{\xi}. \tag{48}$$

In our calculations we will also encounter various moments of influence function J therefore we define following term

$$\bar{J}_\alpha := \frac{1}{\omega_d} \int_{H_1(\mathbf{0})} J(|\boldsymbol{\xi}|)|\boldsymbol{\xi}|^{-\alpha} d\boldsymbol{\xi}, \qquad \text{for } \alpha \in \mathbb{R}. \tag{49}$$

Recall that $J(|\boldsymbol{\xi}|) = 0$ for $\boldsymbol{\xi} \notin H_1(\mathbf{0})$ and $0 \leq J(|\boldsymbol{\xi}|) \leq M$ for $\boldsymbol{\xi} \in H_1(\mathbf{0})$.

Applying the notation, $\mathcal{L}_T^\epsilon$ becomes

$$\mathcal{L}_T^\epsilon(\boldsymbol{u})(\boldsymbol{x}) = \frac{2}{\epsilon\omega_d} \int_{H_1(\mathbf{0})} \omega_{\boldsymbol{\xi}}(\boldsymbol{x}) \frac{J(|\boldsymbol{\xi}|)}{\sqrt{s_{\boldsymbol{\xi}}}} f'(\bar{\boldsymbol{u}}_{\boldsymbol{\xi}}(\boldsymbol{x}) \cdot \boldsymbol{e}_{\boldsymbol{\xi}}/\sqrt{s_{\boldsymbol{\xi}}}) \boldsymbol{e}_{\boldsymbol{\xi}} d\boldsymbol{\xi}. \tag{50}$$

On choosing $\boldsymbol{u} = \boldsymbol{u}^k$ and $\boldsymbol{u} = \tilde{\boldsymbol{u}}^k$ in $\mathcal{L}_T^\epsilon$ given by Equation 50 we get

$$\begin{aligned} I_1 &\leq \frac{2}{\epsilon\omega_d} \int_{H_1(\mathbf{0})} \omega_{\boldsymbol{\xi}}(\boldsymbol{x}_i) \frac{J(|\boldsymbol{\xi}|)}{\sqrt{s_{\boldsymbol{\xi}}}} |f'(\bar{\tilde{\boldsymbol{u}}}_{\boldsymbol{\xi}}^k(\boldsymbol{x}_i) \cdot \boldsymbol{e}_{\boldsymbol{\xi}}/\sqrt{s_{\boldsymbol{\xi}}}) - f'(\bar{\boldsymbol{u}}_{\boldsymbol{\xi}}^k(\boldsymbol{x}_i) \cdot \boldsymbol{e}_{\boldsymbol{\xi}}/\sqrt{s_{\boldsymbol{\xi}}})| d\boldsymbol{\xi} \\ &\leq \frac{2C_2^f}{\epsilon\omega_d} \int_{H_1(\mathbf{0})} \frac{J(|\boldsymbol{\xi}|)}{s_{\boldsymbol{\xi}}} |\bar{\tilde{\boldsymbol{u}}}_{\boldsymbol{\xi}}^k(\boldsymbol{x}_i) - \bar{\boldsymbol{u}}_{\boldsymbol{\xi}}^k(\boldsymbol{x}_i)| d\boldsymbol{\xi}, \end{aligned} \tag{51}$$

where we have applied Equation 8 and used the fact that $|f'(r_1) - f'(r_2)| \leq C_2^f |r_1 - r_2|$ and $0 \leq \omega(\boldsymbol{x}) \leq 1$. We use Lemma 1 to estimate $|\bar{\tilde{\boldsymbol{u}}}_{\boldsymbol{\xi}}^k(\boldsymbol{x}_i) - \bar{\boldsymbol{u}}_{\boldsymbol{\xi}}^k(\boldsymbol{x}_i)|$ as follows

$$\begin{aligned} |\bar{\tilde{\boldsymbol{u}}}_{\boldsymbol{\xi}}^k(\boldsymbol{x}_i) - \bar{\boldsymbol{u}}_{\boldsymbol{\xi}}^k(\boldsymbol{x}_i)| &\leq |\tilde{\boldsymbol{u}}^k(\boldsymbol{x}_i + \epsilon\boldsymbol{\xi}) - \boldsymbol{u}^k(\boldsymbol{x}_i + \epsilon\boldsymbol{\xi})| + |\tilde{\boldsymbol{u}}^k(\boldsymbol{x}_i) - \boldsymbol{u}^k(\boldsymbol{x}_i)| \\ &\leq 2c^\gamma ||\boldsymbol{u}(t^k)||_{C^{0,\gamma}} h^\gamma \leq 2c^\gamma \sup_t ||\boldsymbol{u}(t)||_{C^{0,\gamma}} h^\gamma. \end{aligned} \tag{52}$$

From this we get

$$I_1 \leq \left[\frac{4C_2^f c^\gamma \bar{J}_1}{\epsilon^2} \sup_t ||\boldsymbol{u}(t)||_{C^{0,\gamma}} \right] h^\gamma, \tag{53}$$

where $\bar{J}_\alpha$ for $\alpha \in \mathbb{R}$ is defined in Equation 49. Clearly,

$$\sum_{i, \boldsymbol{x}_i \in D} h^d I_1^2 \leq \left[\frac{4C_2^f c^\gamma \bar{J}_1 \sqrt{|D|}}{\epsilon^2} \sup_t ||\boldsymbol{u}(t)||_{C^{0,\gamma}} \right]^2 h^{2\gamma}. \tag{54}$$

We now estimate I_2 in Equation 46. We will consider g of convex-concave type satisfying $C_i^g < \infty$ for $i = 0, 1, 2, 3$ where $C_0^g = \sup |g(r)|$ and $C_i^g = \sup |g^{(i)}(r)|$ for $i = 1, 2, 3$. It is noted that the upper bound for the choice of quadratic g is also found using the steps presented here. We can write $\mathcal{L}_D^\epsilon(\boldsymbol{u})(\boldsymbol{x})$ (see Equation 15) as follows

$$\mathcal{L}_D^\epsilon(\boldsymbol{u})(\boldsymbol{x}) = \frac{1}{\epsilon^2 \omega_d} \int_{H_1(\mathbf{0})} \omega_{\boldsymbol{\xi}}(\boldsymbol{x}) J(|\boldsymbol{\xi}|)[g'(\theta(\boldsymbol{x} + \epsilon\boldsymbol{\xi}; \boldsymbol{u})) + g'(\theta(\boldsymbol{x}; \boldsymbol{u}))]\boldsymbol{e}_{\boldsymbol{\xi}} d\boldsymbol{\xi}. \tag{55}$$

Using this expression we have the upper bound

$$\begin{aligned}
I_2 = \Bigg| & \frac{1}{\epsilon^2 \omega_d} \int_{H_1(\mathbf{0})} \omega_{\boldsymbol{\xi}}(\boldsymbol{x}_i) J(|\boldsymbol{\xi}|)[g'(\theta(\boldsymbol{x}_i + \epsilon\boldsymbol{\xi}; \tilde{\boldsymbol{u}}^k)) + g'(\theta(\boldsymbol{x}_i; \tilde{\boldsymbol{u}}^k)) \\
& - g'(\theta(\boldsymbol{x}_i + \epsilon\boldsymbol{\xi}; \boldsymbol{u}^k)) + g'(\theta(\boldsymbol{x}_i; \boldsymbol{u}^k))]\boldsymbol{e}_{\boldsymbol{\xi}} d\boldsymbol{\xi} \Bigg| \\
\leq & \frac{1}{\epsilon^2 \omega_d} \int_{H_1(\mathbf{0})} J(|\boldsymbol{\xi}|)(|g'(\theta(\boldsymbol{x}_i + \epsilon\boldsymbol{\xi}; \tilde{\boldsymbol{u}}^k)) - g'(\theta(\boldsymbol{x}_i + \epsilon\boldsymbol{\xi}; \boldsymbol{u}^k))| \\
& + |g'(\theta(\boldsymbol{x}_i; \tilde{\boldsymbol{u}}^k)) - g'(\theta(\boldsymbol{x}_i; \boldsymbol{u}^k))|) d\boldsymbol{\xi} \\
\leq & \frac{C_2^g}{\epsilon^2 \omega_d} \int_{H_1(\mathbf{0})} J(|\boldsymbol{\xi}|)(|\theta(\boldsymbol{x}_i + \epsilon\boldsymbol{\xi}; \tilde{\boldsymbol{u}}^k) - \theta(\boldsymbol{x}_i + \epsilon\boldsymbol{\xi}; \boldsymbol{u}^k)| \\
& + |\theta(\boldsymbol{x}_i; \tilde{\boldsymbol{u}}^k) - \theta(\boldsymbol{x}_i; \boldsymbol{u}^k)|) d\boldsymbol{\xi}.
\end{aligned} \tag{56}$$

We proceed further as follows using expression of θ in Equation 48

$$\begin{aligned}
& |\theta(\boldsymbol{x}_i + \epsilon\boldsymbol{\xi}; \tilde{\boldsymbol{u}}^k) - \theta(\boldsymbol{x}_i + \epsilon\boldsymbol{\xi}; \boldsymbol{u}^k)| \\
\leq & \Bigg| \frac{1}{\omega_d} \int_{H_1(\mathbf{0})} \omega(\boldsymbol{x}_i + \epsilon\boldsymbol{\xi} + \epsilon\boldsymbol{\eta}) J(|\boldsymbol{\eta}|)(\tilde{\boldsymbol{u}}^k(\boldsymbol{x}_i + \epsilon\boldsymbol{\xi} + \epsilon\boldsymbol{\eta}) \\
& - \boldsymbol{u}^k(\boldsymbol{x}_i + \epsilon\boldsymbol{\xi} + \epsilon\boldsymbol{\eta}) - \tilde{\boldsymbol{u}}^k(\boldsymbol{x}_i + \epsilon\boldsymbol{\xi}) + \boldsymbol{u}^k(\boldsymbol{x}_i + \epsilon\boldsymbol{\xi})) \cdot \boldsymbol{e}_{\boldsymbol{\eta}} d\boldsymbol{\eta} \Bigg| \\
\leq & \frac{1}{\omega_d} \int_{H_1(\mathbf{0})} J(|\boldsymbol{\eta}|)(|\tilde{\boldsymbol{u}}^k(\boldsymbol{x}_i + \epsilon\boldsymbol{\xi} + \epsilon\boldsymbol{\eta}) - \boldsymbol{u}^k(\boldsymbol{x}_i + \epsilon\boldsymbol{\xi} + \epsilon\boldsymbol{\eta})| \\
& + |\tilde{\boldsymbol{u}}^k(\boldsymbol{x}_i + \epsilon\boldsymbol{\xi}) - \boldsymbol{u}^k(\boldsymbol{x}_i + \epsilon\boldsymbol{\xi})|) d\boldsymbol{\eta} \\
\leq & 2c^\gamma h^\gamma \sup_t ||\boldsymbol{u}(t)||_{C^{0,\gamma}} \bar{J}_0
\end{aligned} \tag{57}$$

where we used Lemma 1 in last step. We combine above estimate in Equation 56 to get

$$I_2 \leq \left[\frac{4 C_2^g c^\gamma \bar{J}_0^2}{\epsilon^2} \sup_t ||\boldsymbol{u}(t)||_{C^{0,\gamma}} \right] h^\gamma \tag{58}$$

and

$$\sum_{i, \boldsymbol{x}_i \in D} h^d I_2^2 \leq \left[\frac{4 C_2^g c^\gamma \bar{J}_0^2 \sqrt{|D|}}{\epsilon^2} \sup_t ||\boldsymbol{u}(t)||_{C^{0,\gamma}} \right]^2 h^{2\gamma}. \tag{59}$$

Applying Equation 54, Equation 59 and Equation 46 gives

$$\begin{aligned}
||\sigma^k(u)||_{L^2} & \leq \sqrt{\sum_{i, \boldsymbol{x}_i \in D} h^d I_1^2} + \sqrt{\sum_{i, \boldsymbol{x}_i \in D} h^d I_2^2} \\
& \leq \left[\frac{4(C_2^g \bar{J}_0^2 + C_2^f \bar{J}_1) c^\gamma \sqrt{|D|}}{\epsilon^2} \sup_t ||\boldsymbol{u}(t)||_{C^{0,\gamma}} \right] h^\gamma.
\end{aligned}$$

Here we define the constant

$$L_3 = \begin{cases} 4(C_1^f \bar{J}_1 + C_2^g \bar{J}_0^2), & \text{for } g \text{ convex-concave} \\ 4(C_1^f \bar{J}_1 + g''(0)\bar{J}_0^2), & \text{for } g \text{ quadratic} \end{cases} \tag{60}$$

this is also the Lipschitz constant related to Lipschitz continuity of peridynamic force in L^2, see Proposition 2. Thus, we have shown for g convex-concave that

$$||\sigma^k(u)||_{L^2} \leq \left[\frac{L_3 c^\gamma \sqrt{|D|}}{\epsilon^2} \sup_t ||\boldsymbol{u}(t)||_{C^{0,\gamma}} \right] h^\gamma. \tag{61}$$

The same arguments show that an identical inequality holds for quadratic g using the other definition of L_3 and this completes the estimation of the consistency errors.

4.2.5. Stability

In this subsection we establish estimates that ensure stability of the evolution and apply the consistency estimates of the previous subsection to establish Theorem 3. Let e^k be the total error at the k^{th} time step. It is defined as

$$e^k := \left\|\boldsymbol{e}^k(u)\right\|_{L^2} + \left\|\boldsymbol{e}^k(v)\right\|_{L^2}.$$

To simplify the calculations, we collect all the consistency errors and write them as

$$\tau := \sup_t \left(\left\|\tau^k(u)\right\|_{L^2} + \left\|\tau^k(v)\right\|_{L^2} + \left\|\sigma^k(u)\right\|_{L^2} + \left\|\sigma^k(v)\right\|_{L^2} \right),$$

and from our consistency analysis, we know that to leading order in Δt and h that

$$\tau \leq C_t \Delta t + \frac{C_s}{\epsilon^2} h^\gamma \tag{62}$$

where,

$$C_t := \frac{1}{2} \sup_t \left\| \frac{\partial^2 \boldsymbol{u}(t)}{\partial t^2} \right\|_{L^2} + \frac{1}{2} \sup_t \left\| \frac{\partial^3 \boldsymbol{u}(t)}{\partial t^3} \right\|_{L^2}, \tag{63}$$

$$C_s := c^\gamma \sqrt{|D|} \left[\epsilon^2 \sup_t \left\| \frac{\partial^2 \boldsymbol{u}(t)}{\partial t^2} \right\|_{C^{0,\gamma}} + L_3 \sup_t \|\boldsymbol{u}(t)\|_{C^{0,\gamma}} \right]. \tag{64}$$

We take the L^2 norm of Equation 41 and Equation 42 and add them. Using the definition of τ we get

$$\begin{aligned} e^{k+1} \leq\ & e^k + \Delta t \left\|\boldsymbol{e}^{k+1}(v)\right\|_{L^2(D;\mathbb{R}^d)} + \Delta t \tau \\ & + \Delta t \sqrt{\sum_{i, \boldsymbol{x}_i \in D} h^d \left| \mathcal{L}^\epsilon(\hat{\boldsymbol{u}}^k)(\boldsymbol{x}_i) - \mathcal{L}^\epsilon(\tilde{\boldsymbol{u}}^k)(\boldsymbol{x}_i) \right|^2}. \end{aligned} \tag{65}$$

It now remains to estimate the last term in the above equation. We illustrate the calculations for convex-concave g noting the identical steps apply to quadratic g as well. Let

$$\begin{aligned} H :=\ & \sqrt{\sum_{i, \boldsymbol{x}_i \in D} h^d \left| \mathcal{L}^\epsilon(\hat{\boldsymbol{u}}^k)(\boldsymbol{x}_i) - \mathcal{L}^\epsilon(\tilde{\boldsymbol{u}}^k)(\boldsymbol{x}_i) \right|^2} \\ \leq\ & \sqrt{\sum_{i, \boldsymbol{x}_i \in D} h^d \left| \mathcal{L}_T^\epsilon(\hat{\boldsymbol{u}}^k)(\boldsymbol{x}_i) - \mathcal{L}_T^\epsilon(\tilde{\boldsymbol{u}}^k)(\boldsymbol{x}_i) \right|^2} \\ & + \sqrt{\sum_{i, \boldsymbol{x}_i \in D} h^d \left| \mathcal{L}_D^\epsilon(\hat{\boldsymbol{u}}^k)(\boldsymbol{x}_i) - \mathcal{L}_D^\epsilon(\tilde{\boldsymbol{u}}^k)(\boldsymbol{x}_i) \right|^2} \\ =:\ & H_1 + H_2. \end{aligned} \tag{66}$$

Choosing $\boldsymbol{u} = \hat{\boldsymbol{u}}^k$ and $\boldsymbol{u} = \tilde{\boldsymbol{u}}^k$ with $\mathcal{L}_T^\epsilon$ given by Equation 50 we get

$$H_1^2 \leq \sum_{i,\boldsymbol{x}_i \in D} h^d \left| \frac{2C_2^f}{\epsilon^2 \omega_d} \int_{H_1(\mathbf{0})} \frac{J(|\boldsymbol{\xi}|)}{|\boldsymbol{\xi}|} |\bar{\hat{\boldsymbol{u}}}_{\boldsymbol{\xi}}^k(\boldsymbol{x}_i) - \bar{\tilde{\boldsymbol{u}}}_{\boldsymbol{\xi}}^k(\boldsymbol{x}_i)| d\boldsymbol{\xi} \right|^2, \tag{67}$$

where $\bar{\hat{\boldsymbol{u}}}_{\boldsymbol{\xi}}^k(\boldsymbol{x}) = \hat{\boldsymbol{u}}^k(\boldsymbol{x} + \epsilon\boldsymbol{\xi}) - \hat{\boldsymbol{u}}^k(\boldsymbol{x})$.

We will make use of the following inequality in the sequel. Let $p(\boldsymbol{\xi})$ be a scalar valued function of $\boldsymbol{\xi}$ and $\alpha \in \mathbb{R}$ then

$$\begin{aligned}
&\left| \frac{C}{\omega_d} \int_{H_1(\mathbf{0})} \frac{J(|\boldsymbol{\xi}|)}{|\boldsymbol{\xi}|^\alpha} p(\boldsymbol{\xi}) d\boldsymbol{\xi} \right|^2 \\
&\leq \left(\frac{C}{\omega_d} \right)^2 \int_{H_1(\mathbf{0})} \int_{H_1(\mathbf{0})} \frac{J(|\boldsymbol{\xi}|)}{|\boldsymbol{\xi}|^\alpha} \frac{J(|\boldsymbol{\eta}|)}{|\boldsymbol{\eta}|^\alpha} p(\boldsymbol{\xi}) p(\boldsymbol{\eta}) d\boldsymbol{\xi} d\boldsymbol{\eta} \\
&\leq \left(\frac{C}{\omega_d} \right)^2 \int_{H_1(\mathbf{0})} \int_{H_1(\mathbf{0})} \frac{J(|\boldsymbol{\xi}|)}{|\boldsymbol{\xi}|^\alpha} \frac{J(|\boldsymbol{\eta}|)}{|\boldsymbol{\eta}|^\alpha} \frac{p(\boldsymbol{\xi})^2 + p(\boldsymbol{\eta})^2}{2} d\boldsymbol{\xi} d\boldsymbol{\eta} \\
&= C^2 \frac{\bar{J}_\alpha}{\omega_d} \int_{H_1(\mathbf{0})} \frac{J(|\boldsymbol{\xi}|)}{|\boldsymbol{\xi}|^\alpha} p(\boldsymbol{\xi})^2 d\boldsymbol{\xi}.
\end{aligned} \tag{68}$$

On applying Equation 68 in Equation 67 with $C = \frac{2C_2^f}{\epsilon^2}$, $\alpha = 1$, $p(|\boldsymbol{\xi}|) = |\bar{\hat{\boldsymbol{u}}}_{\boldsymbol{\xi}}^k(\boldsymbol{x}_i) - \bar{\tilde{\boldsymbol{u}}}_{\boldsymbol{\xi}}^k(\boldsymbol{x}_i)|$ we get

$$\begin{aligned}
H_1^2 &\leq \sum_{i,\boldsymbol{x}_i \in D} h^d \left(\frac{2C_2^f}{\epsilon^2} \right)^2 \frac{\bar{J}_1}{\omega_d} \int_{H_1(\mathbf{0})} \frac{J(|\boldsymbol{\xi}|)}{|\boldsymbol{\xi}|} |\bar{\hat{\boldsymbol{u}}}_{\boldsymbol{\xi}}^k(\boldsymbol{x}_i) - \bar{\tilde{\boldsymbol{u}}}_{\boldsymbol{\xi}}^k(\boldsymbol{x}_i)|^2 d\boldsymbol{\xi} \\
&\leq \left(\frac{2C_2^f}{\epsilon^2} \right)^2 \frac{\bar{J}_1}{\omega_d} \int_{H_1(\mathbf{0})} \frac{J(|\boldsymbol{\xi}|)}{|\boldsymbol{\xi}|} \\
&\quad \left[\sum_{i,\boldsymbol{x}_i \in D} h^d 2(|\hat{\boldsymbol{u}}^k(\boldsymbol{x}_i + \epsilon\boldsymbol{\xi}) - \tilde{\boldsymbol{u}}^k(\boldsymbol{x}_i + \epsilon\boldsymbol{\xi})|^2 + |\hat{\boldsymbol{u}}^k(\boldsymbol{x}_i) - \tilde{\boldsymbol{u}}^k(\boldsymbol{x}_i)|^2) \right] d\boldsymbol{\xi} \\
&\leq \left(\frac{2C_2^f}{\epsilon^2} \right)^2 \frac{\bar{J}_1}{\omega_d} \int_{H_1(\mathbf{0})} \frac{J(|\boldsymbol{\xi}|)}{|\boldsymbol{\xi}|} \\
&\quad \left[\sum_{i,\boldsymbol{x}_i \in D} h^d 2(|\boldsymbol{e}^k(u)(\boldsymbol{x}_i + \epsilon\boldsymbol{\xi})|^2 + |\boldsymbol{e}^k(u)(\boldsymbol{x}_i)|^2) \right] d\boldsymbol{\xi},
\end{aligned} \tag{69}$$

where we substituted definition of $\bar{\hat{\boldsymbol{u}}}_{\boldsymbol{\xi}}^k$ and $\bar{\tilde{\boldsymbol{u}}}_{\boldsymbol{\xi}}^k$ and used inequality $(a+b)^2 \leq 2a^2 + 2b^2$ in third step, and identified terms as $\boldsymbol{e}^k(u)$ in last step. Since $\boldsymbol{e}^k(u)(\boldsymbol{x}) = \sum_{i,\boldsymbol{x}_i \in D} \boldsymbol{e}_i^k(u) \chi_{U_i}(\boldsymbol{x})$, we have

$$H_1^2 \leq \left(\frac{2C_2^f}{\epsilon^2} \right)^2 \frac{\bar{J}_1}{\omega_d} \int_{H_1(\mathbf{0})} \frac{J(|\boldsymbol{\xi}|)}{|\boldsymbol{\xi}|} 4 ||\boldsymbol{e}^k(u)||_{L^2}^2 d\boldsymbol{\xi},$$

so

$$H_1 \leq \frac{4C_2^f \bar{J}_1}{\epsilon^2} ||\boldsymbol{e}^k(u)||_{L^2}. \tag{70}$$

We now estimate H_2. Note that for $I_2 = |\mathcal{L}_D^\epsilon(\tilde{\boldsymbol{u}}^k)(\boldsymbol{x}_i) - \mathcal{L}_D^\epsilon(\boldsymbol{u}^k)(\boldsymbol{x}_i)|$, we have the inequality given by Equation 56. We now use Equation 56 but with $\tilde{\boldsymbol{u}}^k$ replaced by $\hat{\boldsymbol{u}}^k$ and $\boldsymbol{u}^k$ replaced by $\tilde{\boldsymbol{u}}^k$ together with the identity $\theta(\boldsymbol{x}; \hat{\boldsymbol{u}}^k) - \theta(\boldsymbol{x}; \tilde{\boldsymbol{u}}^k) = \theta(\boldsymbol{x}; \hat{\boldsymbol{u}}^k - \tilde{\boldsymbol{u}}^k) = \theta(\boldsymbol{x}; \boldsymbol{e}^k(u))$, to see that

$$H_2^2 \leq \sum_{i,\boldsymbol{x}_i \in D} h^d \left(\frac{C_2^g}{\epsilon^2 \omega_d} \int_{H_1(\mathbf{0})} J(|\boldsymbol{\xi}|)(|\theta(\boldsymbol{x}_i + \epsilon\boldsymbol{\xi}; \boldsymbol{e}^k(u))| + |\theta(\boldsymbol{x}_i; \boldsymbol{e}^k(u))|) d\boldsymbol{\xi} \right)^2. \tag{71}$$

We use inequality Equation 68 with $C = C_2^g/\epsilon^2$, $\alpha = 0$, and $p(\boldsymbol{\xi}) = |\theta(\boldsymbol{x}_i + \epsilon\boldsymbol{\xi}; \boldsymbol{e}^k(u))| + |\theta(\boldsymbol{x}_i; \boldsymbol{e}^k(u))|$ to get

$$\begin{aligned}
H_2^2 &\leq \sum_{i,\boldsymbol{x}_i \in D} h^d \left(\frac{C_2^g}{\epsilon^2}\right)^2 \frac{\bar{J}_0}{\omega_d} \int_{H_1(\mathbf{0})} J(|\boldsymbol{\xi}|)(|\theta(\boldsymbol{x}_i + \epsilon\boldsymbol{\xi}; \boldsymbol{e}^k(u))| + |\theta(\boldsymbol{x}_i; \boldsymbol{e}^k(u))|)^2 d\boldsymbol{\xi} \\
&\leq \left(\frac{C_2^g}{\epsilon^2}\right)^2 \frac{\bar{J}_0}{\omega_d} \int_{H_1(\mathbf{0})} J(|\boldsymbol{\xi}|) \\
&\quad \left[\sum_{i,\boldsymbol{x}_i \in D} h^d 2(|\theta(\boldsymbol{x}_i + \epsilon\boldsymbol{\xi}; \boldsymbol{e}^k(u))|^2 + |\theta(\boldsymbol{x}_i; \boldsymbol{e}^k(u))|^2)\right] d\boldsymbol{\xi},
\end{aligned} \tag{72}$$

where we used inequality $(a+b)^2 \leq 2a^2 + 2b^2$ in the second step. We now proceed to estimate the first sum in the last line of Equation 72,

$$\begin{aligned}
&\sum_{i,\boldsymbol{x}_i \in D} h^d |\theta(\boldsymbol{x}_i + \epsilon\boldsymbol{\xi}; \boldsymbol{e}^k(u))|^2 \\
&\leq \sum_{i,\boldsymbol{x}_i \in D} h^d \left| \frac{1}{\omega_d} \int_{H_1(\mathbf{0})} J(|\boldsymbol{\eta}|)\omega(\boldsymbol{x}_i + \epsilon\boldsymbol{\xi} + \epsilon\boldsymbol{\eta}) \right. \\
&\qquad \left. (\boldsymbol{e}^k(u)(\boldsymbol{x}_i + \epsilon\boldsymbol{\xi} + \epsilon\boldsymbol{\eta}) - \boldsymbol{e}^k(u)(\boldsymbol{x}_i + \epsilon\boldsymbol{\xi})) \cdot \boldsymbol{e}_{\boldsymbol{\eta}} d\boldsymbol{\eta} \right|^2 \\
&\leq \sum_{i,\boldsymbol{x}_i \in D} h^d \left(\frac{1}{\omega_d} \int_{H_1(\mathbf{0})} J(|\boldsymbol{\eta}|)(|\boldsymbol{e}^k(u)(\boldsymbol{x}_i + \epsilon\boldsymbol{\xi} + \epsilon\boldsymbol{\eta})| + |\boldsymbol{e}^k(u)(\boldsymbol{x}_i + \epsilon\boldsymbol{\xi})|) d\boldsymbol{\eta} \right)^2,
\end{aligned} \tag{73}$$

where we used expression of θ from Equation 48 in first step, and used $0 \leq \omega(\boldsymbol{x}) \leq 1$ in the second step. The second summation on the last line of Equation 72 is also bounded above the same way. We apply inequality Equation 68 with $C = 1$, $\alpha = 0$, and $p(\boldsymbol{\eta}) = |\boldsymbol{e}^k(u)(\boldsymbol{x}_i + \epsilon\boldsymbol{\xi} + \epsilon\boldsymbol{\eta})| + |\boldsymbol{e}^k(u)(\boldsymbol{x}_i + \epsilon\boldsymbol{\xi})|$ to get

$$\begin{aligned}
&\sum_{i,\boldsymbol{x}_i \in D} h^d |\theta(\boldsymbol{x}_i + \epsilon\boldsymbol{\xi}; \boldsymbol{e}^k(u))|^2 \\
&\leq \sum_{i,\boldsymbol{x}_i \in D} h^d \frac{\bar{J}_0}{\omega_d} \int_{H_1(\mathbf{0})} J(|\boldsymbol{\eta}|)(|\boldsymbol{e}^k(u)(\boldsymbol{x}_i + \epsilon\boldsymbol{\xi} + \epsilon\boldsymbol{\eta})| + |\boldsymbol{e}^k(u)(\boldsymbol{x}_i + \epsilon\boldsymbol{\xi})|)^2 d\boldsymbol{\eta} \\
&\leq \frac{\bar{J}_0}{\omega_d} \int_{H_1(\mathbf{0})} J(|\boldsymbol{\eta}|) 2 \sum_{i,\boldsymbol{x}_i \in D} h^d (|\boldsymbol{e}^k(u)(\boldsymbol{x}_i + \epsilon\boldsymbol{\xi} + \epsilon\boldsymbol{\eta})|^2 + |\boldsymbol{e}^k(u)(\boldsymbol{x}_i + \epsilon\boldsymbol{\xi})|^2) d\boldsymbol{\eta} \\
&\leq \frac{\bar{J}_0}{\omega_d} \int_{H_1(\mathbf{0})} J(|\boldsymbol{\eta}|) 4 ||\boldsymbol{e}^k(u)||_{L^2}^2 d\boldsymbol{\eta} \\
&= 4\bar{J}_0^2 ||\boldsymbol{e}^k(u)||_{L^2}^2,
\end{aligned} \tag{74}$$

where as before we have used the Cauchy inequality. We next apply the estimate Equation 74 to Equation 72 to see that

$$H_2^2 \leq 16\bar{J}_0^2 ||\boldsymbol{e}^k(u)||_{L^2}^2 \left(\frac{C_2^g}{\epsilon^2}\right)^2 \frac{\bar{J}_0}{\omega_d} \int_{H_1(\mathbf{0})} J(|\boldsymbol{\xi}|) d\boldsymbol{\xi},$$

so

$$H_2 \leq \frac{4C_2^g \bar{J}_0^2}{\epsilon^2} ||\boldsymbol{e}^k(u)||_{L^2}. \tag{75}$$

Finally, we apply the inequalities given by Equation 70 and Equation 75 to Equation 66 and obtain

$$\begin{aligned} H &= \sqrt{\sum_{i,\boldsymbol{x}_i \in D} h^d \left| \mathcal{L}^\epsilon(\hat{\boldsymbol{u}}^k)(\boldsymbol{x}_i) - \mathcal{L}^\epsilon(\tilde{\boldsymbol{u}}^k)(\boldsymbol{x}_i) \right|^2} \\ &\leq H_1 + H_2 \\ &\leq \frac{4(C_2^f \bar{J}_1 + C_2^g \bar{J}_0^2)}{\epsilon^2} ||\boldsymbol{e}^k(u)||_{L^2} \\ &\leq \left[\frac{L_3}{\epsilon^2} ||\boldsymbol{e}^k(u)||_{L^2} \right]^2, \end{aligned} \tag{76}$$

where $L_3 = 4(C_2^f \bar{J}_1 + C_2^g \bar{J}_0^2)$ for convex-concave g. For the case of quadratic g we have the same inequality but with $L_3 = 4(C_2^f \bar{J}_1 + g''(0)\bar{J}_0^2)$.

Applying the inequality given by Equation 76 to Equation 65 gives

$$e^{k+1} \leq e^k + \Delta t \left\| \boldsymbol{e}^{k+1}(v) \right\|_{L^2(D;\mathbb{R}^d)} + \Delta t \tau + \Delta t \frac{L_3}{\epsilon^2} \left\| \boldsymbol{e}^k(u) \right\|_{L^2(D;\mathbb{R}^d)}.$$

We now add $\Delta t ||e^{k+1}(u)||_{L^2(D;\mathbb{R}^d)} + \Delta t \frac{L_3}{\epsilon^2} ||\boldsymbol{e}^k(v)||_{L^2(D;\mathbb{R}^d)}$ to the right side of the equation above to get

$$\begin{aligned} e^{k+1} &\leq (1 + \Delta t \frac{L_3}{\epsilon^2}) e^k + \Delta t e^{k+1} + \Delta t \tau \\ \Rightarrow e^{k+1} &\leq \frac{(1 + \Delta t L_3/\epsilon^2)}{1 - \Delta t} e^k + \frac{\Delta t}{1 - \Delta t} \tau. \end{aligned}$$

We now recursively substitute e^j as follows

$$\begin{aligned} e^{k+1} &\leq \frac{(1 + \Delta t L_3/\epsilon^2)}{1 - \Delta t} e^k + \frac{\Delta t}{1 - \Delta t} \tau \\ &\leq \left(\frac{(1 + \Delta t L_3/\epsilon^2)}{1 - \Delta t} \right)^2 e^{k-1} + \frac{\Delta t}{1 - \Delta t} \tau \left(1 + \frac{(1 + \Delta t L_3/\epsilon^2)}{1 - \Delta t} \right) \\ &\leq ... \\ &\leq \left(\frac{(1 + \Delta t L_3/\epsilon^2)}{1 - \Delta t} \right)^{k+1} e^0 + \frac{\Delta t}{1 - \Delta t} \tau \sum_{j=0}^{k} \left(\frac{(1 + \Delta t L_3/\epsilon^2)}{1 - \Delta t} \right)^{k-j}. \end{aligned} \tag{77}$$

Since $1/(1 - \Delta t) = 1 + \Delta t + \Delta t^2 + O(\Delta t^3)$, we have

$$\frac{(1 + \Delta t L_3/\epsilon^2)}{1 - \Delta t} \leq 1 + (1 + L_3/\epsilon^2)\Delta t + (1 + L_3/\epsilon^2)\Delta t^2 + O(L_3/\epsilon^2)O(\Delta t^3).$$

Now, for any $k \leq T/\Delta t$ and using the identity $(1 + a)^k \leq \exp[ka]$ for $a \leq 0$, we have

$$\begin{aligned} &\left(\frac{1 + \Delta t L_3/\epsilon^2}{1 - \Delta t} \right)^k \\ &\leq \exp\left[k(1 + L_3/\epsilon^2)\Delta t + k(1 + L_3/\epsilon^2)\Delta t^2 + kO(L_3/\epsilon^2)O(\Delta t^3) \right] \\ &\leq \exp\left[T(1 + L_3/\epsilon^2) + T(1 + L_3/\epsilon^2)\Delta t + O(T L_3/\epsilon^2)O(\Delta t^2) \right]. \end{aligned}$$

We write above equation in more compact form as follows

$$\begin{aligned} &\left(\frac{1 + \Delta t L_3/\epsilon^2}{1 - \Delta t} \right)^k \\ &\leq \exp\left[T(1 + L_3/\epsilon^2)(1 + \Delta t + O(\Delta t^2)) \right]. \end{aligned}$$

We use above estimate in Equation 77 and get following inequality for e^k

$$\begin{aligned} e^{k+1} &\leq \exp\left[T(1+L_3/\epsilon^2)(1+\Delta t+O(\Delta t^2))\right]\left(e^0+(k+1)\tau\Delta t/(1-\Delta t)\right) \\ &\leq \exp\left[T(1+L_3/\epsilon^2)(1+\Delta t+O(\Delta t^2))\right]\left(e^0+T\tau(1+\Delta t+O(\Delta t^2))\right) \end{aligned}$$

where we used the fact that $1/(1-\Delta t) = 1+\Delta t+O(\Delta t^2)$.

Assuming the error in initial data is zero, i.e. $e^0 = 0$, and noting the estimate of τ in Equation 62, we have

$$\sup_k e^k \leq \exp\left[T(1+L_3/\epsilon^2)\right] T\tau$$

and we conclude to leading order that

$$\sup_k e^k \leq \exp\left[T(1+L_3/\epsilon^2)\right] T\left[C_t\Delta t+(C_s/\epsilon^2)h^\gamma\right]. \tag{78}$$

Here the constants C_t and C_s are given by Equation 63 and Equation 64. This shows the stability of the numerical scheme. We note that constant $L_3 = 4(C_1^f\bar{J}_1 + C_2^g\bar{J}_0^2)$, where $C_2^f = \sup|f''(r)|, C_2^g = \sup|g''(r)|$, corresponds to the case when g is convex-concave type. For quadratic g the constant is given by $L_3 = 4(C_1^f\bar{J}_1 + g''(0)\bar{J}_0^2)$.

Next we establish the relation between the nondimensional peridynamic equation analyzed so far to the peridynamic equation with the dimensional quantities. We also estimate the total error incurred for Plexiglass material and the maximum allowed simulation time based on the convergence analysis in Theorem 3.

5. Quantifying the error

In this section we show how to apply the a-priori error bound to numerical simulations carried out using quantities with dimensions. As an example we consider the numerical simulation of a propagating crack in Plexiglass at room temperature. Here the dynamics is modeled in terms of quantities with dimensions. We show how to transform the peridynamic equation of motion for Plexiglass into an equivalent evolution in terms of non dimensional quantities Equation 12. We then apply our a-priori error bounds to the equivalent non dimensional peridynamics Section 4.2. In this way obtain the dimensionless simulation time for which the error remains within an acceptable limit. One can then transform the dimensionless time back to the actual time of the fracture propagation given in micro-seconds for which the a-priori simulation error is acceptable. We find that the acceptable simulation time predicted by a-priori analysis is smaller than can be seen in the numerical experiments. This is to be expected as a-priori estimates are naturally pessimistic. We explain the reasons for this difference in the last part of this section. To keep the following presentation simple, we will assume that the dimension is 2, the potential function $g = 0$ and $\boldsymbol{b} = \boldsymbol{0}$.

Suppose $\bar{D}$ is the material domain with characteristic length scale L_0 and suppose $\bar{\boldsymbol{x}} \in \bar{D}$ are coordinates with dimensions of length. Let $\bar{T}$ denote the simulation time with dimensions of time and $\bar{t} \in [0, \bar{T}]$. Let $\bar{\epsilon}$ denote the size of horizon with units of length. The displacement field is $\bar{\boldsymbol{u}}(\bar{\boldsymbol{x}}, \bar{t})$ and has units of length. The influence function $\bar{J}(\bar{\xi}) = a(1-\xi)$ is non dimensional and its argument $\bar{\xi} = |\bar{\boldsymbol{x}} - \bar{\boldsymbol{y}}|/\bar{\epsilon}$ is also non dimensional. The non dimensional parameter $a > 0$ is a fixed positive constant. Last we note that the boundary function ω is dimensionless and its argument is also dimensionless.

To fix ideas we consider an explicit potential function $\bar{f}(\bar{r}) = \bar{C}(1-\exp[-\bar{\beta}\bar{r}^2])$ where $\bar{r}$ has units of $\sqrt{\text{length}}$, $\bar{C}$ has units of force/length, and $\bar{\beta}$ has units of 1/length. Let the bulk modulus K, density $\bar{\rho}$, and critical energy release rate G correspond to Plexiglass at room temperature. Following equations 94, 95, and 97 of Lipton et al. (2018), the parameters $\bar{C}, \bar{\beta}$ are given by

$$\bar{C} = \frac{G}{2(\omega_1/\omega_2)M}, \quad \bar{\beta} = \frac{\lambda}{(1/4)\bar{C}M}, \quad M = \int_0^1 \bar{J}(\xi)\xi^2 d\xi, \tag{79}$$

where $\omega_1 = 2, \omega_2 = \pi$. Here the Lamé parameter is related to K by $\lambda = 3K/5$. For $\bar{J}(\xi) = a(1-\xi)$, $M = a/12$. Substituting, we have

$$\bar{C} = \frac{3\pi G}{a}, \quad \bar{\beta} = \frac{48K}{5\pi G} \tag{80}$$

and also

$$\bar{C}\bar{\beta} = \frac{144}{5a}K. \tag{81}$$

The solution $\bar{\boldsymbol{u}}$ satisfies

$$\bar{\rho}\ddot{\bar{\boldsymbol{u}}}(\bar{\boldsymbol{x}}, \bar{t}) = \bar{\mathcal{L}}_T^{\bar{\epsilon}}(\bar{\boldsymbol{u}})(\bar{\boldsymbol{x}}, \bar{t}), \qquad \forall (\bar{\boldsymbol{x}}, \bar{t}) \in \bar{D} \times [0, \bar{T}]. \tag{82}$$

The solution $\bar{\boldsymbol{u}}$ takes the boundary condition $\bar{\boldsymbol{u}}(t) = \boldsymbol{0}$ for all $\bar{\boldsymbol{x}} \in \partial\bar{D}$ and the initial condition $\bar{\boldsymbol{u}}(0) = \bar{\boldsymbol{u}}_0, \dot{\bar{\boldsymbol{u}}}(0) = \bar{\boldsymbol{v}}_0$.

5.1. Nondimensionalization

Now we associate a local wave speed for the peridynamic material and an associated local time scale given by

$$v_0 = \sqrt{\frac{\bar{C}\bar{\beta}}{\bar{\rho}}}, \quad T_0 = \frac{L_0}{v_0}. \tag{83}$$

The change to non-dimensional variables is given by

$$x = \frac{\bar{\boldsymbol{x}}}{L_0}, \quad t = \frac{\bar{t}}{T_0}, \quad \bar{\epsilon} = \frac{\epsilon}{L_0}, \quad \boldsymbol{u}(x,t) = \frac{\bar{\boldsymbol{u}}(\bar{\boldsymbol{x}}, \bar{t})}{L_0}. \tag{84}$$

From above it is easy to see that $\bar{S}(\bar{\boldsymbol{x}}, \bar{\boldsymbol{y}}, \bar{t}) = \frac{\bar{\boldsymbol{u}}(\bar{\boldsymbol{y}}, \bar{t}) - \bar{\boldsymbol{u}}(\bar{\boldsymbol{x}}, \bar{t})}{|\bar{\boldsymbol{y}} - \bar{\boldsymbol{x}}|} \cdot \frac{\bar{\boldsymbol{y}} - \bar{\boldsymbol{x}}}{|\bar{\boldsymbol{y}} - \bar{\boldsymbol{x}}|} = S(\boldsymbol{x}, \boldsymbol{y}, t)$. We write

$$\bar{r} = \sqrt{|\bar{\boldsymbol{x}} - \bar{\boldsymbol{y}}|}\, \bar{S} = \sqrt{L_0}\sqrt{|\boldsymbol{x} - \boldsymbol{y}|}\, S = \sqrt{L_0}\, r, \tag{85}$$

where $r = \sqrt{|\boldsymbol{x} - \boldsymbol{y}|}\, S$. The non-dimensional potential function f is related to $\bar{f}$ by

$$f(r) = \frac{\bar{f}(\sqrt{L_0} r)}{L_0 \bar{\rho} v_0^2} = \frac{1}{L_0 \bar{\rho} v_0^2} \bar{C}(1 - \exp[-L_0 \bar{\beta} r^2]). \tag{86}$$

It is now clear that the dimension of $\bar{f}$ is the same as $L_0 \bar{\rho} v_0^2$ and therefore f is non-dimensional. We have,

$$f'(r) = \frac{\bar{f}'(\sqrt{L_0} r)}{\sqrt{L_0}\bar{\rho} v_0^2} = \frac{2\bar{C}\bar{\beta} r}{\bar{\rho} v_0^2} \exp[-L_0 \bar{\beta} r^2]. \tag{87}$$

Collecting results we now see that the peridynamic equation 82 is equivalent to the non-dimensional equation of motion 12 with density $\rho = 1$, i.e.,

$$\left(\frac{\bar{\rho} v_0^2}{L_0}\right) \partial_{tt} \boldsymbol{u} = \bar{\rho} \partial_{\bar{t}\bar{t}} \bar{\boldsymbol{u}} = \bar{\mathcal{L}}_T^{\bar{\epsilon}}(\bar{\boldsymbol{u}})(\bar{\boldsymbol{x}}) = \left(\frac{\bar{\rho} v_0^2}{L_0}\right) \mathcal{L}_T^{\epsilon}(\boldsymbol{u})(\boldsymbol{x}), \tag{88}$$

so

$$\ddot{\boldsymbol{u}} = \mathcal{L}_T^{\epsilon}(\boldsymbol{u})(\boldsymbol{x}). \tag{89}$$

5.2. Lipschitz continuity constant and bound on error

The exact solution is in $\boldsymbol{u} \in C_0^{0,1}(D;\mathbb{R}^2)$, and the bound on the spatial discretization error is given by, see Equation 78,

$$\sup_k e^k \leq \exp\left[T(1+L_3/\epsilon^2)\right] T(C_s/\epsilon^2)h, \tag{90}$$

where

$$L_3 = 4C_2^f \bar{J}_1, \quad C_2^f = \sup_r |f''(r)|, \quad \bar{J}_1 = \frac{1}{\omega_2}\int_{H_1(\mathbf{0})} J(|\boldsymbol{\xi}|)/|\boldsymbol{\xi}| d\boldsymbol{\xi}, \quad \omega_2 = |H_1(\mathbf{0})| = \pi$$

and

$$\begin{aligned} C_s &= \sqrt{2L_0}\left[\epsilon^2 \sup_t \left\| \frac{\partial^2 \boldsymbol{u}(t)}{\partial t^2}\right\|_{C^{0,\gamma}} + L_3 \sup_t \|\boldsymbol{u}(t)\|_{C^{0,\gamma}}\right] \\ &\approx L_3\sqrt{2}\sqrt{L_0}\sup_t \|\boldsymbol{u}(t)\|_{C^{0,\gamma}}, \end{aligned}$$

where we have ignored the order ϵ^2 term.

For $f(r) = \frac{1}{L_0\bar{\rho}v_0^2}\bar{C}(1-\exp[-L_0\bar{\beta}r^2])$ and $J(r) = a(1-\xi)$, it can be seen that

$$C_2^f = \frac{2\bar{C}\bar{\beta}}{\bar{\rho}v_0^2}, \quad \bar{J}_1 = a. \tag{91}$$

We have $\bar{C}\bar{\beta} = \bar{\rho}v_0^2$ from Equation 83. So

$$L_3 = \frac{8a}{\epsilon^2}. \tag{92}$$

The upper bound on error is given by

$$\sup_k e^k \leq \sqrt{2L_0}\exp[(1+\frac{8a}{\epsilon^2})T]T\frac{8a}{\epsilon^2}\sup_t \|\boldsymbol{u}(t)\|_{C^{0,\gamma}} h/\epsilon^2,$$

and the a-priori upper bound on the relative error is denoted by α where

$$\alpha = \sqrt{2L_0}\exp[(1+\frac{8a}{\epsilon^2})T]8a\frac{Th}{\epsilon^2} \tag{93}$$

5.3. Numerical value of α

We set $L_0 = 1, \epsilon = 1/10, h = 1/100$ and we fix $a = 0.001$ and $v_0 = \sqrt{\frac{\bar{C}\bar{\beta}}{\bar{\rho}}}$. The material properties of Plexiglass at room temperature are given by the density $\bar{\rho} = 1200\,kg/m^3$, the bulk modulus $K = 25\,GPa$, and the critical energy release rate $G = 500\,Jm^{-2}$. We then have

$$\alpha = \exp[1.8T]0.012T. \tag{94}$$

Here the relative error upper bound $\alpha < 1/10$ when the non-dimensional time $T \leq \frac{2}{1.8} = 1.111$. Therefore the actual time in seconds of the simulation can be $\bar{T} = T_0 \times T \leq (L_0/v_0) \times 1.111 = 1.433\mu$s.

5.4. Discussion on error accumulation in the numerics

Fracture in notched Plexiglass samples can last up to several hundred microseconds. From the previous subsection we see that error increases by factor 1/10 every 1.433μs for nonlinear peridynamic material. This gives us about 5μs of simulation time till the a-priori bound on the relative error is about 1/2. However, from the numerical experiments conducted in the following section we find that the discrete simulation is stable and converges with h at a linear rate for a larger amount of time than predicted by the a-priori estimates.

To explain this we first note that the region where nonlinearity is strong is always restricted to a very small region, with area $L_0 \times 2\bar{\epsilon}$ in 2-d for a single crack see Lipton et al. (2018); Lipton (2016). For points in the region away from the crack the deformation is smooth. We can argue that in this region the material behaves like a linear elastic material up to a small error of the order of $O(\bar{\epsilon})$. This has been shown for this model when the solution is sufficiently smooth and using [Proposition 6, Jha and Lipton (2018b)] we write

$$\bar{\mathcal{L}}_T^{\bar{\epsilon}}(\bar{\boldsymbol{u}})(\bar{\boldsymbol{x}}) = \nabla \cdot \mathbb{C}\mathcal{E}\bar{\boldsymbol{u}}(\bar{\boldsymbol{x}}) + O(\bar{\epsilon}), \tag{95}$$

where

$$\mathcal{E}\bar{\boldsymbol{u}}(\bar{\boldsymbol{x}}) = \frac{1}{2}(\nabla\bar{\boldsymbol{u}}(\bar{\boldsymbol{x}}) + \nabla\bar{\boldsymbol{u}}(\bar{\boldsymbol{x}})^T), \tag{96}$$

$$\mathbb{C}_{ijkl} = 2\mu\frac{\delta_{ik}\delta_{jl} + \delta_{il}\delta_{jk}}{2} + \lambda\delta_{ij}\delta_{kl}, \tag{97}$$

$$\lambda = \mu = \frac{\bar{f}''(0)}{8}\int_0^1 J(\xi)\xi^2 d\xi = \bar{C}\bar{\beta}\frac{a}{48}, \tag{98}$$

where last equation is for $d = 2$ and for $J(\xi) = a(1-\xi)$. We now observe that for the non-dimensional function $f(r) = \frac{1}{L_0\bar{\rho}\bar{v}_0^2}\bar{C}(1 - \exp[-L_0\bar{\beta}r^2])$, $f''(0) = 2$. Using this we can write

$$\bar{\mathcal{L}}_T^{\bar{\epsilon}}(\bar{\boldsymbol{u}})(\bar{\boldsymbol{x}}) = \frac{\bar{C}\bar{\beta}}{L_0}\frac{a}{48}\nabla \cdot \hat{\mathbb{C}}\mathcal{E}\boldsymbol{u}(\boldsymbol{x}) + O(\bar{\epsilon}), \tag{99}$$

where $\hat{\mathbb{C}}$ is given by Equation 97 for the choice $\lambda = \mu = 1$.

Substituting Equation 95 into Equation 89 we get

$$\bar{\mathcal{L}}_T^{\bar{\epsilon}}(\boldsymbol{u})(\boldsymbol{x}) = \left(\frac{\bar{\rho}\tilde{v}_0^2}{L_0}\right)\nabla \cdot \hat{\mathbb{C}}\mathcal{E}\boldsymbol{u}(\boldsymbol{x}) + O(\bar{\epsilon}), \tag{100}$$

with

$$\tilde{v}_0 = \sqrt{\frac{\bar{C}\bar{\beta}}{48\bar{\rho}}} = \sqrt{\frac{\lambda}{\bar{\rho}}}. \tag{101}$$

where we have used the relation Equation 81 and $\lambda = \mu$ and $\tilde{v}_0$ is the s-wave speed in Plexiglass.

It follows from Equation 100, that for regions where nonlinearity is negligible then the solution should be an approximation to the solution of the linear elastic wave equation. This is shown for smooth solutions in [Theorem 5, Jha and Lipton (2018b)] so the total error accumulated at each time step is far less than in the nonlinear region. The error due to the truly nonlinear peridynamic interaction is restricted to a region of small area $2L_0\bar{\epsilon}$. This explains why simulations in the next section exhibit a linear rate of convergence in h for a longer time than predicted from the a-priori estimates.

6. Numerical results

In this section, we present numerical simulations that support the theoretical upper bound on the convergence rate. We also show the sharp crack propagation in the sample under the bending load. We specify the

Parameters \ Poisson's ratio	$\nu = 0.245$	$\nu = 0.25$
c	4712.4	4712.4
C	-1.0623×10^{12}	0
β	1.7533×10^{8}	1.5279×10^{8}
$r* = \frac{1}{\sqrt{2\beta}}$	5.3402×10^{-5}	5.7206×10^{-5}

Table 1: Peridynamic material parameters assuming bulk modulus $K = 25\,GPa$ and critical energy release rate $G_c = 500\,J/m^{-2}$. Density is $\rho = 1200\,kg/m^3$.

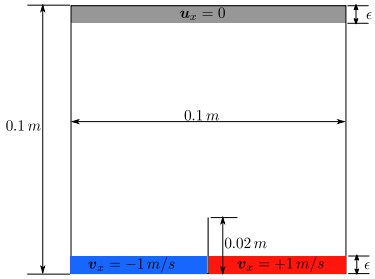

Figure 4: Material domain $D = [0, 0.1\,m]^2$ with crack of length $0.02\,m$. The x-component of displacement is fixed along a collar of thickness equal to the horizon on top. On the bottom the velocity $\boldsymbol{v}_x = \pm 1\,m/s$ along x-direction is specified on either side of the crack to make the crack propagate upwards.

density $\rho = 1200\,kg/m^3$, bulk modulus $K = 25\,GPa$, and critical energy release rate $G_c = 500\,Jm^{-2}$. The pairwise interaction and the hydrostatic interaction are characterized by potentials $f(r) = c(1 - \exp[-\beta r^2])$ and $g(r) = Cr^2/2$ respectively. The influence function is $J(r) = 1 - r$. We present results when hydrostatic force is active (when Poisson's ratio $\nu = 0.245$) and when hydrostatic force is inactive (when $\nu = 0.25$). Equations 94, 95, and 97 of Lipton et al. (2018) relate parameters c, β, C to the Lamè parameters λ, μ and the critical energy release rate G_c. In Table 1 we list the values of parameters. The critical bond strain between material point $\boldsymbol{y}$ and $\boldsymbol{x}$ is $S_c = r^*/\sqrt{|\boldsymbol{y} - \boldsymbol{x}|}$ where $r^* = 1/\sqrt{2\beta}$.

We note that the mesh nodes near the boundary suffer from reduced stiffness due to lack of bonds. This is known as the surface effect. To counter the surface effect, the parameters c, β, C have to be adjusted for the nodes closer to the boundary so that the stiffness of the volume represented by the nodes near the boundary is same as the stiffness of volumes represented by the interior nodes. In the numerical implementation same value of parameters are used. For the type of problems considered in this work, the damage is only seen near pre-crack and during the evolution new damage zones are created in the interior. Looking at the damage profile Figure 5 and Figure 9 we can see that surface effects are not visible and no damage is seen near the boundary. This suggests that the surface effect does not play a major role in the simulations considered in this work.

We consider the central difference time discretization described by Equation 35 and Equation 36 on a uniform square mesh of mesh size h. We place nodes at the center of each square cell. Area represented by each node is simply h^2. We can write the peridynamic force $\mathcal{L}^\epsilon(\hat{\boldsymbol{u}}^k)(\boldsymbol{x}_i)$ as follows

$$\mathcal{L}^\epsilon(\hat{\boldsymbol{u}}^k)(\boldsymbol{x}_i) = \int_{H_\epsilon(\boldsymbol{x}_i)} (w_1(\boldsymbol{y}, \boldsymbol{x}_i) + w_2(\boldsymbol{y}, \boldsymbol{x}_i))d\boldsymbol{y}, \tag{102}$$

where w_1 and w_2 can be determined from expression of $\mathcal{L}^\epsilon$ in Equation 13. In the simulation we approximate $\mathcal{L}^\epsilon(\hat{\boldsymbol{u}}^k)(\boldsymbol{x}_i)$ as below

$$\mathcal{L}^\epsilon(\hat{\boldsymbol{u}}^k)(\boldsymbol{x}_i) \approx \sum_{\boldsymbol{x}_j \in D_h \cap H_\epsilon(\boldsymbol{x}_i)} (w_1(\boldsymbol{x}_j, \boldsymbol{x}_i) + w_w(\boldsymbol{x}_j, \boldsymbol{x}_i))V_j \bar{V}_{ij}, \tag{103}$$

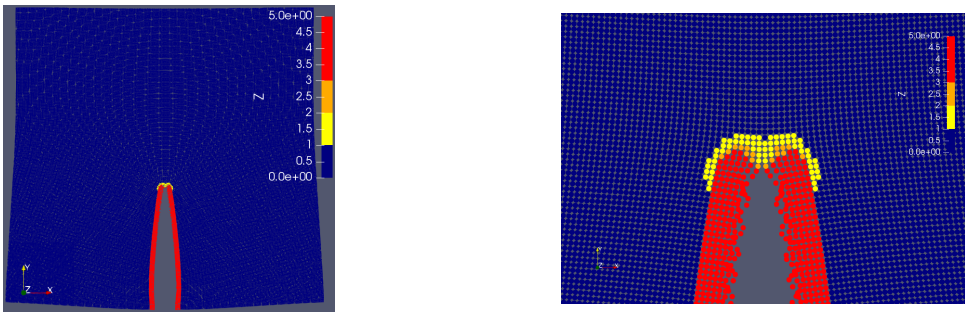

(a) (b)

Figure 5: (a) Color plot of damage function Z on deformed material domain at time $t = 34\,\mu s$. Dark blue represents undamaged material $Z < 1$, $Z \approx 1$ is yellow at crack tip, red is softening material. The plot is for a horizon $\epsilon = 2\,mm$ and $h = \epsilon/8$. Here, the displacements are scaled by 100 and damage function is cut off at 5 to highlight the crack zone. The maximum displacement is $4.4\,mm$ and the maximum value of $Z(x)$ is 82 at $t = 34\,\mu s$. (b) View near the crack tip.

where $V_j = h^2$ is the area (volume in 3-d) represented by node $\boldsymbol{x}_j$. The area (volume in 3-d) correction $\bar{V}_{ij}$ is the ratio of part of the area V_j which is within the horizon of $\boldsymbol{x}_i$ and the area V_j. The numerical results are presented in the following section.

6.1. Crack propagation: Fracture energy and numerical convergence study

We consider a 2-d domain $D = [0, 0.1\,m]^2$ (with unit thickness in the third direction) with a vertical pre-crack of length $0.02\,m$. We use a uniform square mesh of size h. The boundary conditions are described in Figure 4. The simulation time is $T = 34\,\mu s$ and the time step is $\Delta t = 0.004\,\mu s$. In what follows we run the simulations for three different horizons $\epsilon = 8\,mm, 4\,mm, 2\,mm$. For the coarsest horizon $\epsilon = 8\,mm$, the number of mesh nodes are (approximately) $0.9 \times 10^3, 3.5 \times 10^3, 13.7 \times 10^3$ for $h = 4, 2, 1\,mm$ respectively. The memory consumed are 10 MB, 16 MB, 95 MB respectively. For the finest horizon, $\epsilon = 2\,mm$, the number of nodes is $11 \times 10^3, 44 \times 10^3, 174 \times 10^3$ for $h = 1, 0.5, 0.25\,mm$ respectively. The memory consumed are 16.4 MB, 99.4 MB, 1126.4 MB respectively. All computations were performed on a single workstation in parallel using 20 threads.

6.1.1. Fracture energy of crack zone

The extent of damage at a material point $\boldsymbol{x}$ is given by the function $Z(\boldsymbol{x})$

$$Z(\boldsymbol{x}) = \max_{\boldsymbol{y} \in H_\epsilon(\boldsymbol{x}) \cap D} \frac{S(\boldsymbol{y}, \boldsymbol{x}; \boldsymbol{u})}{S_c}. \tag{104}$$

We define the crack zone as the set of material points which have $Z > 1$. We compute the peridynamic energy of crack zone and compare it with the Griffith's fracture energy. For a crack of length l, the Griffith's fracture energy (G.E.) will be $G.E. = G_c \times l$. The peridynamic fracture energy (P.E.) is given by

$$P.E. = \int_{\substack{\boldsymbol{x} \in D, \\ Z(\boldsymbol{x}) \geq 1}} \left[\frac{1}{\epsilon^d \omega_d} \int_{H_\epsilon(\boldsymbol{x})} |\boldsymbol{y} - \boldsymbol{x}| \mathcal{W}^\epsilon(S(\boldsymbol{y}, \boldsymbol{x}, \boldsymbol{u}))\, d\boldsymbol{y} \right] d\boldsymbol{x},$$

where $\mathcal{W}^\epsilon(S(\boldsymbol{y}, \boldsymbol{x}, \boldsymbol{u}))$ is the bond-based potential, see Equation 3. For the choice of $f(r)$ and $g(r)$, only bond-based potential f contributes to the fracture energy, therefore $P.E.$ is computed only from bond-based interaction.

Figure 5 shows the plot of Z at time $t = 34\,\mu s$ for horizon $\epsilon = 2\,mm$ and $h = 0.25\,mm$. The figure on the right shows the Z field near a crack tip. In Figure 6 we plot the peridynamic and Griffith's fracture energy as a function of crack length. The absolute error between the peridynamic and Griffith's fracture energy remain below 5% for simulation time upto $34\,\mu s$.

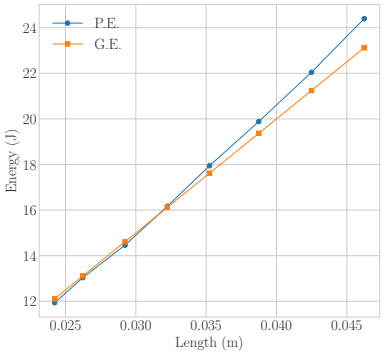

Figure 6: Crack length vs peridynamic fracture energy (P.E.) and Griffith's fracture energy (G.E.). G.E. is simply $G_c \times l$ where $G_c = 500\, Jm^{-2}$. Plot is for $\epsilon = 2\, mm$.

6.1.2. Convergence rate

Consider a fixed horizon ϵ and three different mesh sizes $h_1 = \epsilon/2, h_2 = \epsilon/4, h_3 = \epsilon/8$. We compute the convergence rate as follows. Let $\boldsymbol{u}_1, \boldsymbol{u}_2, \boldsymbol{u}_3$ be approximate solutions corresponding to meshes of size h_1, h_2, h_3, and let $\boldsymbol{u}$ be the exact solution. We suppose for $h' < h$ that $\underline{C}h^\alpha \leq ||\boldsymbol{u}_h - \boldsymbol{u}_{h'}|| = \overline{C}h^\alpha$ with $\underline{C} \leq \overline{C}$ and $\alpha > 0$, and fix the ratio of mesh size $h_1/h_2 = h_2/h_3 = r$. A straight forward calculation gives

$$\alpha \leq \frac{\log(||\boldsymbol{u}_1 - \boldsymbol{u}_2||) - \log(||\boldsymbol{u}_2 - \boldsymbol{u}_3||) + \log(\overline{C}) - \log(\underline{C})}{\log(r)}, \tag{105}$$

so an upper bound on the convergence rate is at least as big as

$$b = \frac{\log(||\boldsymbol{u}_1 - \boldsymbol{u}_2||) - \log(||\boldsymbol{u}_2 - \boldsymbol{u}_3||)}{\log(r)}. \tag{106}$$

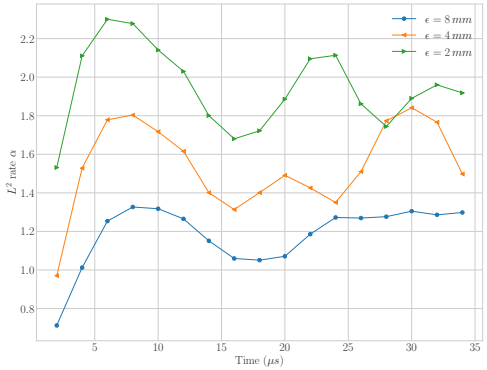

Figure 7: Convergence rate with respect to mesh size for different fixed size of horizons.

We calculate the convergence rate estimate b for mesh sizes $h = \epsilon/2, \epsilon/4, \epsilon/8$ and plot it for every $2\,\mu s$ for times up to $34\,\mu s$, see Figure 7. It is seen that the convergence rate is at least 1 up to the final time of $34\,\mu s$. These numerical results show a convergence at a rate that is at least as good as the linear a-priori convergence rate obtained in Theorem 3.

6.2. Bending test with pre-crack

We consider a 2-d material domain (with unit thickness in third direction) $D = [0, 0.25\, m] \times [0, 0.05\, m]$ with single and double vertical cracks. We fix horizon to $\epsilon = 0.75\, mm$ and mesh size $h = 0.25\, mm$. The

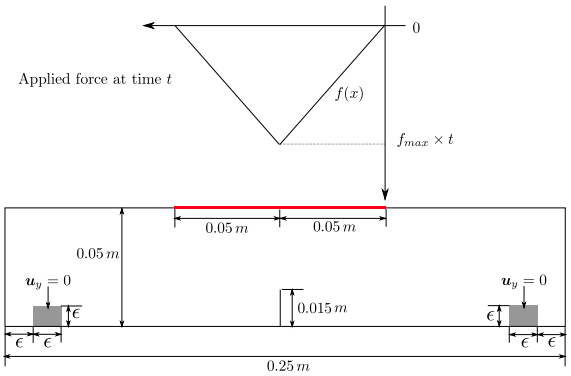

Figure 8: Material domain $D = [0, 0.25\,m] \times [0, 0.05\,m]$ with single verticle crack of length $0.015\,m$ at mid point of bottom edge. We apply linear in time distributed load, along negative y-direction, on part of the top edge. At any time t, the load is zero at the end points of loading line (red line) and is $f_{max} \times t$ at the midpoint. We take constant $f_{max} = -2.5 \times 10^{14}$. We fix a vertical displacement on two support regions shown in the figure. Horizon is $\epsilon = 0.75\,mm$.

boundary conditions are described in Figure 8 for single crack. For the double crack problem, the two vertical cracks are symmetrically located at distance $0.02\,m$ along x-axis from the mid point $x = 0.125\,m, y = 0$. With time step $\Delta t = 0.0035\,\mu s$ we run simulations upto time $T = 350\,\mu s$. Material properties correspond to the Poisson's ration $\nu = 0.25$, see Table 1.

In Figure 9 damage profile at various times are shown for both single and double crack problem. The material exhibits a sharp crack propagation. In Figure 10 we plot the fracture energy as a function of total crack length. The error in energy remain below 5% till $220.5\,\mu s$ for single crack problem and $245\,\mu s$ for double crack problem.

7. Conclusions

In this article, we present an a-priori convergence analysis for a class of nonlinear nonlocal state based peridynamic models. We have shown that the convergence rate applies, even when the fields do not have well-defined spatial derivatives. The results are valid for two different classes of state-based peridynamic models depending on the potential functions associated with the dilatational energy. For both models the potential function characterizing the energy due to tensile strain is of convex-concave type while the potential function for the dilatational strain can be either convex-concave or quadratic. The convergence rate of the discrete approximation to the true solution in the mean square norm is given by $C(\Delta t + h^\gamma/\epsilon^2)$. Here the constant depends on the Hölder and L^2 norm of the true solution and its time derivatives. The Lipschitz property of the nonlocal, nonlinear force together with boundedness of the nonlocal kernel plays an important role. It ensures that the error in the nonlocal force remains bounded when replacing the exact solution with its approximation. This, in turn, implies that even in the presence of mechanical instabilities the global approximation error remains controlled by the local truncation error in space and time. We have described the connection between the non-dimensionalized dynamics used in the a-priori convergence analysis and the simulated dynamics using dimensional quantities. The numerics are carried out for Plexiglass. The a-priori estimates predict a simulation time of a few microseconds before the relative error grows too large. On the other hand the numerical simulation with crack propagation looks to be stable and one can control the error by choosing the time step and spatial discretization sufficiently small. The simulation shows a linear convergence rate with respect to mesh size for simulation times ten times larger than predicted by the a-priori estimates. This is due to the fact that the nonlinearity is isolated on a set of small area related to the crack set. Away from the crack set the evolution is linearly elastic and characterized by the shear wave speed of Plexiglass. This observation motivates future work that will address a-posteriori error estimation and mesh adaptivity.

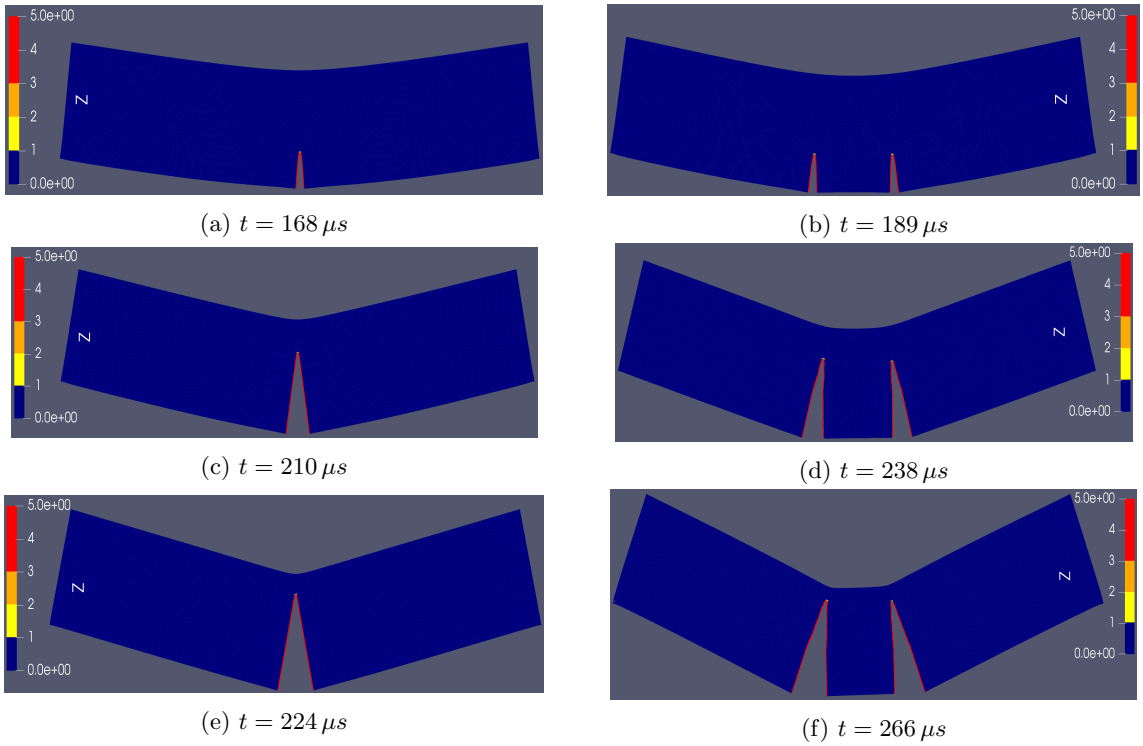

(a) $t = 168\,\mu s$ (b) $t = 189\,\mu s$

(c) $t = 210\,\mu s$ (d) $t = 238\,\mu s$

(e) $t = 224\,\mu s$ (f) $t = 266\,\mu s$

Figure 9: Damage profile under bending load. Plots on left are for single crack and plots on right are for double crack.

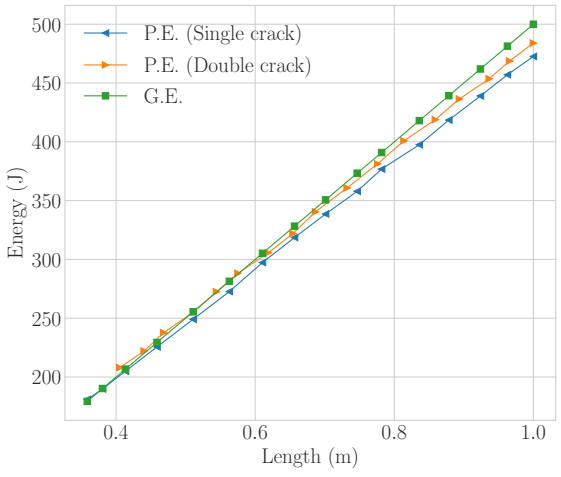

Figure 10: Crack length vs peridynamic fracture energy (P.E.) and Griffith's fracture energy (G.E.). Here crack length and fracture energy of single crack and double crack are normalized by crack length $L = 0.0386\,m$ at time $t = 220.5\,\mu s$ and crack length $L = 0.0706\,m$ at time $t = 245\,\mu s$ respectively.

References

Agwai, A., Guven, I., Madenci, E., 2011. Predicting crack propagation with peridynamics: a comparative study. International journal of fracture 171 (1), 65–78.

Aksoylu, B., Mengesha, T., 2010. Results on nonlocal boundary value problems. Numerical functional analysis and optimization 31 (12), 1301–1317.

Aksoylu, B., Parks, M. L., 2011. Variational theory and domain decomposition for nonlocal problems. Applied Mathematics and Computation 217 (14), 6498–6515.

Aksoylu, B., Unlu, Z., 2014. Conditioning analysis of nonlocal integral operators in fractional sobolev spaces. SIAM Journal on Numerical Analysis 52, 653–677.

Bobaru, F., Hu, W., 2012. The meaning, selection, and use of the peridynamic horizon and its relation to crack branching in brittle materials. International journal of fracture 176 (2), 215–222.

Bobaru, F., Yang, M., Alves, L. F., Silling, S. A., Askari, E., Xu, J., 2009. Convergence, adaptive refinement, and scaling in 1d peridynamics. International Journal for Numerical Methods in Engineering 77 (6), 852–877.

Chen, X., Gunzburger, M., 2011. Continuous and discontinuous finite element methods for a peridynamics model of mechanics. Computer Methods in Applied Mechanics and Engineering 200 (9), 1237–1250.

Driver, B. K., June 2003. Analysis tools with applications. Lecture Notes.
URL http://math.ucsd.edu/~driver/240-01-02/Lecture_Notes/anal.pdf

Du, Q., Gunzburger, M., Lehoucq, R. B., Zhou, K., 2012. Analysis and approximation of nonlocal diffusion problems with volume constraints. SIAM review 54 (4), 667–696.

D'Elia, M., Gunzburger, M., 2013. The fractional laplacian operator on bounded domains as a special case of the nonlocal diffusion operator. Computers & Mathematics with Applications 66 (7), 1245–1260.

Emmrich, E., Lehoucq, R. B., Puhst, D., 2013. Peridynamics: a nonlocal continuum theory. In: Meshfree Methods for Partial Differential Equations VI. Springer, pp. 45–65.

Bobaru, F., Foster, J. T., Geubelle, P. H., Silling, S. A., 2016. Handbook of peridynamic modeling. CRC press.

Foster, J. T., Silling, S. A., Chen, W., 2011. An energy based failure criterion for use with peridynamic states. International Journal for Multiscale Computational Engineering 9 (6).

Ghajari, M., Iannucci, L., Curtis, P., 2014. A peridynamic material model for the analysis of dynamic crack propagation in orthotropic media. Computer Methods in Applied Mechanics and Engineering 276, 431–452.

Ha, Y. D., Bobaru, F., 2010. Studies of dynamic crack propagation and crack branching with peridynamics. International Journal of Fracture 162 (1-2), 229–244.

Jha, P. K., Lipton, R., October 2017. Finite element approximation of nonlinear nonlocal models. arXiv preprint arXiv:1710.07661.

Jha, P. K., Lipton, R., 2018a. Numerical analysis of nonlocal fracture models in Hölder space. SIAM Journal on Numerical Analysis 56 (2), 906–941.
URL https://doi.org/10.1137/17M1112236

Jha, P. K., Lipton, R., 2018b. Numerical convergence of nonlinear nonlocal continuum models to local elastodynamics. International Journal for Numerical Methods in Engineering 114 (13), 1389–1410.
URL https://onlinelibrary.wiley.com/doi/abs/10.1002/nme.5791

Lindsay, P., Parks, M., Prakash, A., 2016. Enabling fast, stable and accurate peridynamic computations using multi-time-step integration. Computer Methods in Applied Mechanics and Engineering 306, 382–405.

Lipton, R., 2014. Dynamic brittle fracture as a small horizon limit of peridynamics. Journal of Elasticity 117 (1), 21–50.

Lipton, R., 2016. Cohesive dynamics and brittle fracture. Journal of Elasticity 124 (2), 143–191.

Lipton, R., Said, E., Jha, P. K., 2018. Dynamic brittle fracture from nonlocal double-well potentials: A state-based model. Handbook of Nonlocal Continuum Mechanics for Materials and Structures, 1–27.
URL https://doi.org/10.1007/978-3-319-22977-5_33-1

Lipton, R., Silling, S., Lehoucq, R., 2016. Complex fracture nucleation and evolution with nonlocal elastodynamics. arXiv preprint arXiv:1602.00247.

Mengesha, T., Du, Q., 2013. Analysis of a scalar peridynamic model with a sign changing kernel. Discrete Contin. Dynam. Systems B 18, 1415–1437.

Mengesha, T., Du, Q., 2015. On the variational limit of a class of nonlocal functionals related to peridynamics. Nonlinearity 28 (11), 3999.

Nochetto, R. H., Otárola, E., Salgado, A. J., 2015. A pde approach to fractional diffusion in general domains: a priori error analysis. Foundations of Computational Mathematics 15 (3), 733–791.

Silling, S., Weckner, O., Askari, E., Bobaru, F., 2010. Crack nucleation in a peridynamic solid. International Journal of Fracture 162 (1-2), 219–227.

Silling, S. A., 2000. Reformulation of elasticity theory for discontinuities and long-range forces. Journal of the Mechanics and Physics of Solids 48 (1), 175–209.

Silling, S. A., Askari, E., 2005. A meshfree method based on the peridynamic model of solid mechanics. Computers & structures 83 (17), 1526–1535.

Silling, S. A., Bobaru, F., 2005. Peridynamic modeling of membranes and fibers. International Journal of Non-Linear Mechanics 40 (2), 395–409.

Silling, S. A., Epton, M., Weckner, O., Xu, J., Askari, E., 2007. Peridynamic states and constitutive modeling. Journal of Elasticity 88 (2), 151–184.

Silling, S. A., Lehoucq, R. B., 2008. Convergence of peridynamics to classical elasticity theory. Journal of Elasticity 93 (1), 13–37.
Tian, X., Du, Q., 2013. Analysis and comparison of different approximations to nonlocal diffusion and linear peridynamic equations. SIAM Journal on Numerical Analysis 51 (6), 3458–3482.
Weckner, O., Emmrich, E., 2005. Numerical simulation of the dynamics of a nonlocal, inhomogeneous, infinite bar. J. Comput. Appl. Mech 6 (2), 311–319.

Appendix A Proof of Lipschitz continuity for the non-local force

In this section, we prove Proposition 1 and Proposition 2.

A.1 Proof of Proposition 1

Recall that $I = [0, T]$ is the time domain, $X = C_0^{0,\gamma}(D;\mathbb{R}^d)\times C_0^{0,\gamma}(D;\mathbb{R}^d)$, and $F^\epsilon(y,t) = (F_1^\epsilon(y,t), F_2^\epsilon(y,t))^T$, where $F_1^\epsilon(y,t) = y^2$ and $F_2^\epsilon(y,t) = \mathcal{L}^\epsilon(y^1) + \boldsymbol{b}(t)$. Given $t \in I$ and $y = (y^1, y^2)^T, z = (z^1, z^2)^T \in X$, we have

$$\begin{aligned}&\|F^\epsilon(y,t) - F^\epsilon(z,t)\|_X\\ &= \left\|y^2 - z^2\right\|_{C^{0,\gamma}(D;\mathbb{R}^d)} + \left\|\mathcal{L}^\epsilon(y^1) - \mathcal{L}^\epsilon(z^1)\right\|_{C^{0,\gamma}(D;\mathbb{R}^d)}\end{aligned} \tag{107}$$

and

$$\|F^\epsilon(y,t)\|_X = \left\|y^2\right\|_{C^{0,\gamma}(D;\mathbb{R}^d)} + \left\|\mathcal{L}^\epsilon(y^1)\right\|_{C^{0,\gamma}(D;\mathbb{R}^d)} + b, \tag{108}$$

where $b = \sup_t ||\boldsymbol{b}(t)||_{C^{0,\gamma}}$.

Thus, to prove Equation 21 and Equation 22 of Proposition 1 we need to study the terms associated with $\mathcal{L}^\epsilon$ in the equations listed above. The peridynamic force $\mathcal{L}^\epsilon$ is sum of two forces, the tensile force $\mathcal{L}_T^\epsilon$ and the dilatational force $\mathcal{L}_D^\epsilon$. So for $\boldsymbol{u}, \boldsymbol{v} \in C_0^{0,\gamma}(D;\mathbb{R}^d)$ we have

$$\begin{aligned}&\|\mathcal{L}^\epsilon(\boldsymbol{u}) - \mathcal{L}^\epsilon(\boldsymbol{v})\|_{C^{0,\gamma}(D;\mathbb{R}^d)}\\ &\le \|\mathcal{L}_T^\epsilon(\boldsymbol{u}) - \mathcal{L}_T^\epsilon(\boldsymbol{v})\|_{C^{0,\gamma}(D;\mathbb{R}^d)} + \|\mathcal{L}_D^\epsilon(\boldsymbol{u}) - \mathcal{L}_D^\epsilon(\boldsymbol{v})\|_{C^{0,\gamma}(D;\mathbb{R}^d)}\end{aligned} \tag{109}$$

and

$$\|\mathcal{L}^\epsilon(\boldsymbol{u})\|_{C^{0,\gamma}(D;\mathbb{R}^d)} \le \|\mathcal{L}_T^\epsilon(\boldsymbol{u})\|_{C^{0,\gamma}(D;\mathbb{R}^d)} + \|\mathcal{L}_D^\epsilon(\boldsymbol{u})\|_{C^{0,\gamma}(D;\mathbb{R}^d)}. \tag{110}$$

We conclude listing estimates that will be used in the sequel. For $\boldsymbol{u} \in C_0^{0,\gamma}(D;\mathbb{R}^d)$ and $\omega \in C_0^{0,\gamma}(D;[0,1])$ one easily deduces the estimates

$$\begin{aligned}|\boldsymbol{u}(\boldsymbol{x}+\epsilon\boldsymbol{\xi}) - \boldsymbol{u}(\boldsymbol{x})| &\le (\epsilon|\boldsymbol{\xi}|)^\gamma ||\boldsymbol{u}||_{C^{0,\gamma}},\\ |\boldsymbol{u}(\boldsymbol{x}+\epsilon\boldsymbol{\xi}) - \boldsymbol{u}(\boldsymbol{y}+\epsilon\boldsymbol{\xi})| &\le |\boldsymbol{x}-\boldsymbol{y}|^\gamma ||\boldsymbol{u}||_{C^{0,\gamma}},\\ |\omega(\boldsymbol{x}+\epsilon\boldsymbol{\xi}) - \omega(\boldsymbol{y}+\epsilon\boldsymbol{\xi})| &\le |\boldsymbol{x}-\boldsymbol{y}|^\gamma ||\omega||_{C^{0,\gamma}},\end{aligned} \tag{111}$$

for $\boldsymbol{x}, \boldsymbol{y} \in D$ and $\boldsymbol{\xi} \in H_1(\boldsymbol{0})$. Since $\boldsymbol{u}$ and ω are extended by zero outside D these estimates also hold for all points outside D.

A.1.1 Lipschitz continuity in Hölder space

In this subsection, we provide upper bounds on Equation 109.

We employ the notations used in Section 4.2.4. Recall that, for $\boldsymbol{\xi} \in H_1(\boldsymbol{0})$, we define

$$\begin{aligned}s_{\boldsymbol{\xi}} &:= \epsilon|\boldsymbol{\xi}|,\ \boldsymbol{e}_{\boldsymbol{\xi}} := \frac{\boldsymbol{\xi}}{|\boldsymbol{\xi}|},\\ \omega_{\boldsymbol{\xi}}(\boldsymbol{x}) &:= \omega(\boldsymbol{x}+\epsilon\boldsymbol{\xi})\omega(\boldsymbol{x}),\\ \bar{\boldsymbol{u}}_{\boldsymbol{\xi}}(\boldsymbol{x}) &:= \boldsymbol{u}(\boldsymbol{x}+\epsilon\boldsymbol{\xi}) - \boldsymbol{u}(\boldsymbol{x})\end{aligned} \tag{112}$$

and

$$\bar{J}_\alpha := \frac{1}{\omega_d}\int_{H_1(\mathbf{0})} J(|\boldsymbol{\xi}|)|\boldsymbol{\xi}|^{-\alpha} d\boldsymbol{\xi}, \qquad \text{for } \alpha \in \mathbb{R}. \tag{113}$$

Hydrostatic strain simplifies to

$$\theta(\boldsymbol{x};\boldsymbol{u}) = \frac{1}{\omega_d}\int_{H_1(\mathbf{0})} \omega(\boldsymbol{x}+\epsilon\boldsymbol{\xi}) J(|\boldsymbol{\xi}|)\bar{\boldsymbol{u}}_{\boldsymbol{\xi}}(\boldsymbol{x})\cdot \boldsymbol{e}_{\boldsymbol{\xi}} d\boldsymbol{\xi}. \tag{114}$$

Peridynamic force $\mathcal{L}_T^\epsilon(\boldsymbol{u})$ and $\mathcal{L}_D^\epsilon(\boldsymbol{u})$ can be written as

$$\mathcal{L}_T^\epsilon(\boldsymbol{u})(\boldsymbol{x}) = \frac{2}{\epsilon\omega_d}\int_{H_1(\mathbf{0})} \omega_{\boldsymbol{\xi}}(\boldsymbol{x})\frac{J(|\boldsymbol{\xi}|)}{\sqrt{s_{\boldsymbol{\xi}}}} f'(\bar{\boldsymbol{u}}_{\boldsymbol{\xi}}(\boldsymbol{x})\cdot \boldsymbol{e}_{\boldsymbol{\xi}}/\sqrt{s_{\boldsymbol{\xi}}})\boldsymbol{e}_{\boldsymbol{\xi}} d\boldsymbol{\xi}, \tag{115}$$

$$\mathcal{L}_D^\epsilon(\boldsymbol{u})(\boldsymbol{x}) = \frac{1}{\epsilon^2\omega_d}\int_{H_1(\mathbf{0})} \omega_{\boldsymbol{\xi}}(\boldsymbol{x}) J(|\boldsymbol{\xi}|)[g'(\theta(\boldsymbol{x}+\epsilon\boldsymbol{\xi};\boldsymbol{u})) + g'(\theta(\boldsymbol{x};\boldsymbol{u}))]\boldsymbol{e}_{\boldsymbol{\xi}} d\boldsymbol{\xi}. \tag{116}$$

Non-local tensile force. For any $\boldsymbol{u},\boldsymbol{v} \in C_0^{0,\gamma}(D;\mathbb{R}^d)$, we provide upper bounds on

$$\begin{aligned}
&\|\mathcal{L}_T^\epsilon(\boldsymbol{u}) - \mathcal{L}_T^\epsilon(\boldsymbol{v})\|_{C^{0,\gamma}(D;\mathbb{R}^d)} \\
&= \sup_{\boldsymbol{x}\in D} |\mathcal{L}_T^\epsilon(\boldsymbol{u})(\boldsymbol{x}) - \mathcal{L}_T^\epsilon(\boldsymbol{v})(\boldsymbol{x})| \\
&+ \sup_{\boldsymbol{x},\boldsymbol{y}\in D,\boldsymbol{x}\neq\boldsymbol{y}} \frac{|(\mathcal{L}_T^\epsilon(\boldsymbol{u})(\boldsymbol{x}) - \mathcal{L}_T^\epsilon(\boldsymbol{v})(\boldsymbol{x})) - (\mathcal{L}_T^\epsilon(\boldsymbol{u})(\boldsymbol{y}) - \mathcal{L}_T^\epsilon(\boldsymbol{v})(\boldsymbol{y}))|}{|\boldsymbol{x}-\boldsymbol{y}|^\gamma}.
\end{aligned} \tag{117}$$

Using simplified form of $\mathcal{L}_T^\epsilon$ in Equation 115 and proceeding as in Section 4.2.4 we see that

$$\begin{aligned}
&|\mathcal{L}_T^\epsilon(\boldsymbol{u})(\boldsymbol{x}) - \mathcal{L}_T^\epsilon(\boldsymbol{v})(\boldsymbol{x})| \\
&= \left|\frac{2}{\epsilon\omega_d}\int_{H_1(\mathbf{0})} \omega_{\boldsymbol{\xi}}(\boldsymbol{x})\frac{J(|\boldsymbol{\xi}|)}{\sqrt{s_{\boldsymbol{\xi}}}}\left[f'(\bar{\boldsymbol{u}}_{\boldsymbol{\xi}}(\boldsymbol{x})\cdot\boldsymbol{e}_{\boldsymbol{\xi}}/\sqrt{s_{\boldsymbol{\xi}}}) - f'(\bar{\boldsymbol{v}}_{\boldsymbol{\xi}}(\boldsymbol{x})\cdot\boldsymbol{e}_{\boldsymbol{\xi}}/\sqrt{s_{\boldsymbol{\xi}}})\right]\boldsymbol{e}_{\boldsymbol{\xi}} d\boldsymbol{\xi}\right| \\
&\leq \frac{2}{\epsilon\omega_d}\int_{H_1(\mathbf{0})} \omega_{\boldsymbol{\xi}}(\boldsymbol{x})\frac{J(|\boldsymbol{\xi}|)}{\sqrt{s_{\boldsymbol{\xi}}}}\left|f'(\bar{\boldsymbol{u}}_{\boldsymbol{\xi}}(\boldsymbol{x})\cdot\boldsymbol{e}_{\boldsymbol{\xi}}/\sqrt{s_{\boldsymbol{\xi}}}) - f'(\bar{\boldsymbol{v}}_{\boldsymbol{\xi}}(\boldsymbol{x})\cdot\boldsymbol{e}_{\boldsymbol{\xi}}/\sqrt{s_{\boldsymbol{\xi}}})\right| d\boldsymbol{\xi} \\
&\leq \frac{2C_2^f}{\epsilon\omega_d}\int_{H_1(\mathbf{0})} \frac{J(|\boldsymbol{\xi}|)}{s_{\boldsymbol{\xi}}}\left|\bar{\boldsymbol{u}}_{\boldsymbol{\xi}}(\boldsymbol{x}) - \bar{\boldsymbol{v}}_{\boldsymbol{\xi}}(\boldsymbol{x})\right| d\boldsymbol{\xi}.
\end{aligned} \tag{118}$$

A straightforward calculation gives the estimate

$$\begin{aligned}
|\boldsymbol{u}_{\boldsymbol{\xi}}(\boldsymbol{x}) - \boldsymbol{v}_{\boldsymbol{\xi}}(\boldsymbol{x})| &= |\boldsymbol{u}(\boldsymbol{x}+\epsilon\boldsymbol{\xi}) - \boldsymbol{u}(\boldsymbol{x}) - (\boldsymbol{v}(\boldsymbol{x}+\epsilon\boldsymbol{\xi}) - \boldsymbol{v}(\boldsymbol{x}))| \\
&\leq |\boldsymbol{u}(\boldsymbol{x}+\epsilon\boldsymbol{\xi}) - \boldsymbol{v}(\boldsymbol{x}+\epsilon\boldsymbol{\xi})| + |\boldsymbol{u}(\boldsymbol{x}) - \boldsymbol{v}(\boldsymbol{x})| \leq 2||\boldsymbol{u}-\boldsymbol{v}||_{C^{0,\gamma}}
\end{aligned}$$

and on applying this to Equation 118 we get

$$|\mathcal{L}_T^\epsilon(\boldsymbol{u})(\boldsymbol{x}) - \mathcal{L}_T^\epsilon(\boldsymbol{v})(\boldsymbol{x})| \leq \frac{4C_2^f\bar{J}_1}{\epsilon^2}||\boldsymbol{u}-\boldsymbol{v}||_{C^{0,\gamma}}, \tag{119}$$

where $\bar{J}_1$ is given by Equation 113. Next we derive a bound on

$$\begin{aligned}
&\frac{|(\mathcal{L}_T^\epsilon(\boldsymbol{u})(\boldsymbol{x}) - \mathcal{L}_T^\epsilon(\boldsymbol{v})(\boldsymbol{x})) - (\mathcal{L}_T^\epsilon(\boldsymbol{u})(\boldsymbol{y}) - \mathcal{L}_T^\epsilon(\boldsymbol{v})(\boldsymbol{y}))|}{|\boldsymbol{x}-\boldsymbol{y}|^\gamma} \\
&= \frac{1}{|\boldsymbol{x}-\boldsymbol{y}|^\gamma}\left|\frac{2}{\epsilon\omega_d}\int_{H_1(\mathbf{0})}\frac{J(|\boldsymbol{\xi}|)}{\sqrt{s_{\boldsymbol{\xi}}}}\left[\omega_{\boldsymbol{\xi}}(\boldsymbol{x})(f'(\bar{\boldsymbol{u}}_{\boldsymbol{\xi}}(\boldsymbol{x})\cdot\boldsymbol{e}_{\boldsymbol{\xi}}/\sqrt{s_{\boldsymbol{\xi}}}) - f'(\bar{\boldsymbol{v}}_{\boldsymbol{\xi}}(\boldsymbol{x})\cdot\boldsymbol{e}_{\boldsymbol{\xi}}/\sqrt{s_{\boldsymbol{\xi}}}))\right.\right. \\
&\qquad \left.\left. -\omega_{\boldsymbol{\xi}}(\boldsymbol{y})(f'(\bar{\boldsymbol{u}}_{\boldsymbol{\xi}}(\boldsymbol{y})\cdot\boldsymbol{e}_{\boldsymbol{\xi}}/\sqrt{s_{\boldsymbol{\xi}}}) - f'(\bar{\boldsymbol{v}}_{\boldsymbol{\xi}}(\boldsymbol{y})\cdot\boldsymbol{e}_{\boldsymbol{\xi}}/\sqrt{s_{\boldsymbol{\xi}}}))\right]\boldsymbol{e}_{\boldsymbol{\xi}} d\boldsymbol{\xi}\right|.
\end{aligned}$$

Let

$$H := \frac{1}{|\boldsymbol{x}-\boldsymbol{y}|^\gamma}\Big|\omega_{\boldsymbol{\xi}}(\boldsymbol{x})(f'(\bar{\boldsymbol{u}}_{\boldsymbol{\xi}}(\boldsymbol{x})\cdot\boldsymbol{e}_{\boldsymbol{\xi}}/\sqrt{s_{\boldsymbol{\xi}}}) - f'(\bar{\boldsymbol{v}}_{\boldsymbol{\xi}}(\boldsymbol{x})\cdot\boldsymbol{e}_{\boldsymbol{\xi}}/\sqrt{s_{\boldsymbol{\xi}}})) - \omega_{\boldsymbol{\xi}}(\boldsymbol{y})(f'(\bar{\boldsymbol{u}}_{\boldsymbol{\xi}}(\boldsymbol{y})\cdot\boldsymbol{e}_{\boldsymbol{\xi}}/\sqrt{s_{\boldsymbol{\xi}}}) - f'(\bar{\boldsymbol{v}}_{\boldsymbol{\xi}}(\boldsymbol{y})\cdot\boldsymbol{e}_{\boldsymbol{\xi}}/\sqrt{s_{\boldsymbol{\xi}}}))\Big|. \tag{120}$$

Then

$$\frac{|(\mathcal{L}_T^\epsilon(\boldsymbol{u})(\boldsymbol{x}) - \mathcal{L}_T^\epsilon(\boldsymbol{v})(\boldsymbol{x})) - (\mathcal{L}_T^\epsilon(\boldsymbol{u})(\boldsymbol{y}) - \mathcal{L}_T^\epsilon(\boldsymbol{v})(\boldsymbol{y}))|}{|\boldsymbol{x}-\boldsymbol{y}|^\gamma} \leq \frac{2}{\epsilon\omega_d}\int_{H_1(\mathbf{0})}\frac{J(|\boldsymbol{\xi}|)}{\sqrt{s_{\boldsymbol{\xi}}}}H d\boldsymbol{\xi}. \tag{121}$$

To analyze H we consider the function $\boldsymbol{r}:[0,1]\times D\to\mathbb{R}^d$ given by

$$\boldsymbol{r}(l,\boldsymbol{x}) := \bar{\boldsymbol{v}}_{\boldsymbol{\xi}}(\boldsymbol{x}) + l(\bar{\boldsymbol{u}}_{\boldsymbol{\xi}}(\boldsymbol{x}) - \bar{\boldsymbol{v}}_{\boldsymbol{\xi}}(\boldsymbol{x})), \tag{122}$$

and $\partial\boldsymbol{r}(l,\boldsymbol{x})/\partial l = \bar{\boldsymbol{u}}_{\boldsymbol{\xi}}(\boldsymbol{x}) - \bar{\boldsymbol{v}}_{\boldsymbol{\xi}}(\boldsymbol{x})$. We write

$$\begin{aligned} &f'(\bar{\boldsymbol{u}}_{\boldsymbol{\xi}}(\boldsymbol{x})\cdot\boldsymbol{e}_{\boldsymbol{\xi}}/\sqrt{s_{\boldsymbol{\xi}}}) - f'(\bar{\boldsymbol{v}}_{\boldsymbol{\xi}}(\boldsymbol{x})\cdot\boldsymbol{e}_{\boldsymbol{\xi}}/\sqrt{s_{\boldsymbol{\xi}}}) \\ &= \int_0^1 \frac{\partial f'(\boldsymbol{r}(l,\boldsymbol{x})\cdot\boldsymbol{e}_{\boldsymbol{\xi}}/\sqrt{s_{\boldsymbol{\xi}}})}{\partial l}dl \\ &= \int_0^1 \frac{\partial f'(\boldsymbol{r}\cdot\boldsymbol{e}_{\boldsymbol{\xi}}/\sqrt{s_{\boldsymbol{\xi}}})}{\partial \boldsymbol{r}}\Big|_{\boldsymbol{r}=\boldsymbol{r}(l,\boldsymbol{x})}\cdot\frac{\partial\boldsymbol{r}(l,\boldsymbol{x})}{\partial l}dl \\ &= \int_0^1 f''(\boldsymbol{r}(l,\boldsymbol{x})\cdot\boldsymbol{e}_{\boldsymbol{\xi}}/\sqrt{s_{\boldsymbol{\xi}}})\frac{\boldsymbol{e}_{\boldsymbol{\xi}}}{\sqrt{s_{\boldsymbol{\xi}}}}\cdot(\bar{\boldsymbol{u}}_{\boldsymbol{\xi}}(\boldsymbol{x}) - \bar{\boldsymbol{v}}_{\boldsymbol{\xi}}(\boldsymbol{x}))dl. \end{aligned} \tag{123}$$

and similarly we have

$$\begin{aligned} &f'(\bar{\boldsymbol{u}}_{\boldsymbol{\xi}}(\boldsymbol{y})\cdot\boldsymbol{e}_{\boldsymbol{\xi}}/\sqrt{s_{\boldsymbol{\xi}}}) - f'(\bar{\boldsymbol{v}}_{\boldsymbol{\xi}}(\boldsymbol{y})\cdot\boldsymbol{e}_{\boldsymbol{\xi}}/\sqrt{s_{\boldsymbol{\xi}}}) \\ &= \int_0^1 f''(\boldsymbol{r}(l,\boldsymbol{y})\cdot\boldsymbol{e}_{\boldsymbol{\xi}}/\sqrt{s_{\boldsymbol{\xi}}})\frac{\boldsymbol{e}_{\boldsymbol{\xi}}}{\sqrt{s_{\boldsymbol{\xi}}}}\cdot(\bar{\boldsymbol{u}}_{\boldsymbol{\xi}}(\boldsymbol{y}) - \bar{\boldsymbol{v}}_{\boldsymbol{\xi}}(\boldsymbol{y}))dl. \end{aligned} \tag{124}$$

Substituting Equation 123 and Equation 124 into Equation 120 gives

$$\begin{aligned} H &= \frac{1}{|\boldsymbol{x}-\boldsymbol{y}|^\gamma}\Big|\int_0^1 \big[\omega_{\boldsymbol{\xi}}(\boldsymbol{x})f''(\boldsymbol{r}(l,\boldsymbol{x})\cdot\boldsymbol{e}_{\boldsymbol{\xi}}/\sqrt{s_{\boldsymbol{\xi}}})(\bar{\boldsymbol{u}}_{\boldsymbol{\xi}}(\boldsymbol{x}) - \bar{\boldsymbol{v}}_{\boldsymbol{\xi}}(\boldsymbol{x})) \\ &\quad -\omega_{\boldsymbol{\xi}}(\boldsymbol{y})f''(\boldsymbol{r}(l,\boldsymbol{y})\cdot\boldsymbol{e}_{\boldsymbol{\xi}}/\sqrt{s_{\boldsymbol{\xi}}})(\bar{\boldsymbol{u}}_{\boldsymbol{\xi}}(\boldsymbol{y}) - \bar{\boldsymbol{v}}_{\boldsymbol{\xi}}(\boldsymbol{y}))\big]\cdot\frac{\boldsymbol{e}_{\boldsymbol{\xi}}}{\sqrt{s_{\boldsymbol{\xi}}}}d\boldsymbol{\xi}\Big|. \\ &\leq \frac{1}{|\boldsymbol{x}-\boldsymbol{y}|^\gamma}\frac{1}{\sqrt{s_{\boldsymbol{\xi}}}}\int_0^1 \Big|\omega_{\boldsymbol{\xi}}(\boldsymbol{x})f''(\boldsymbol{r}(l,\boldsymbol{x})\cdot\boldsymbol{e}_{\boldsymbol{\xi}}/\sqrt{s_{\boldsymbol{\xi}}})(\bar{\boldsymbol{u}}_{\boldsymbol{\xi}}(\boldsymbol{x}) - \bar{\boldsymbol{v}}_{\boldsymbol{\xi}}(\boldsymbol{x})) \\ &\quad - \omega_{\boldsymbol{\xi}}(\boldsymbol{y})f''(\boldsymbol{r}(l,\boldsymbol{y})\cdot\boldsymbol{e}_{\boldsymbol{\xi}}/\sqrt{s_{\boldsymbol{\xi}}})(\bar{\boldsymbol{u}}_{\boldsymbol{\xi}}(\boldsymbol{y}) - \bar{\boldsymbol{v}}_{\boldsymbol{\xi}}(\boldsymbol{y}))\Big|d\boldsymbol{\xi}. \end{aligned}$$

We now add and subtract $\omega_{\boldsymbol{\xi}}(\boldsymbol{x})f''(\boldsymbol{r}(l,\boldsymbol{x})\cdot\boldsymbol{e}_{\boldsymbol{\xi}}/\sqrt{s_{\boldsymbol{\xi}}})(\bar{\boldsymbol{u}}_{\boldsymbol{\xi}}(\boldsymbol{y}) - \bar{\boldsymbol{v}}_{\boldsymbol{\xi}}(\boldsymbol{y}))$, and note $0\leq\omega_{\boldsymbol{\xi}}\leq 1$, to get

$$\begin{aligned} H &\leq \frac{1}{|\boldsymbol{x}-\boldsymbol{y}|^\gamma}\frac{1}{\sqrt{s_{\boldsymbol{\xi}}}}\int_0^1 |f''(\boldsymbol{r}(l,\boldsymbol{x})\cdot\boldsymbol{e}_{\boldsymbol{\xi}}/\sqrt{s_{\boldsymbol{\xi}}})||\bar{\boldsymbol{u}}_{\boldsymbol{\xi}}(\boldsymbol{x}) - \bar{\boldsymbol{v}}_{\boldsymbol{\xi}}(\boldsymbol{x}) - \bar{\boldsymbol{u}}_{\boldsymbol{\xi}}(\boldsymbol{y}) + \bar{\boldsymbol{v}}_{\boldsymbol{\xi}}(\boldsymbol{y})|dl \\ &\quad + \frac{1}{|\boldsymbol{x}-\boldsymbol{y}|^\gamma}\frac{1}{\sqrt{s_{\boldsymbol{\xi}}}}\int_0^1 |\omega_{\boldsymbol{\xi}}(\boldsymbol{x})f''(\boldsymbol{r}(l,\boldsymbol{x})\cdot\boldsymbol{e}_{\boldsymbol{\xi}}/\sqrt{s_{\boldsymbol{\xi}}}) - \omega_{\boldsymbol{\xi}}(\boldsymbol{y})f''(\boldsymbol{r}(l,\boldsymbol{y})\cdot\boldsymbol{e}_{\boldsymbol{\xi}}/\sqrt{s_{\boldsymbol{\xi}}})| \\ &\qquad |\bar{\boldsymbol{u}}_{\boldsymbol{\xi}}(\boldsymbol{y}) - \bar{\boldsymbol{v}}_{\boldsymbol{\xi}}(\boldsymbol{y})|dl \\ &=: H_1 + H_2, \end{aligned} \tag{125}$$

where we denoted first and second term on right hand side as H_1 and H_2. Using the estimate

$$\frac{|\bar{\boldsymbol{u}}_{\boldsymbol{\xi}}(\boldsymbol{x}) - \bar{\boldsymbol{v}}_{\boldsymbol{\xi}}(\boldsymbol{x}) - \bar{\boldsymbol{u}}_{\boldsymbol{\xi}}(\boldsymbol{y}) + \bar{\boldsymbol{v}}_{\boldsymbol{\xi}}(\boldsymbol{y})|}{|\boldsymbol{x}-\boldsymbol{y}|^{\gamma}} \leq 2||\boldsymbol{u}-\boldsymbol{v}||_{C^{0,\gamma}}.$$

and $|f''(r)| \leq C_2^f$ we see that

$$\begin{aligned} H_1 &\leq \frac{C_2^f}{|\boldsymbol{x}-\boldsymbol{y}|^{\gamma}\sqrt{s_{\boldsymbol{\xi}}}} \int_0^1 |\bar{\boldsymbol{u}}_{\boldsymbol{\xi}}(\boldsymbol{x}) - \bar{\boldsymbol{v}}_{\boldsymbol{\xi}}(\boldsymbol{x}) - \bar{\boldsymbol{u}}_{\boldsymbol{\xi}}(\boldsymbol{y}) + \bar{\boldsymbol{v}}_{\boldsymbol{\xi}}(\boldsymbol{y})| dl \\ &= \frac{C_2^f}{|\boldsymbol{x}-\boldsymbol{y}|^{\gamma}\sqrt{s_{\boldsymbol{\xi}}}} |\bar{\boldsymbol{u}}_{\boldsymbol{\xi}}(\boldsymbol{x}) - \bar{\boldsymbol{v}}_{\boldsymbol{\xi}}(\boldsymbol{x}) - \bar{\boldsymbol{u}}_{\boldsymbol{\xi}}(\boldsymbol{y}) + \bar{\boldsymbol{v}}_{\boldsymbol{\xi}}(\boldsymbol{y})| \\ &\leq \frac{2C_2^f}{\sqrt{s_{\boldsymbol{\xi}}}} ||\boldsymbol{u}-\boldsymbol{v}||_{C^{0,\gamma}}. \end{aligned} \tag{126}$$

To bound H_2, we add and subtract $\omega_{\boldsymbol{\xi}}(\boldsymbol{x}) f''(\boldsymbol{r}(l,\boldsymbol{y})\cdot \boldsymbol{e}_{\boldsymbol{\xi}}/\sqrt{s_{\boldsymbol{\xi}}})$ and further split the terms

$$\begin{aligned} H_2 &\leq \int_0^1 \frac{|f''(\boldsymbol{r}(l,\boldsymbol{x})\cdot \boldsymbol{e}_{\boldsymbol{\xi}}/\sqrt{s_{\boldsymbol{\xi}}}) - f''(\boldsymbol{r}(l,\boldsymbol{y})\cdot \boldsymbol{e}_{\boldsymbol{\xi}}/\sqrt{s_{\boldsymbol{\xi}}})|}{|\boldsymbol{x}-\boldsymbol{y}|^{\gamma}\sqrt{s_{\boldsymbol{\xi}}}} |\bar{\boldsymbol{u}}_{\boldsymbol{\xi}}(\boldsymbol{y}) - \bar{\boldsymbol{v}}_{\boldsymbol{\xi}}(\boldsymbol{y})| dl \\ &+ \int_0^1 \frac{|\omega_{\boldsymbol{\xi}}(\boldsymbol{x}) - \omega_{\boldsymbol{\xi}}(\boldsymbol{y})|}{|\boldsymbol{x}-\boldsymbol{y}|^{\gamma}\sqrt{s_{\boldsymbol{\xi}}}} |f''(\boldsymbol{r}(l,\boldsymbol{y})\cdot \boldsymbol{e}_{\boldsymbol{\xi}}/\sqrt{s_{\boldsymbol{\xi}}})||\bar{\boldsymbol{u}}_{\boldsymbol{\xi}}(\boldsymbol{y}) - \bar{\boldsymbol{v}}_{\boldsymbol{\xi}}(\boldsymbol{y})| dl \\ &=: H_3 + H_4, \end{aligned} \tag{127}$$

where we used the fact that $0 \leq \omega_{\boldsymbol{\xi}} \leq 1$ in first term.

We consider H_3 first. With $|f'''(r)| \leq C_3^f$ and $0 \leq l, 1-l \leq 1$ for $l \in [0,1]$, we have

$$\begin{aligned} &\frac{|f''(\boldsymbol{r}(l,\boldsymbol{x})\cdot \boldsymbol{e}_{\boldsymbol{\xi}}/\sqrt{s_{\boldsymbol{\xi}}}) - f''(\boldsymbol{r}(l,\boldsymbol{y})\cdot \boldsymbol{e}_{\boldsymbol{\xi}}/\sqrt{s_{\boldsymbol{\xi}}})|}{|\boldsymbol{x}-\boldsymbol{y}|^{\gamma}} \\ &\leq \frac{C_3^f}{\sqrt{s_{\boldsymbol{\xi}}}} \frac{|\boldsymbol{r}(l,\boldsymbol{x}) - \boldsymbol{r}(l,\boldsymbol{y})|}{|\boldsymbol{x}-\boldsymbol{y}|^{\gamma}} \\ &\leq \frac{C_3^f}{\sqrt{s_{\boldsymbol{\xi}}}} \frac{|1-l||\bar{\boldsymbol{v}}_{\boldsymbol{\xi}}(\boldsymbol{x}) - \bar{\boldsymbol{v}}_{\boldsymbol{\xi}}(\boldsymbol{y})| + |l||\bar{\boldsymbol{u}}_{\boldsymbol{\xi}}(\boldsymbol{x}) - \bar{\boldsymbol{u}}_{\boldsymbol{\xi}}(\boldsymbol{y})|}{|\boldsymbol{x}-\boldsymbol{y}|^{\gamma}} \\ &\leq \frac{C_3^f}{\sqrt{s_{\boldsymbol{\xi}}}} \left(\frac{|\bar{\boldsymbol{v}}_{\boldsymbol{\xi}}(\boldsymbol{x}) - \bar{\boldsymbol{v}}_{\boldsymbol{\xi}}(\boldsymbol{y})|}{|\boldsymbol{x}-\boldsymbol{y}|^{\gamma}} + \frac{|\bar{\boldsymbol{u}}_{\boldsymbol{\xi}}(\boldsymbol{x}) - \bar{\boldsymbol{u}}_{\boldsymbol{\xi}}(\boldsymbol{y})|}{|\boldsymbol{x}-\boldsymbol{y}|^{\gamma}} \right) \end{aligned}$$

Following estimates

$$\frac{|\bar{\boldsymbol{v}}_{\boldsymbol{\xi}}(\boldsymbol{x}) - \bar{\boldsymbol{v}}_{\boldsymbol{\xi}}(\boldsymbol{y})|}{|\boldsymbol{x}-\boldsymbol{y}|^{\gamma}} \leq 2||\boldsymbol{v}||_{C^{0,\gamma}}, \quad \frac{|\bar{\boldsymbol{u}}_{\boldsymbol{\xi}}(\boldsymbol{x}) - \bar{\boldsymbol{u}}_{\boldsymbol{\xi}}(\boldsymbol{y})|}{|\boldsymbol{x}-\boldsymbol{y}|^{\gamma}} \leq 2||\boldsymbol{u}||_{C^{0,\gamma}}$$

delivers

$$\frac{|f''(\boldsymbol{r}(l,\boldsymbol{x})\cdot \boldsymbol{e}_{\boldsymbol{\xi}}/\sqrt{s_{\boldsymbol{\xi}}}) - f''(\boldsymbol{r}(l,\boldsymbol{y})\cdot \boldsymbol{e}_{\boldsymbol{\xi}}/\sqrt{s_{\boldsymbol{\xi}}})|}{|\boldsymbol{x}-\boldsymbol{y}|^{\gamma}} \leq \frac{2C_3^f}{\sqrt{s_{\boldsymbol{\xi}}}} (||\boldsymbol{u}||_{C^{0,\gamma}} + ||\boldsymbol{v}||_{C^{0,\gamma}}). \tag{128}$$

We use the inequality above together with the estimate

$$|\bar{\boldsymbol{u}}_{\boldsymbol{\xi}}(\boldsymbol{y}) - \bar{\boldsymbol{v}}_{\boldsymbol{\xi}}(\boldsymbol{y})| \leq 2s_{\boldsymbol{\xi}}^{\gamma} ||\boldsymbol{u}-\boldsymbol{v}||_{C^{0,\gamma}}$$

to get

$$H_3 \leq \frac{4C_3^f}{s_{\boldsymbol{\xi}}^{1-\gamma}} (||\boldsymbol{u}||_{C^{0,\gamma}} + ||\boldsymbol{v}||_{C^{0,\gamma}}) ||\boldsymbol{u}-\boldsymbol{v}||_{C^{0,\gamma}}. \tag{129}$$

We now consider H_4 in Equation 127. Using $|f''(r)| \leq C_2^f$, $|\bar{\boldsymbol{u}}_{\boldsymbol{\xi}}(\boldsymbol{y}) - \bar{\boldsymbol{v}}_{\boldsymbol{\xi}}(\boldsymbol{y})| \leq 2||\boldsymbol{u}-\boldsymbol{v}||_{C^{0,\gamma}}$, and the following estimate

$$\begin{aligned}\frac{|\omega_{\boldsymbol{\xi}}(\boldsymbol{x}) - \omega_{\boldsymbol{\xi}}(\boldsymbol{y})|}{|\boldsymbol{x}-\boldsymbol{y}|^\gamma} &= \frac{|\omega(\boldsymbol{x}+\epsilon\boldsymbol{\xi})\omega(\boldsymbol{x}) - \omega(\boldsymbol{y}+\epsilon\boldsymbol{\xi})\omega(\boldsymbol{y})|}{|\boldsymbol{x}-\boldsymbol{y}|^\gamma} \\ &\leq \frac{|\omega(\boldsymbol{x}+\epsilon\boldsymbol{\xi})||\omega(\boldsymbol{x}) - \omega(\boldsymbol{y})|}{|\boldsymbol{x}-\boldsymbol{y}|^\gamma} + \frac{|\omega(\boldsymbol{y})||\omega(\boldsymbol{x}+\epsilon\boldsymbol{y}) - \omega(\boldsymbol{y}+\epsilon\boldsymbol{\xi})|}{|\boldsymbol{x}-\boldsymbol{y}|^\gamma} \\ &\leq 2||\omega||_{C^{0,\gamma}}, \end{aligned} \tag{130}$$

we have

$$H_4 \leq \frac{4C_2^f||\omega||_{C^{0,\gamma}}}{\sqrt{s_{\boldsymbol{\xi}}}}||\boldsymbol{u}-\boldsymbol{v}||_{C^{0,\gamma}}. \tag{131}$$

Applying the inequalities Equation 129 and Equation 131 to Equation 127 gives

$$H_2 \leq \left[\frac{4C_3^f}{s_{\boldsymbol{\xi}}^{1-\gamma}}(||\boldsymbol{u}||_{C^{0,\gamma}} + ||\boldsymbol{v}||_{C^{0,\gamma}}) + \frac{4C_2^f||\omega||_{C^{0,\gamma}}}{\sqrt{s_{\boldsymbol{\xi}}}}\right]||\boldsymbol{u}-\boldsymbol{v}||_{C^{0,\gamma}}. \tag{132}$$

Applying the upper bounds on H_1 and H_2 shows that

$$H \leq \left[\frac{4C_3^f}{s_{\boldsymbol{\xi}}^{1-\gamma}}(||\boldsymbol{u}||_{C^{0,\gamma}} + ||\boldsymbol{v}||_{C^{0,\gamma}}) + \frac{4C_2^f(1+||\omega||_{C^{0,\gamma}})}{\sqrt{s_{\boldsymbol{\xi}}}}\right]||\boldsymbol{u}-\boldsymbol{v}||_{C^{0,\gamma}}. \tag{133}$$

We substitute the upper bound on H in Equation 121 to find that

$$\begin{aligned}&\frac{|(\mathcal{L}_T^\epsilon(\boldsymbol{u})(\boldsymbol{x}) - \mathcal{L}_T^\epsilon(\boldsymbol{v})(\boldsymbol{x})) - (\mathcal{L}_T^\epsilon(\boldsymbol{u})(\boldsymbol{y}) - \mathcal{L}_T^\epsilon(\boldsymbol{v})(\boldsymbol{y}))|}{|\boldsymbol{x}-\boldsymbol{y}|^\gamma} \\ &\leq \frac{2}{\epsilon\omega_d}\int_{H_1(\boldsymbol{0})}\frac{J(|\boldsymbol{\xi}|)}{\sqrt{s_{\boldsymbol{\xi}}}}\left[\frac{4C_3^f}{s_{\boldsymbol{\xi}}^{1-\gamma}}(||\boldsymbol{u}||_{C^{0,\gamma}} + ||\boldsymbol{v}||_{C^{0,\gamma}})\right. \\ &\quad \left.+\frac{4C_2^f(1+||\omega||_{C^{0,\gamma}})}{\sqrt{s_{\boldsymbol{\xi}}}}\right]||\boldsymbol{u}-\boldsymbol{v}||_{C^{0,\gamma}}d\boldsymbol{\xi} \\ &= \left[\frac{8C_3^f\bar{J}_{3/2-\gamma}}{\epsilon^{5/2-\gamma}}(||\boldsymbol{u}||_{C^{0,\gamma}} + ||\boldsymbol{v}||_{C^{0,\gamma}}) + \frac{8C_2^f(1+||\omega||_{C^{0,\gamma}})\bar{J}_1}{\epsilon^2}\right]||\boldsymbol{u}-\boldsymbol{v}||_{C^{0,\gamma}}, \end{aligned} \tag{134}$$

where $\bar{J}_\alpha$ is defined in Equation 113. Application of Equation 119 and Equation 134 deliver

$$\begin{aligned}&\|\mathcal{L}_T^\epsilon(\boldsymbol{u}) - \mathcal{L}_T^\epsilon(\boldsymbol{v})\|_{C^{0,\gamma}} \\ &\leq \left[\frac{8C_3^f\bar{J}_{3/2-\gamma}}{\epsilon^{5/2-\gamma}}(||\boldsymbol{u}||_{C^{0,\gamma}} + ||\boldsymbol{v}||_{C^{0,\gamma}}) + \frac{8C_2^f(2+||\omega||_{C^{0,\gamma}})\bar{J}_1}{\epsilon^2}\right]||\boldsymbol{u}-\boldsymbol{v}||_{C^{0,\gamma}}, \end{aligned} \tag{135}$$

and we have established the Lipschitz continuity of the non-local force due to tensile strain.

Non-local hydrostatic force. Now we establish the Lipschitz continuity for the non-local dilatational force. For any $\boldsymbol{u}, \boldsymbol{v} \in C_0^{0,\gamma}(D;\mathbb{R}^d)$ we write

$$\begin{aligned}&\|\mathcal{L}_D^\epsilon(\boldsymbol{u}) - \mathcal{L}_D^\epsilon(\boldsymbol{v})\|_{C^{0,\gamma}(D;\mathbb{R}^d)} \\ &= \sup_{\boldsymbol{x}\in D}|\mathcal{L}_D^\epsilon(\boldsymbol{u})(\boldsymbol{x}) - \mathcal{L}_D^\epsilon(\boldsymbol{v})(\boldsymbol{x})| \\ &+ \sup_{\boldsymbol{x},\boldsymbol{y}\in D,\boldsymbol{x}\neq\boldsymbol{y}}\frac{|(\mathcal{L}_D^\epsilon(\boldsymbol{u})(\boldsymbol{x}) - \mathcal{L}_D^\epsilon(\boldsymbol{v})(\boldsymbol{x})) - (\mathcal{L}_D^\epsilon(\boldsymbol{u})(\boldsymbol{y}) - \mathcal{L}_D^\epsilon(\boldsymbol{v})(\boldsymbol{y}))|}{|\boldsymbol{x}-\boldsymbol{y}|^\gamma}. \end{aligned} \tag{136}$$

The potential function g can either be a quadratic function, e.g., $g(r) = \beta r^2/2$ or it can be a convex-concave function, see Figure 2a. Here we present the derivation of Lipschitz continuity for the convex-concave type g. The proof for the quadratic potential functions g is identical.

Let g be a bounded convex-concave potential function with bounded derivatives expressed by Equation 10. We begin by estimating $|\theta(\boldsymbol{x};\boldsymbol{u}) - \theta(\boldsymbol{x};\boldsymbol{v})|$ where $\theta(\boldsymbol{x};\boldsymbol{u})$ is given by Equation 114. Application of the inequality $|\bar{\boldsymbol{u}}_{\boldsymbol{\xi}}(\boldsymbol{x}) - \bar{\boldsymbol{v}}_{\boldsymbol{\xi}}(\boldsymbol{x})| \leq 2||\boldsymbol{u}-\boldsymbol{v}||_{C^{0,\gamma}}$, and a straightforward calculation shows that

$$|\theta(\boldsymbol{x};\boldsymbol{u}) - \theta(\boldsymbol{x};\boldsymbol{v})| \leq 2\bar{J}_0||\boldsymbol{u}-\boldsymbol{v}||_{C^{0,\gamma}}. \tag{137}$$

We now bound $|\theta(\boldsymbol{x};\boldsymbol{u}) - \theta(\boldsymbol{y};\boldsymbol{u})|$ as follows

$$\begin{aligned}
|\theta(\boldsymbol{x};\boldsymbol{u}) - \theta(\boldsymbol{y};\boldsymbol{u})| &= \left|\frac{1}{\omega_d}\int_{H_1(\boldsymbol{0})} J(|\boldsymbol{\xi}|)\left[\omega(\boldsymbol{x}+\epsilon\boldsymbol{\xi})\bar{\boldsymbol{u}}_{\boldsymbol{\xi}}(\boldsymbol{x}) - \omega(\boldsymbol{y}+\epsilon\boldsymbol{\xi})\bar{\boldsymbol{u}}_{\boldsymbol{\xi}}(\boldsymbol{y})\right]\cdot\boldsymbol{e}_{\boldsymbol{\xi}}d\boldsymbol{\xi}\right| \\
&\leq \frac{1}{\omega_d}\int_{H_1(\boldsymbol{0})} J(|\boldsymbol{\xi}|)|\omega(\boldsymbol{x}+\epsilon\boldsymbol{\xi})\bar{\boldsymbol{u}}_{\boldsymbol{\xi}}(\boldsymbol{x}) - \omega(\boldsymbol{y}+\epsilon\boldsymbol{\xi})\bar{\boldsymbol{u}}_{\boldsymbol{\xi}}(\boldsymbol{y})|d\boldsymbol{\xi} \\
&\leq \frac{1}{\omega_d}\int_{H_1(\boldsymbol{0})} J(|\boldsymbol{\xi}|)|\omega(\boldsymbol{x}+\epsilon\boldsymbol{\xi})||\bar{\boldsymbol{u}}_{\boldsymbol{\xi}}(\boldsymbol{x}) - \bar{\boldsymbol{u}}_{\boldsymbol{\xi}}(\boldsymbol{y})|d\boldsymbol{\xi} \\
&\quad + \frac{1}{\omega_d}\int_{H_1(\boldsymbol{0})} J(|\boldsymbol{\xi}|)|\omega(\boldsymbol{x}+\epsilon\boldsymbol{\xi}) - \omega(\boldsymbol{y}+\epsilon\boldsymbol{\xi})||\bar{\boldsymbol{u}}_{\boldsymbol{\xi}}(\boldsymbol{y})|d\boldsymbol{\xi},
\end{aligned} \tag{138}$$

where we used $|\boldsymbol{e}_{\boldsymbol{\xi}}| = 1$ and Cauchy's inequality in the first equation, added and subtracted $\omega(\boldsymbol{x}+\epsilon\boldsymbol{\xi})\bar{\boldsymbol{u}}_{\boldsymbol{\xi}}(\boldsymbol{y})$ in the second equation and used the triangle inequality. Applying $|\bar{\boldsymbol{u}}_{\boldsymbol{\xi}}(\boldsymbol{x}) - \bar{\boldsymbol{u}}_{\boldsymbol{\xi}}(\boldsymbol{y})| \leq 2|\boldsymbol{x}-\boldsymbol{y}|^{\gamma}||\boldsymbol{u}||_{C^{0,\gamma}}$, $|\omega(\boldsymbol{x}+\epsilon\boldsymbol{\xi}) - \omega(\boldsymbol{y}+\epsilon\boldsymbol{\xi})| \leq |\boldsymbol{x}-\boldsymbol{y}|^{\gamma}||\omega||_{C^{0,\gamma}}$, and $|\bar{\boldsymbol{u}}_{\boldsymbol{\xi}}(\boldsymbol{y})| \leq 2||\boldsymbol{u}||_{C^{0,\gamma}}$ gives

$$\begin{aligned}
|\theta(\boldsymbol{x};\boldsymbol{u}) - \theta(\boldsymbol{y};\boldsymbol{u})| &\leq \frac{1}{\omega_d}\int_{H_1(\boldsymbol{0})} J(|\boldsymbol{\xi}|)2|\boldsymbol{x}-\boldsymbol{y}|^{\gamma}||\boldsymbol{u}||_{C^{0,\gamma}}d\boldsymbol{\xi} \\
&\quad + \frac{1}{\omega_d}\int_{H_1(\boldsymbol{0})} J(|\boldsymbol{\xi}|)|\boldsymbol{x}-\boldsymbol{y}|^{\gamma}||\omega||_{C^{0,\gamma}}2||\boldsymbol{u}||_{C^{0,\gamma}},
\end{aligned}$$

i.e.,

$$|\theta(\boldsymbol{x};\boldsymbol{u}) - \theta(\boldsymbol{y};\boldsymbol{u})| \leq 2\bar{J}_0(1+||\omega||_{C^{0,\gamma}})||\boldsymbol{u}||_{C^{0,\gamma}}|\boldsymbol{x}-\boldsymbol{y}|^{\gamma}. \tag{139}$$

We note that estimate Equation 137 and Equation 139 holds for all $\boldsymbol{x},\boldsymbol{y} \in D$ as well as for $\boldsymbol{x}$ and $\boldsymbol{y}$ in the layer of thickness 2ϵ surrounding D.

Using Equation 116 we have

$$\begin{aligned}
|\mathcal{L}_D^{\epsilon}(\boldsymbol{u})(\boldsymbol{x}) - \mathcal{L}_D^{\epsilon}(\boldsymbol{v})(\boldsymbol{x})| &= \Bigg|\frac{1}{\epsilon^2\omega_d}\int_{H_1(\boldsymbol{0})} \omega_{\boldsymbol{\xi}}(\boldsymbol{x})J(|\boldsymbol{\xi}|)[g'(\theta(\boldsymbol{x}+\epsilon\boldsymbol{\xi};\boldsymbol{u})) + g'(\theta(\boldsymbol{x};\boldsymbol{u})) \\
&\qquad - g'(\theta(\boldsymbol{x}+\epsilon\boldsymbol{\xi};\boldsymbol{v})) - g'(\theta(\boldsymbol{x};\boldsymbol{v}))]\boldsymbol{e}_{\boldsymbol{\xi}}d\boldsymbol{\xi}\Bigg| \\
&\leq \frac{1}{\epsilon^2\omega_d}\int_{H_1(\boldsymbol{0})} J(|\boldsymbol{\xi}|)\Big|g'(\theta(\boldsymbol{x}+\epsilon\boldsymbol{\xi};\boldsymbol{u})) + g'(\theta(\boldsymbol{x};\boldsymbol{u})) \\
&\qquad - g'(\theta(\boldsymbol{x}+\epsilon\boldsymbol{\xi};\boldsymbol{v})) - g'(\theta(\boldsymbol{x};\boldsymbol{v}))\Big|d\boldsymbol{\xi} \\
&\leq \frac{1}{\epsilon^2\omega_d}\int_{H_1(\boldsymbol{0})} J(|\boldsymbol{\xi}|)\left\{\Big|g'(\theta(\boldsymbol{x}+\epsilon\boldsymbol{\xi};\boldsymbol{u})) - g'(\theta(\boldsymbol{x}+\epsilon\boldsymbol{\xi};\boldsymbol{v}))\Big|\right. \\
&\qquad \left. + \Big|g'(\theta(\boldsymbol{x};\boldsymbol{u})) - g'(\theta(\boldsymbol{x};\boldsymbol{v}))\Big|\right\}d\boldsymbol{\xi}.
\end{aligned} \tag{140}$$

Since $|g'(r_1) - g'(r_2)| \leq C_2^g |r_1 - r_2|$, we have

$$\begin{aligned} |g'(\theta(\boldsymbol{x};\boldsymbol{u})) - g'(\theta(\boldsymbol{x};\boldsymbol{v}))| &\leq C_2^g |\theta(\boldsymbol{x};\boldsymbol{u}) - \theta(\boldsymbol{x};\boldsymbol{v})| \\ &\leq 2C_2^g \bar{J}_0 ||\boldsymbol{u} - \boldsymbol{v}||_{C^{0,\gamma}}, \end{aligned}$$

where we used Equation 137. Similarly we have

$$|g'(\theta(\boldsymbol{x} + \epsilon\boldsymbol{\xi};\boldsymbol{u})) - g'(\theta(\boldsymbol{x} + \epsilon\boldsymbol{\xi};\boldsymbol{v}))| \leq 2C_2^g \bar{J}_0 ||\boldsymbol{u} - \boldsymbol{v}||_{C^{0,\gamma}}.$$

and we arrive at the estimate

$$|\mathcal{L}_D^\epsilon(\boldsymbol{u})(\boldsymbol{x}) - \mathcal{L}_D^\epsilon(\boldsymbol{v})(\boldsymbol{x})| \leq \frac{4C_2^g \bar{J}_0^2}{\epsilon^2} ||\boldsymbol{u} - \boldsymbol{v}||_{C^{0,\gamma}}. \tag{141}$$

Now we estimate

$$\frac{|(\mathcal{L}_D^\epsilon(\boldsymbol{u})(\boldsymbol{x}) - \mathcal{L}_D^\epsilon(\boldsymbol{v})(\boldsymbol{x})) - (\mathcal{L}_D^\epsilon(\boldsymbol{u})(\boldsymbol{y}) - \mathcal{L}_D^\epsilon(\boldsymbol{v})(\boldsymbol{y}))|}{|\boldsymbol{x} - \boldsymbol{y}|^\gamma}.$$

We write

$$\begin{aligned} \mathcal{L}_D^\epsilon(\boldsymbol{u})(\boldsymbol{x}) - \mathcal{L}_D^\epsilon(\boldsymbol{v})(\boldsymbol{x}) = \frac{1}{\epsilon^2 \omega_d} \int_{H_1(\mathbf{0})} \omega_{\boldsymbol{\xi}}(\boldsymbol{x}) J(|\boldsymbol{\xi}|) [g'(\theta(\boldsymbol{x} + \epsilon\boldsymbol{\xi};\boldsymbol{u})) + g'(\theta(\boldsymbol{x};\boldsymbol{u})) \\ - g'(\theta(\boldsymbol{x} + \epsilon\boldsymbol{\xi};\boldsymbol{v})) - g'(\theta(\boldsymbol{x};\boldsymbol{v}))] \boldsymbol{e}_{\boldsymbol{\xi}} d\boldsymbol{\xi} \end{aligned}$$

and

$$\begin{aligned} \mathcal{L}_D^\epsilon(\boldsymbol{u})(\boldsymbol{y}) - \mathcal{L}_D^\epsilon(\boldsymbol{v})(\boldsymbol{y}) = \frac{1}{\epsilon^2 \omega_d} \int_{H_1(\mathbf{0})} \omega_{\boldsymbol{\xi}}(\boldsymbol{y}) J(|\boldsymbol{\xi}|) [g'(\theta(\boldsymbol{y} + \epsilon\boldsymbol{\xi};\boldsymbol{u})) + g'(\theta(\boldsymbol{y};\boldsymbol{u})) \\ - g'(\theta(\boldsymbol{y} + \epsilon\boldsymbol{\xi};\boldsymbol{v})) - g'(\theta(\boldsymbol{y};\boldsymbol{v}))] \boldsymbol{e}_{\boldsymbol{\xi}} d\boldsymbol{\xi}. \end{aligned}$$

to find

$$\begin{aligned} &|(\mathcal{L}_D^\epsilon(\boldsymbol{u})(\boldsymbol{x}) - \mathcal{L}_D^\epsilon(\boldsymbol{v})(\boldsymbol{x})) - (\mathcal{L}_D^\epsilon(\boldsymbol{u})(\boldsymbol{y}) - \mathcal{L}_D^\epsilon(\boldsymbol{v})(\boldsymbol{y}))| \\ &= \left| \frac{1}{\epsilon^2 \omega_d} \int_{H_1(\mathbf{0})} J(|\boldsymbol{\xi}|) \right. \\ &\Big(\omega_{\boldsymbol{\xi}}(\boldsymbol{x}) [g'(\theta(\boldsymbol{x} + \epsilon\boldsymbol{\xi};\boldsymbol{u})) + g'(\theta(\boldsymbol{x};\boldsymbol{u})) - g'(\theta(\boldsymbol{x} + \epsilon\boldsymbol{\xi};\boldsymbol{v})) - g'(\theta(\boldsymbol{x};\boldsymbol{v}))] \\ &- \omega_{\boldsymbol{\xi}}(\boldsymbol{y}) [g'(\theta(\boldsymbol{y} + \epsilon\boldsymbol{\xi};\boldsymbol{u})) + g'(\theta(\boldsymbol{y};\boldsymbol{u})) - g'(\theta(\boldsymbol{y} + \epsilon\boldsymbol{\xi};\boldsymbol{v})) - g'(\theta(\boldsymbol{y};\boldsymbol{v}))] \Big) \boldsymbol{e}_{\boldsymbol{\xi}} d\boldsymbol{\xi} \left. \right| \\ &\leq \frac{1}{\epsilon^2 \omega_d} \int_{H_1(\mathbf{0})} J(|\boldsymbol{\xi}|) \\ &\Big| \omega_{\boldsymbol{\xi}}(\boldsymbol{x}) [g'(\theta(\boldsymbol{x} + \epsilon\boldsymbol{\xi};\boldsymbol{u})) + g'(\theta(\boldsymbol{x};\boldsymbol{u})) - g'(\theta(\boldsymbol{x} + \epsilon\boldsymbol{\xi};\boldsymbol{v})) - g'(\theta(\boldsymbol{x};\boldsymbol{v}))] \\ &- \omega_{\boldsymbol{\xi}}(\boldsymbol{y}) [g'(\theta(\boldsymbol{y} + \epsilon\boldsymbol{\xi};\boldsymbol{u})) + g'(\theta(\boldsymbol{y};\boldsymbol{u})) - g'(\theta(\boldsymbol{y} + \epsilon\boldsymbol{\xi};\boldsymbol{v})) - g'(\theta(\boldsymbol{y};\boldsymbol{v}))] \Big| d\boldsymbol{\xi} \\ &= \frac{1}{\epsilon^2 \omega_d} \int_{H_1(\mathbf{0})} J(|\boldsymbol{\xi}|) \Big| \Big(\omega_{\boldsymbol{\xi}}(\boldsymbol{x}) [g'(\theta(\boldsymbol{x} + \epsilon\boldsymbol{\xi};\boldsymbol{u})) - g'(\theta(\boldsymbol{x} + \epsilon\boldsymbol{\xi};\boldsymbol{v}))] \\ &\qquad - \omega_{\boldsymbol{\xi}}(\boldsymbol{y}) [g'(\theta(\boldsymbol{y} + \epsilon\boldsymbol{\xi};\boldsymbol{u})) - g'(\theta(\boldsymbol{y} + \epsilon\boldsymbol{\xi};\boldsymbol{v}))] \Big) \\ &\qquad + \Big(\omega_{\boldsymbol{\xi}}(\boldsymbol{x}) [g'(\theta(\boldsymbol{x};\boldsymbol{u})) - g'(\theta(\boldsymbol{x};\boldsymbol{v}))] \\ &\qquad - \omega_{\boldsymbol{\xi}}(\boldsymbol{y}) [g'(\theta(\boldsymbol{y};\boldsymbol{u})) - g'(\theta(\boldsymbol{y};\boldsymbol{v}))] \Big) \Big| d\boldsymbol{\xi}, \end{aligned} \tag{142}$$

where we have rearranged the terms in last step. Application of the triangle inequality gives

$$\begin{aligned}
&|(\mathcal{L}_D^\epsilon(\boldsymbol{u})(\boldsymbol{x}) - \mathcal{L}_D^\epsilon(\boldsymbol{v})(\boldsymbol{x})) - (\mathcal{L}_D^\epsilon(\boldsymbol{u})(\boldsymbol{y}) - \mathcal{L}_D^\epsilon(\boldsymbol{v})(\boldsymbol{y}))| \\
&\leq \frac{1}{\epsilon^2\omega_d}\int_{H_1(\mathbf{0})} J(|\boldsymbol{\xi}|)\Bigg(\Big|\omega_{\boldsymbol{\xi}}(\boldsymbol{x})[g'(\theta(\boldsymbol{x}+\epsilon\boldsymbol{\xi};\boldsymbol{u})) - g'(\theta(\boldsymbol{x}+\epsilon\boldsymbol{\xi};\boldsymbol{v}))] \\
&\qquad - \omega_{\boldsymbol{\xi}}(\boldsymbol{y})[g'(\theta(\boldsymbol{y}+\epsilon\boldsymbol{\xi};\boldsymbol{u})) - g'(\theta(\boldsymbol{y}+\epsilon\boldsymbol{\xi};\boldsymbol{v}))]\Big| \\
&\qquad + \Big|\omega_{\boldsymbol{\xi}}(\boldsymbol{x})[g'(\theta(\boldsymbol{x};\boldsymbol{u})) - g'(\theta(\boldsymbol{x};\boldsymbol{v}))] \\
&\qquad - \omega_{\boldsymbol{\xi}}(\boldsymbol{y})[g'(\theta(\boldsymbol{y};\boldsymbol{u})) - g'(\theta(\boldsymbol{y};\boldsymbol{v}))]\Big|\Bigg)d\boldsymbol{\xi}. \qquad (143)
\end{aligned}$$

Now write $h_{\boldsymbol{\xi}} : \mathbb{R}^d \times \mathbb{R}^d \to \mathbb{R}^+$ given by

$$h_{\boldsymbol{\xi}}(\boldsymbol{x},\boldsymbol{y}) := \Big|\omega_{\boldsymbol{\xi}}(\boldsymbol{x})[g'(\theta(\boldsymbol{x};\boldsymbol{u})) - g'(\theta(\boldsymbol{x};\boldsymbol{v}))] - \omega_{\boldsymbol{\xi}}(\boldsymbol{y})[g'(\theta(\boldsymbol{y};\boldsymbol{u})) - g'(\theta(\boldsymbol{y};\boldsymbol{v}))]\Big|. \qquad (144)$$

and

$$\begin{aligned}
&|(\mathcal{L}_D^\epsilon(\boldsymbol{u})(\boldsymbol{x}) - \mathcal{L}_D^\epsilon(\boldsymbol{v})(\boldsymbol{x})) - (\mathcal{L}_D^\epsilon(\boldsymbol{u})(\boldsymbol{y}) - \mathcal{L}_D^\epsilon(\boldsymbol{v})(\boldsymbol{y}))| \\
&\leq \frac{1}{\epsilon^2\omega_d}\int_{H_1(\mathbf{0})} J(|\boldsymbol{\xi}|)(h_{\boldsymbol{\xi}}(\boldsymbol{x}+\epsilon\boldsymbol{\xi},\boldsymbol{y}+\epsilon\boldsymbol{\xi}) + h(\boldsymbol{x},\boldsymbol{y}))d\boldsymbol{\xi}. \qquad (145)
\end{aligned}$$

We now estimate $h_{\boldsymbol{\xi}}(\boldsymbol{x},\boldsymbol{y})$ for any $\boldsymbol{x},\boldsymbol{y}$ in D and in the layer of thickness ϵ surrounding D.

Proceeding as before we define $r : [0,1] \times D \to \mathbb{R}$ as follows

$$r(l,\boldsymbol{x}) := \theta(\boldsymbol{x};\boldsymbol{v}) + l(\theta(\boldsymbol{x};\boldsymbol{u}) - \theta(\boldsymbol{x};\boldsymbol{v})), \qquad (146)$$

so $\frac{\partial r(l,\boldsymbol{x})}{\partial l} = \theta(\boldsymbol{x};\boldsymbol{u}) - \theta(\boldsymbol{x};\boldsymbol{v})$. We also have

$$\begin{aligned}
g'(\theta(\boldsymbol{x};\boldsymbol{u})) - g'(\theta(\boldsymbol{x};\boldsymbol{v})) &= g'(r(1,\boldsymbol{x})) - g'(r(0,\boldsymbol{x})) \\
&= \int_0^1 \frac{\partial g'(r(l,\boldsymbol{x}))}{\partial l}dl \\
&= \int_0^1 g''(r(l,\boldsymbol{x}))(\theta(\boldsymbol{x};\boldsymbol{u}) - \theta(\boldsymbol{x};\boldsymbol{v}))dl. \qquad (147)
\end{aligned}$$

Similarly,

$$g'(\theta(\boldsymbol{y};\boldsymbol{u})) - g'(\theta(\boldsymbol{y};\boldsymbol{v})) = \int_0^1 g''(r(l,\boldsymbol{y}))(\theta(\boldsymbol{y};\boldsymbol{u}) - \theta(\boldsymbol{y};\boldsymbol{v}))dl. \qquad (148)$$

Substitution of Equation 147 and Equation 148 in $h_{\boldsymbol{\xi}}(\boldsymbol{x},\boldsymbol{y})$ gives

$$\begin{aligned}
h_{\boldsymbol{\xi}}(\boldsymbol{x},\boldsymbol{y}) &= \Big|\int_0^1 (\omega_{\boldsymbol{\xi}}(\boldsymbol{x})g''(r(l,\boldsymbol{x}))(\theta(\boldsymbol{x};\boldsymbol{u}) - \theta(\boldsymbol{x};\boldsymbol{v})) \\
&\qquad - \omega_{\boldsymbol{\xi}}(\boldsymbol{y})g''(r(l,\boldsymbol{y}))(\theta(\boldsymbol{y};\boldsymbol{u}) - \theta(\boldsymbol{y};\boldsymbol{v})))dl\Big| \\
&\leq \int_0^1 \Big|\omega_{\boldsymbol{\xi}}(\boldsymbol{x})g''(r(l,\boldsymbol{x}))(\theta(\boldsymbol{x};\boldsymbol{u}) - \theta(\boldsymbol{x};\boldsymbol{v})) \\
&\qquad - \omega_{\boldsymbol{\xi}}(\boldsymbol{y})g''(r(l,\boldsymbol{y}))(\theta(\boldsymbol{y};\boldsymbol{u}) - \theta(\boldsymbol{y};\boldsymbol{v}))\Big|dl.
\end{aligned}$$

Adding and subtracting $\omega_{\boldsymbol{\xi}}(\boldsymbol{x})g''(r(l,\boldsymbol{x}))(\theta(\boldsymbol{y};\boldsymbol{u})-\theta(\boldsymbol{y};\boldsymbol{v}))$ gives

$$\begin{aligned}h_{\boldsymbol{\xi}}(\boldsymbol{x},\boldsymbol{y}) &\leq \int_0^1 |\omega_{\boldsymbol{\xi}}(\boldsymbol{x})|\,|g''(r(l,\boldsymbol{x}))|\,|(\theta(\boldsymbol{x};\boldsymbol{u})-\theta(\boldsymbol{x};\boldsymbol{v}))-(\theta(\boldsymbol{y};\boldsymbol{u})-\theta(\boldsymbol{y};\boldsymbol{v}))|dl\\ &+\int_0^1 |\omega_{\boldsymbol{\xi}}(\boldsymbol{x})g''(r(l,\boldsymbol{x}))-\omega_{\boldsymbol{\xi}}(\boldsymbol{y})g''(r(l,\boldsymbol{y}))|\,|\theta(\boldsymbol{y};\boldsymbol{u})-\theta(\boldsymbol{y};\boldsymbol{v})|dl\\ &=: I_1+I_2,\end{aligned} \tag{149}$$

For I_1, we note that $0\leq\omega(\boldsymbol{x})\leq 1$ and $|g''(r)|\leq C_2^g$ and proceed further to find that

$$\begin{aligned}I_1 &\leq C_2^g|(\theta(\boldsymbol{x};\boldsymbol{u})-\theta(\boldsymbol{x};\boldsymbol{v}))-(\theta(\boldsymbol{y};\boldsymbol{u})-\theta(\boldsymbol{y};\boldsymbol{v}))|\\ &= C_2^g|\theta(\boldsymbol{x};\boldsymbol{u}-\boldsymbol{v})-\theta(\boldsymbol{y};\boldsymbol{u}-\boldsymbol{v})|.\end{aligned} \tag{150}$$

Using the estimate given in Equation 139 we see that

$$I_1\leq 2\bar{J}_0C_2^g(1+||\omega||_{C^{0,\gamma}})||\boldsymbol{u}-\boldsymbol{v}||_{C^{0,\gamma}}|\boldsymbol{x}-\boldsymbol{y}|^\gamma. \tag{151}$$

Now we apply the inequality given in Equation 137 to I_2 to find that

$$I_2\leq 2\bar{J}_0||\boldsymbol{u}-\boldsymbol{v}||_{C^{0,\gamma}}\int_0^1|\omega_{\boldsymbol{\xi}}(\boldsymbol{x})g''(r(l,\boldsymbol{x}))-\omega_{\boldsymbol{\xi}}(\boldsymbol{y})g''(r(l,\boldsymbol{y}))|dl.$$

Adding and subtracting $\omega_{\boldsymbol{\xi}}(\boldsymbol{x})g''(r(l,\boldsymbol{y}))$ gives

$$\begin{aligned}I_2 &\leq 2\bar{J}_0||\boldsymbol{u}-\boldsymbol{v}||_{C^{0,\gamma}}\int_0^1|\omega_{\boldsymbol{\xi}}(\boldsymbol{x})|\,|g''(r(l,\boldsymbol{x}))-g''(r(l,\boldsymbol{y}))|dl\\ &+2\bar{J}_0||\boldsymbol{u}-\boldsymbol{v}||_{C^{0,\gamma}}\int_0^1|\omega_{\boldsymbol{\xi}}(\boldsymbol{x})-\omega_{\boldsymbol{\xi}}(\boldsymbol{y})|\,|g''(r(l,\boldsymbol{y}))|dl\\ &\leq 2C_3^g\bar{J}_0||\boldsymbol{u}-\boldsymbol{v}||_{C^{0,\gamma}}\int_0^1|r(l,\boldsymbol{x})-r(l,\boldsymbol{y})|dl\\ &+2C_2^g\bar{J}_0||\boldsymbol{u}-\boldsymbol{v}||_{C^{0,\gamma}}\int_0^1|\omega_{\boldsymbol{\xi}}(\boldsymbol{x})-\omega_{\boldsymbol{\xi}}(\boldsymbol{y})|dl.\end{aligned}$$

The quantity $|r(l,\boldsymbol{x})-r(l,\boldsymbol{y})|$ (see Equation 146) can be estimated as follows

$$\begin{aligned}&|r(l,\boldsymbol{x})-r(l,\boldsymbol{y})|\\ &=|(1-l)\theta(\boldsymbol{x};\boldsymbol{v})+l\theta(\boldsymbol{x};\boldsymbol{u})-((1-l)\theta(\boldsymbol{y};\boldsymbol{v})+l\theta(\boldsymbol{y};\boldsymbol{u}))|\\ &\leq|1-l|\,|\theta(\boldsymbol{x};\boldsymbol{v})-\theta(\boldsymbol{y};\boldsymbol{v})|+|l|\,|\theta(\boldsymbol{x};\boldsymbol{u})-\theta(\boldsymbol{y};\boldsymbol{u})|\\ &\leq|\theta(\boldsymbol{x};\boldsymbol{v})-\theta(\boldsymbol{y};\boldsymbol{v})|+|\theta(\boldsymbol{x};\boldsymbol{u})-\theta(\boldsymbol{y};\boldsymbol{u})|\\ &\leq 2\bar{J}_0(1+||\omega||_{C^{0,\gamma}})||\boldsymbol{v}||_{C^{0,\gamma}}|\boldsymbol{x}-\boldsymbol{y}|^\gamma+2\bar{J}_0(1+||\omega||_{C^{0,\gamma}})||\boldsymbol{u}||_{C^{0,\gamma}}|\boldsymbol{x}-\boldsymbol{y}|^\gamma\\ &=2\bar{J}_0(1+||\omega||_{C^{0,\gamma}})(||\boldsymbol{u}||_{C^{0,\gamma}}+||\boldsymbol{v}||_{C^{0,\gamma}})|\boldsymbol{x}-\boldsymbol{y}|^\gamma,\end{aligned} \tag{152}$$

where we used the fact that $l\in[0,1]$ and Equation 139. Using the inequality above and $|\omega_{\boldsymbol{\xi}}(\boldsymbol{x})-\omega_{\boldsymbol{\xi}}(\boldsymbol{y})|\leq 2|\boldsymbol{x}-\boldsymbol{y}|^\gamma||\omega||_{C^{0,\gamma}}$ we get

$$\begin{aligned}I_2 &\leq 2C_3^g\bar{J}_0||\boldsymbol{u}-\boldsymbol{v}||_{C^{0,\gamma}}2\bar{J}_0(1+||\omega||_{C^{0,\gamma}})(||\boldsymbol{u}||_{C^{0,\gamma}}+||\boldsymbol{v}||_{C^{0,\gamma}})\,|\boldsymbol{x}-\boldsymbol{y}|^\gamma\\ &+2C_2^g\bar{J}_0||\boldsymbol{u}-\boldsymbol{v}||_{C^{0,\gamma}}2|\boldsymbol{x}-\boldsymbol{y}|^\gamma|\,||\omega||_{C^{0,\gamma}}\\ &\leq 4\bar{J}_0(1+||\omega||_{C^{0,\gamma}})\,[C_3^g\bar{J}_0(||\boldsymbol{u}||_{C^{0,\gamma}}+||\boldsymbol{v}||_{C^{0,\gamma}})+C_2^g]\,||\boldsymbol{u}-\boldsymbol{v}||_{C^{0,\gamma}}\,|\boldsymbol{x}-\boldsymbol{y}|^\gamma.\end{aligned} \tag{153}$$

Substituting Equation 151 and Equation 153 into Equation 149 gives

$$\begin{aligned}&h_{\boldsymbol{\xi}}(\boldsymbol{x},\boldsymbol{y})\\ &\leq 6\bar{J}_0(1+||\omega||_{C^{0,\gamma}})\,[C_3^g\bar{J}_0(||\boldsymbol{u}||_{C^{0,\gamma}}+||\boldsymbol{v}||_{C^{0,\gamma}})+C_2^g]\,||\boldsymbol{u}-\boldsymbol{v}||_{C^{0,\gamma}}\,|\boldsymbol{x}-\boldsymbol{y}|^\gamma.\end{aligned} \tag{154}$$

We now apply Equation 154 to Equation 145 and divide both sides by $|\boldsymbol{x}-\boldsymbol{y}|^\gamma$ to see that

$$\begin{aligned}
&\frac{|(\mathcal{L}_D^\epsilon(\boldsymbol{u})(\boldsymbol{x})-\mathcal{L}_D^\epsilon(\boldsymbol{v})(\boldsymbol{x}))-(\mathcal{L}_D^\epsilon(\boldsymbol{u})(\boldsymbol{y})-\mathcal{L}_D^\epsilon(\boldsymbol{v})(\boldsymbol{y}))|}{|\boldsymbol{x}-\boldsymbol{y}|^\gamma}\\
&\leq \frac{1}{\epsilon^2\omega_d}\int_{H_1(\mathbf{0})} J(|\boldsymbol{\xi}|)\\
&\quad 2\times 6\bar{J}_0(1+||\omega||_{C^{0,\gamma}})\left[C_3^g\bar{J}_0(||\boldsymbol{u}||_{C^{0,\gamma}}+||\boldsymbol{v}||_{C^{0,\gamma}})+C_2^g\right]||\boldsymbol{u}-\boldsymbol{v}||_{C^{0,\gamma}}\,d\boldsymbol{\xi}\\
&= \frac{12\bar{J}_0^2(1+||\omega||_{C^{0,\gamma}})\left[C_3^g\bar{J}_0(||\boldsymbol{u}||_{C^{0,\gamma}}+||\boldsymbol{v}||_{C^{0,\gamma}})+C_2^g\right]}{\epsilon^2}||\boldsymbol{u}-\boldsymbol{v}||_{C^{0,\gamma}}. \qquad (155)
\end{aligned}$$

Collecting results inequalities Equation 141 and Equation 155 deliver the upper bound given by

$$\begin{aligned}
&||\mathcal{L}_D^\epsilon(\boldsymbol{u})-\mathcal{L}_D^\epsilon(\boldsymbol{v})||_{C^{0,\gamma}}\\
&\leq \frac{16\bar{J}_0^2(1+||\omega||_{C^{0,\gamma}})\left[C_3^g\bar{J}_0(||\boldsymbol{u}||_{C^{0,\gamma}}+||\boldsymbol{v}||_{C^{0,\gamma}})+C_2^g\right]}{\epsilon^2}||\boldsymbol{u}-\boldsymbol{v}||_{C^{0,\gamma}}. \qquad (156)
\end{aligned}$$

Lipschitz continuity for $\mathcal{L}^\epsilon(\boldsymbol{u})$. Using Equation 135 and Equation 156 we get

$$\begin{aligned}
&||\mathcal{L}^\epsilon(\boldsymbol{u})-\mathcal{L}^\epsilon(\boldsymbol{v})||_{C^{0,\gamma}}\\
&\leq \left(\frac{8C_3^f\bar{J}_{3/2-\gamma}}{\epsilon^{5/2-\gamma}}(||\boldsymbol{u}||_{C^{0,\gamma}}+||\boldsymbol{v}||_{C^{0,\gamma}})+\frac{8C_2^f(2+||\omega||_{C^{0,\gamma}})\bar{J}_1}{\epsilon^2}\right.\\
&\left.+\frac{16\bar{J}_0^2(1+||\omega||_{C^{0,\gamma}})\left[C_3^g\bar{J}_0(||\boldsymbol{u}||_{C^{0,\gamma}}+||\boldsymbol{v}||_{C^{0,\gamma}})+C_2^g\right]}{\epsilon^2}\right)||\boldsymbol{u}-\boldsymbol{v}||_{C^{0,\gamma}}. \qquad (157)
\end{aligned}$$

Let $\alpha(\gamma)$ defined as follows: $\alpha(\gamma)=0$ if $\gamma\geq 1/2$ and $\alpha(\gamma)=1/2-\gamma$ if $\gamma\leq 1/2$. It is easy to verify that, for all $\gamma\in(0,1]$ and $0<\epsilon\leq 1$

$$\max\left\{\frac{1}{\epsilon^2},\frac{1}{\epsilon^{5/2-\gamma}}\right\}\leq\frac{1}{\epsilon^{2+\alpha(\gamma)}}. \qquad (158)$$

Using $\alpha(\gamma)$ and renaming the constants we have

$$\begin{aligned}
&||\mathcal{L}^\epsilon(\boldsymbol{u})-\mathcal{L}^\epsilon(\boldsymbol{v})||_{C^{0,\gamma}}\\
&\leq \frac{L_1(1+||\omega||_{C^{0,\gamma}})(1+||\boldsymbol{u}||_{C^{0,\gamma}}+||\boldsymbol{v}||_{C^{0,\gamma}})}{\epsilon^{2+\alpha(\gamma)}}||\boldsymbol{u}-\boldsymbol{v}||_{C^{0,\gamma}}. \qquad (159)
\end{aligned}$$

To complete the proof of Equation 21, we substitute the inequality above into Equation 108 to obtain

$$\begin{aligned}
&\|F^\epsilon(y,t)-F^\epsilon(z,t)\|_X\\
&\leq ||y^2-z^2||_{C^{0,\gamma}}+\frac{L_1(1+||\omega||_{C^{0,\gamma}})(1+||y^1||_{C^{0,\gamma}}+||z^1||_{C^{0,\gamma}})}{\epsilon^{2+\alpha(\gamma)}}||y^1-z^1||_{C^{0,\gamma}}\\
&\leq \frac{L_1(1+||\omega||_{C^{0,\gamma}})(1+||y||_X+||z||_X)}{\epsilon^{2+\alpha(\gamma)}}||y-z||_X, \qquad (160)
\end{aligned}$$

and Equation 21 is proved.

A.1.2 Bound on the non-local force in the Hölder norm

In this subsection, we bound $||\mathcal{L}^\epsilon(\boldsymbol{u})||_{C^{0,\gamma}}$ from above. It follows from Equation 115 and a straightforward calculation similar to the previous sections that

$$\begin{aligned}
|\mathcal{L}_T^\epsilon(\boldsymbol{u})(\boldsymbol{x})| &\leq \frac{2C_1^f\bar{J}_{1/2}}{\epsilon^{3/2}},\\
\frac{|\mathcal{L}_T^\epsilon(\boldsymbol{u})(\boldsymbol{x})-\mathcal{L}_T^\epsilon(\boldsymbol{u})(\boldsymbol{y})|}{|\boldsymbol{x}-\boldsymbol{y}|^\gamma} &\leq \frac{4C_2^f\bar{J}_1||\boldsymbol{u}||_{C^{0,\gamma}}+4C_1^f\bar{J}_{1/2}||\omega||_{C^{0,\gamma}}}{\epsilon^2}. \qquad (161)
\end{aligned}$$

Next we consider the non-local dilatational force $\mathcal{L}_D^\epsilon$. We show how to calculate the bounds for the case of a convex-concave potential function g. When g is quadratic we can still proceed along identical lines. We use the formula for $\mathcal{L}_D^\epsilon(\boldsymbol{u})(\boldsymbol{x})$ given by Equation 116 and perform a straightforward calculation to obtain the upper bound given by

$$|\mathcal{L}_D^\epsilon(\boldsymbol{u})(\boldsymbol{x})| \leq \frac{2C_1^g \bar{J}_0}{\epsilon^2}. \tag{162}$$

We have the estimate

$$\begin{aligned}
&|\mathcal{L}_D^\epsilon(\boldsymbol{u})(\boldsymbol{x}) - \mathcal{L}_D^\epsilon(\boldsymbol{u})(\boldsymbol{y})| \\
&\leq \frac{1}{\epsilon^2\omega_d}\int_{H_1(\boldsymbol{0})} J(|\boldsymbol{\xi}|)\Big|\omega_{\boldsymbol{\xi}}(\boldsymbol{x})(g'(\theta(\boldsymbol{x}+\epsilon\boldsymbol{\xi};\boldsymbol{u})) + g'(\theta(\boldsymbol{x};\boldsymbol{u})))) \\
&\qquad - \omega_{\boldsymbol{\xi}}(\boldsymbol{y})(g'(\theta(\boldsymbol{y}+\epsilon\boldsymbol{\xi};\boldsymbol{u})) + g'(\theta(\boldsymbol{y};\boldsymbol{u})))\Big| d\boldsymbol{\xi} \\
&\leq \frac{1}{\epsilon^2\omega_d}\int_{H_1(\boldsymbol{0})} J(|\boldsymbol{\xi}|)\Big|\omega_{\boldsymbol{\xi}}(\boldsymbol{x})g'(\theta(\boldsymbol{x}+\epsilon\boldsymbol{\xi};\boldsymbol{u})) - \omega_{\boldsymbol{\xi}}(\boldsymbol{y})g'(\theta(\boldsymbol{y}+\epsilon\boldsymbol{\xi};\boldsymbol{u}))\Big| d\boldsymbol{\xi} \\
&+ \frac{1}{\epsilon^2\omega_d}\int_{H_1(\boldsymbol{0})} J(|\boldsymbol{\xi}|)\Big|\omega_{\boldsymbol{\xi}}(\boldsymbol{x})g'(\theta(\boldsymbol{x};\boldsymbol{u})) - \omega_{\boldsymbol{\xi}}(\boldsymbol{y})g'(\theta(\boldsymbol{y};\boldsymbol{u}))\Big| d\boldsymbol{\xi}.
\end{aligned} \tag{163}$$

Using $|\omega_{\boldsymbol{\xi}}(\boldsymbol{x}) - \omega_{\boldsymbol{\xi}}(\boldsymbol{y})| \leq 2|\boldsymbol{x}-\boldsymbol{y}|^\gamma ||\omega||_{C^{0,\gamma}}$, $|g'(r_1) - g'(r_2)| \leq C_2^g |r_1 - r_2|$, $|g'(r)| \leq C_1^g$, and the estimate on $|\theta(\boldsymbol{x};\boldsymbol{u}) - \theta(\boldsymbol{y};\boldsymbol{u})|$ given by Equation 139, we obtain

$$\begin{aligned}
&|\mathcal{L}_D^\epsilon(\boldsymbol{u})(\boldsymbol{x}) - \mathcal{L}_D^\epsilon(\boldsymbol{u})(\boldsymbol{y})| \\
&\leq \frac{[2\bar{J}_0 C_2^g(1+||\omega||_{C^{0,\gamma}})||\boldsymbol{u}||_{C^{0,\gamma}} + 2C_1^g||\omega||_{C^{0,\gamma}}||\boldsymbol{u}||_{C^{0,\gamma}}]}{\epsilon^2}|\boldsymbol{x}-\boldsymbol{y}|^\gamma.
\end{aligned} \tag{164}$$

Last we combine results and rename the constants to get

$$||\mathcal{L}^\epsilon(\boldsymbol{u})||_{C^{0,\gamma}} \leq \frac{L_2(1+||\omega||_{C^{0,\gamma}})(1+||\boldsymbol{u}||_{C^{0,\gamma}})}{\epsilon^2}. \tag{165}$$

This completes the proof of Equation 22.

A.2 Proof of Proposition 2

Given $\boldsymbol{u}, \boldsymbol{v} \in L_0^2(D;\mathbb{R}^d)$ we find upper bounds on the Lipschitz continuity of the nonlocal force with respect to the L^2 norm. Motivated by the inequality

$$||\mathcal{L}^\epsilon(\boldsymbol{u}) - \mathcal{L}^\epsilon(\boldsymbol{v})||_{L^2} \leq ||\mathcal{L}_T^\epsilon(\boldsymbol{u}) - \mathcal{L}_T^\epsilon(\boldsymbol{v})||_{L^2} + ||\mathcal{L}_D^\epsilon(\boldsymbol{u}) - \mathcal{L}_D^\epsilon(\boldsymbol{u})||_{L^2}., \tag{166}$$

we bound the Lipschitz continuity of the nonlocal forces due to tensile strain and dilatational strain separately. We study $\mathcal{L}_T^\epsilon$ first. It is evident from Equation 115 and using the estimate $|f'(r_1) - f'(r_2)| \leq C_2^f|r_1 - r_2|$, and arguments similar to previous sections that we have

$$\begin{aligned}
&|\mathcal{L}_T^\epsilon(\boldsymbol{u})(\boldsymbol{x}) - \mathcal{L}_T^\epsilon(\boldsymbol{v})(\boldsymbol{x})| \\
&\leq \frac{2}{\epsilon\omega_d}\int_{H_1(\boldsymbol{0})} \frac{J(|\boldsymbol{\xi}|)}{\sqrt{s_{\boldsymbol{\xi}}}}|f'(\bar{\boldsymbol{u}}_{\boldsymbol{\xi}}(\boldsymbol{x}).\boldsymbol{e}_{\boldsymbol{\xi}}/\sqrt{s_{\boldsymbol{\xi}}}) - f'(\bar{\boldsymbol{v}}_{\boldsymbol{\xi}}(\boldsymbol{x}).\boldsymbol{e}_{\boldsymbol{\xi}}/\sqrt{s_{\boldsymbol{\xi}}})|d\boldsymbol{\xi} \\
&\leq \frac{2C_2^f}{\epsilon^2\omega_d}\int_{H_1(\boldsymbol{0})} \frac{J(|\boldsymbol{\xi}|)}{|\boldsymbol{\xi}|}|\bar{\boldsymbol{u}}_{\boldsymbol{\xi}}(\boldsymbol{x}) - \bar{\boldsymbol{v}}_{\boldsymbol{\xi}}(\boldsymbol{x})|d\boldsymbol{\xi},
\end{aligned} \tag{167}$$

where we also substituted $s_{\boldsymbol{\xi}} = \epsilon|\boldsymbol{\xi}|$.

We apply Equation 68 to Equation 167 with $C = \frac{2C_2^f}{\epsilon^2}$, $\alpha = 1$, and $p(\boldsymbol{\xi}) = |\bar{\boldsymbol{u}}_{\boldsymbol{\xi}}(\boldsymbol{x}) - \bar{\boldsymbol{v}}_{\boldsymbol{\xi}}(\boldsymbol{x})|$ to get

$$\begin{aligned}
&||\mathcal{L}_T^\epsilon(\boldsymbol{u}) - \mathcal{L}_T^\epsilon(\boldsymbol{v})||_{L^2}^2 \\
&\leq \int_D |\mathcal{L}_T^\epsilon(\boldsymbol{u})(\boldsymbol{x}) - \mathcal{L}_T^\epsilon(\boldsymbol{v})(\boldsymbol{x})|^2 d\boldsymbol{x} \\
&\leq \int_D \left(\frac{2C_2^f}{\epsilon^2}\right)^2 \frac{\bar{J}_1}{\omega_d} \int_{H_1(\mathbf{0})} \frac{J(|\boldsymbol{\xi}|)}{|\boldsymbol{\xi}|} |\bar{\boldsymbol{u}}_{\boldsymbol{\xi}}(\boldsymbol{x}) - \bar{\boldsymbol{v}}_{\boldsymbol{\xi}}(\boldsymbol{x})|^2 d\boldsymbol{\xi} d\boldsymbol{x} \\
&= \left(\frac{2C_2^f}{\epsilon^2}\right)^2 \frac{\bar{J}_1}{\omega_d} \int_{H_1(\mathbf{0})} \frac{J(|\boldsymbol{\xi}|)}{|\boldsymbol{\xi}|} \left[\int_D |\bar{\boldsymbol{u}}_{\boldsymbol{\xi}}(\boldsymbol{x}) - \bar{\boldsymbol{v}}_{\boldsymbol{\xi}}(\boldsymbol{x})|^2 d\boldsymbol{x}\right] d\boldsymbol{\xi},
\end{aligned} \tag{168}$$

where we interchanged integration in last step. Using

$$\int_D |\bar{\boldsymbol{u}}_{\boldsymbol{\xi}}(\boldsymbol{x}) - \bar{\boldsymbol{v}}_{\boldsymbol{\xi}}(\boldsymbol{x})|^2 d\boldsymbol{x} \leq 2||\boldsymbol{u} - \boldsymbol{v}||_{L^2}^2 \tag{169}$$

we conclude that

$$||\mathcal{L}_T^\epsilon(\boldsymbol{u}) - \mathcal{L}_T^\epsilon(\boldsymbol{v})||_{L^2} \leq \frac{4C_2^f \bar{J}_1}{\epsilon^2} ||\boldsymbol{u} - \boldsymbol{v}||_{L^2}. \tag{170}$$

In estimating $||\mathcal{L}_D^\epsilon(\boldsymbol{u}) - \mathcal{L}_D^\epsilon(\boldsymbol{v})||_{L^2}$ we will consider convex-concave g noting that the case of quadratic g is dealt in a similar fashion. From Equation 116 and using estimate $|g'(r_1) - g'(r_2)| \leq C_2^g |r_1 - r_2|$, and proceeding as before we have

$$\begin{aligned}
&|\mathcal{L}_D^\epsilon(\boldsymbol{u})(\boldsymbol{x}) - \mathcal{L}_D^\epsilon(\boldsymbol{v})(\boldsymbol{x})| \\
&\leq \frac{1}{\epsilon^2 \omega_d} \int_{H_1(\mathbf{0})} J(|\boldsymbol{\xi}|)[|g'(\theta(\boldsymbol{x} + \epsilon\boldsymbol{\xi}; \boldsymbol{u})) - g'(\theta(\boldsymbol{x} + \epsilon\boldsymbol{\xi}; \boldsymbol{v}))| \\
&\qquad + |g'(\theta(\boldsymbol{x}; \boldsymbol{u})) - g'(\theta(\boldsymbol{x}; \boldsymbol{v}))|] d\boldsymbol{\xi} \\
&\leq \frac{C_2^g}{\epsilon^2 \omega_d} \int_{H_1(\mathbf{0})} J(|\boldsymbol{\xi}|)[|\theta(\boldsymbol{x} + \epsilon\boldsymbol{\xi}; \boldsymbol{u}) - \theta(\boldsymbol{x} + \epsilon\boldsymbol{\xi}; \boldsymbol{v})| + |\theta(\boldsymbol{x}; \boldsymbol{u}) - \theta(\boldsymbol{x}; \boldsymbol{v})|] d\boldsymbol{\xi} \\
&= \frac{C_2^g}{\epsilon^2 \omega_d} \int_{H_1(\mathbf{0})} J(|\boldsymbol{\xi}|)[|\theta(\boldsymbol{x} + \epsilon\boldsymbol{\xi}; \boldsymbol{u} - \boldsymbol{v})| + |\theta(\boldsymbol{x}; \boldsymbol{u} - \boldsymbol{v})|] d\boldsymbol{\xi}.
\end{aligned} \tag{171}$$

Squaring Equation 171 and applying inequality Equation 68 with $C = \frac{C_2^g}{\epsilon^2}$, $\alpha = 0$, and $p(\boldsymbol{\xi}) = |\theta(\boldsymbol{x} + \epsilon\boldsymbol{\xi}; \boldsymbol{u} - \boldsymbol{v})| + |\theta(\boldsymbol{x}; \boldsymbol{u} - \boldsymbol{v})|$ gives

$$\begin{aligned}
&||\mathcal{L}_D^\epsilon(\boldsymbol{u}) - \mathcal{L}_D^\epsilon(\boldsymbol{v})||_{L^2}^2 \\
&\leq \int_D \left(\frac{C_2^g}{\epsilon^2}\right)^2 \frac{\bar{J}_0}{\omega_d} \int_{H_1(\mathbf{0})} J(|\boldsymbol{\xi}|)(|\theta(\boldsymbol{x} + \epsilon\boldsymbol{\xi}; \boldsymbol{u} - \boldsymbol{v})| + |\theta(\boldsymbol{x}; \boldsymbol{u} - \boldsymbol{v})|)^2 d\boldsymbol{\xi} d\boldsymbol{x} \\
&\leq \left(\frac{C_2^g}{\epsilon^2}\right)^2 \frac{\bar{J}_0}{\omega_d} \int_{H_1(\mathbf{0})} J(|\boldsymbol{\xi}|) \left[\int_D 2(|\theta(\boldsymbol{x} + \epsilon\boldsymbol{\xi}; \boldsymbol{u} - \boldsymbol{v})|^2 + |\theta(\boldsymbol{x}; \boldsymbol{u} - \boldsymbol{v})|^2) d\boldsymbol{x}\right] d\boldsymbol{\xi},
\end{aligned} \tag{172}$$

where we used Cauchy's inequality and exchanged integration in the last step. It is easy to verify that

$$\int_D |\theta(\boldsymbol{x} + \epsilon\boldsymbol{\xi}; \boldsymbol{u})|^2 d\boldsymbol{x} \leq 2\bar{J}_0^2 ||\boldsymbol{u}||_{L^2}^2$$

holds for all $\boldsymbol{\xi} \in H_1(\mathbf{0})$. Combining this estimate and Equation 172 we see that

$$||\mathcal{L}_D^\epsilon(\boldsymbol{u}) - \mathcal{L}_D^\epsilon(\boldsymbol{v})||_{L^2} \leq \frac{4C_2^g \bar{J}_0^2}{\epsilon^2} ||\boldsymbol{u} - \boldsymbol{v}||_{L^2}. \tag{173}$$

Estimates Equation 170 and Equation 173 together delivers (after renaming the constants)

$$||\mathcal{L}^\epsilon(\boldsymbol{u}) - \mathcal{L}^\epsilon(\boldsymbol{v})||_{L^2} \leq \frac{L_3}{\epsilon^2}||\boldsymbol{u} - \boldsymbol{v}||_{L^2}, \tag{174}$$

where L_3 is given by Equation 60. This completes the proof of Proposition 2.

Appendix B Energy stability of the semi-discrete scheme

In this section, we establish Theorem 2 for convex-concave potential functions g as well as for quadratic potential functions. We recall the semi-discrete problem introduced in Section 4.1. We first introduce the semi-discrete boundary condition by setting $\hat{\boldsymbol{u}}_i(t) = \boldsymbol{0}$ for all t and for all $\boldsymbol{x}_i \notin D$. Let $\{\hat{\boldsymbol{u}}_i(t)\}_{i,\boldsymbol{x}_i\in D}$ denote the semi-discrete approximate solution which satisfies the following evolution, for all $t \in [0,T]$ and i such that $\boldsymbol{x}_i \in D$,

$$\ddot{\hat{\boldsymbol{u}}}_i(t) = \mathcal{L}^\epsilon(\hat{\boldsymbol{u}}(t))(\boldsymbol{x}_i) + \boldsymbol{b}(\boldsymbol{x}_i, t), \tag{175}$$

where $\hat{\boldsymbol{u}}(t)$ is the piecewise constant extension of $\{\hat{\boldsymbol{u}}(t)\}_{i,\boldsymbol{x}_i\in D}$, given by

$$\hat{\boldsymbol{u}}(t,\boldsymbol{x}) = \sum_{i,\boldsymbol{x}_i\in D} \hat{\boldsymbol{u}}_i(t)\chi_{U_i}(\boldsymbol{x}).$$

Let $\hat{\mathcal{L}}^\epsilon(\hat{\boldsymbol{u}}(t))(\boldsymbol{x})$ be defined as

$$\hat{\mathcal{L}}^\epsilon(\hat{\boldsymbol{u}}(t))(\boldsymbol{x}) = \sum_{i,\boldsymbol{x}_i\in D} \mathcal{L}^\epsilon(\hat{\boldsymbol{u}}(t))(\boldsymbol{x}_i)\chi_{U_i}(\boldsymbol{x})$$

and define $\hat{\boldsymbol{b}}(t)$ similarly. From Equation 175 noting the definition of piecewise constant extension

$$\begin{aligned}\ddot{\hat{\boldsymbol{u}}}(\boldsymbol{x},t) &= \hat{\mathcal{L}}^\epsilon(\hat{\boldsymbol{u}}(t))(\boldsymbol{x}) + \hat{\boldsymbol{b}}(\boldsymbol{x},t)\\ &= \mathcal{L}^\epsilon(\hat{\boldsymbol{u}}(t))(\boldsymbol{x}) + \hat{\boldsymbol{b}}(\boldsymbol{x},t) + \sigma(\boldsymbol{x},t),\end{aligned} \tag{176}$$

where the error term $\sigma(\boldsymbol{x},t)$ is given by

$$\sigma(\boldsymbol{x},t) := \hat{\mathcal{L}}^\epsilon(\hat{\boldsymbol{u}}(t))(\boldsymbol{x}) - \mathcal{L}^\epsilon(\hat{\boldsymbol{u}}(t))(\boldsymbol{x}). \tag{177}$$

We split σ into two parts

$$\begin{aligned}\sigma(\boldsymbol{x},t) &= \left[\hat{\mathcal{L}^\epsilon_T}(\hat{\boldsymbol{u}}(t))(\boldsymbol{x}) - \mathcal{L}^\epsilon_T(\hat{\boldsymbol{u}}(t))(\boldsymbol{x})\right] + \left[\hat{\mathcal{L}^\epsilon_D}(\hat{\boldsymbol{u}}(t))(\boldsymbol{x}) - \mathcal{L}^\epsilon_D(\hat{\boldsymbol{u}}(t))(\boldsymbol{x})\right]\\ &=: \sigma_T(\boldsymbol{x},t) + \sigma_D(\boldsymbol{x},t).\end{aligned} \tag{178}$$

Multiplying both sides of Equation 176 by $\dot{\hat{\boldsymbol{u}}}(t)$ and integrating over D gives

$$(\ddot{\hat{\boldsymbol{u}}}(t), \dot{\hat{\boldsymbol{u}}}(t)) = (\mathcal{L}^\epsilon(\hat{\boldsymbol{u}}(t)), \dot{\hat{\boldsymbol{u}}}(t)) + (\hat{\boldsymbol{b}}(t), \dot{\hat{\boldsymbol{u}}}(t)) + (\sigma(t), \dot{\hat{\boldsymbol{u}}}(t)), \tag{179}$$

where $(\cdot,\cdot)$ denotes the L^2-inner product.

B.1 Estimating σ

We proceed by estimating L^2-norm of $\sigma(t)$. It follows easily from Equation 115 that

$$|\sigma_T(\boldsymbol{x},t)| \leq \frac{4C_1^f \bar{J}_{1/2}}{\epsilon^{3/2}} \quad \Rightarrow ||\sigma_T(t)||_{L^2} \leq \frac{4C_1^f \bar{J}_{1/2}\sqrt{|D|}}{\epsilon^{3/2}}. \tag{180}$$

We now deal with two cases of g separately.

1. Convex-concave type g: In this case, we can easily show from Equation 116 that

$$|\sigma_D(\boldsymbol{x},t)| \leq \frac{4C_1^g \bar{J}_0}{\epsilon^2} \quad \Rightarrow ||\sigma_D(t)||_{L^2} \leq \frac{4C_1^g \bar{J}_0 \sqrt{|D|}}{\epsilon^2}. \tag{181}$$

2. Quadratic type g: In this case we have $g'(r) = g''(0)r$. Let $\boldsymbol{x} \in U_i$, i.e. in the unit cell of the i^{th} mesh node. To simplify the calculations let $\boldsymbol{u} = \hat{\boldsymbol{u}}(t)$ (and later we will use the fact that $\hat{\boldsymbol{u}}$ is piecewise constant function). From Equation 116, we have

$$\begin{aligned}
|\sigma_D(\boldsymbol{x},t)| &= |\mathcal{L}_D^\epsilon(\boldsymbol{u})(\boldsymbol{x}_i) - \mathcal{L}_D^\epsilon(\boldsymbol{u})(\boldsymbol{x})| \\
&= \left| \frac{g''(0)}{\epsilon^2 \omega_d} \int_{H_1(\mathbf{0})} J(|\boldsymbol{\xi}|) \Big[\omega_{\boldsymbol{\xi}}(\boldsymbol{x}_i)(\theta(\boldsymbol{x}_i + \epsilon\boldsymbol{\xi}; \boldsymbol{u}) + \theta(\boldsymbol{x}_i; \boldsymbol{u})) \right. \\
&\qquad \left. - \omega_{\boldsymbol{\xi}}(\boldsymbol{x})(\theta(\boldsymbol{x} + \epsilon\boldsymbol{\xi}; \boldsymbol{u}) + \theta(\boldsymbol{x}; \boldsymbol{u})) \Big] \boldsymbol{e}_{\boldsymbol{\xi}} d\boldsymbol{\xi} \right|.
\end{aligned} \tag{182}$$

Now consider the function $a(\boldsymbol{x}, \boldsymbol{\xi})$ defined as

$$a(\boldsymbol{x}, \boldsymbol{\xi}) = \theta(\boldsymbol{x} + \epsilon\boldsymbol{\xi}; \boldsymbol{u}). \tag{183}$$

We then have

$$\begin{aligned}
&|\sigma_D(\boldsymbol{x},t)| \\
&= \left| \frac{g''(0)}{\epsilon^2 \omega_d} \int_{H_1(\mathbf{0})} J(|\boldsymbol{\xi}|) \Big[\omega_{\boldsymbol{\xi}}(\boldsymbol{x}_i)(a(\boldsymbol{x}_i, \boldsymbol{\xi}) + a(\boldsymbol{x}_i, \mathbf{0})) \right. \\
&\qquad \left. - \omega_{\boldsymbol{\xi}}(\boldsymbol{x})(a(\boldsymbol{x}, \boldsymbol{\xi}) + a(\boldsymbol{x}, \mathbf{0})) \Big] \boldsymbol{e}_{\boldsymbol{\xi}} d\boldsymbol{\xi} \right| \\
&\leq \frac{g''(0)}{\epsilon^2 \omega_d} \int_{H_1(\mathbf{0})} J(|\boldsymbol{\xi}|)(|a(\boldsymbol{x}_i, \boldsymbol{\xi})| + |a(\boldsymbol{x}_i, \mathbf{0})| + |a(\boldsymbol{x}, \boldsymbol{\xi})| + |a(\boldsymbol{x}, \mathbf{0})|) d\boldsymbol{\xi}.
\end{aligned} \tag{184}$$

Let

$$b_{\boldsymbol{\xi}} := |a(\boldsymbol{x}_i, \boldsymbol{\xi})| + |a(\boldsymbol{x}_i, \mathbf{0})| + |a(\boldsymbol{x}, \boldsymbol{\xi})| + |a(\boldsymbol{x}, \mathbf{0})| \tag{185}$$

then using the inequality Equation 68 with $C = \frac{g''(0)}{\epsilon^2}$, $\alpha = 0$, and $p(\boldsymbol{\xi}) = b_{\boldsymbol{\xi}}$, we get

$$|\sigma_D(\boldsymbol{x},t)|^2 \leq \left(\frac{g''(0)}{\epsilon^2} \right)^2 \frac{\bar{J}_0}{\omega_d} \int_{H_1(\mathbf{0})} J(|\boldsymbol{\xi}|) b_{\boldsymbol{\xi}}^2 d\boldsymbol{\xi}. \tag{186}$$

Thus on an interchange of integration we have

$$\begin{aligned}
||\sigma_D(t)||_{L^2}^2 &= \int_D |\sigma_D(\boldsymbol{x},t)|^2 d\boldsymbol{x} \\
&\leq \sum_{i, \boldsymbol{x}_i \in D} \int_{U_i} |\sigma_D(\boldsymbol{x},t)|^2 d\boldsymbol{x} \\
&\leq \left(\frac{g''(0)}{\epsilon^2} \right)^2 \frac{\bar{J}_0}{\omega_d} \int_{H_1(\mathbf{0})} J(|\boldsymbol{\xi}|) \left[\sum_{i, \boldsymbol{x}_i \in D} \int_{U_i} b_{\boldsymbol{\xi}}^2 d\boldsymbol{x} \right] d\boldsymbol{\xi}.
\end{aligned} \tag{187}$$

We denote the term inside square bracket as I and estimate it next. Recalling the definition of $b_{\boldsymbol{\xi}}$ in Equation 185 and using the identity $(\sum_{n=1}^4 c_n)^2 \leq 4 \sum_{n=1}^4 c_n^2$ we have

$$I \leq 4 \sum_{i, \boldsymbol{x}_i \in D} \int_{U_i} (|a(\boldsymbol{x}_i, \boldsymbol{\xi})|^2 + |a(\boldsymbol{x}_i, \mathbf{0})|^2 + |a(\boldsymbol{x}, \boldsymbol{\xi})|^2 + |a(\boldsymbol{x}, \mathbf{0})|^2) d\boldsymbol{x}. \tag{188}$$

For $\boldsymbol{x}$ either in D or in layer of thickness ϵ surrounding D and $\boldsymbol{\xi} \in H_1(\mathbf{0})$, we have from the definition of $a(\boldsymbol{x}, \boldsymbol{\xi})$

$$\begin{aligned}|a(\boldsymbol{x},\boldsymbol{\xi})|^2 &= |\theta(\boldsymbol{x}+\epsilon\boldsymbol{\xi},\boldsymbol{u})|^2 \\ &= \left|\frac{1}{\omega_d}\int_{H_1(\mathbf{0})} \omega(\boldsymbol{x}+\epsilon\boldsymbol{\xi}+\epsilon\boldsymbol{\eta})J(|\boldsymbol{\eta}|)\bar{\boldsymbol{u}}_{\boldsymbol{\eta}}(\boldsymbol{x}+\epsilon\boldsymbol{\xi})\cdot\boldsymbol{e}_{\boldsymbol{\eta}}d\boldsymbol{\eta}\right|^2 \\ &\leq \left|\frac{1}{\omega_d}\int_{H_1(\mathbf{0})} J(|\boldsymbol{\eta}|)(|\boldsymbol{u}(\boldsymbol{x}+\epsilon\boldsymbol{\xi}+\epsilon\boldsymbol{\eta})|+|\boldsymbol{u}(\boldsymbol{x}+\epsilon\boldsymbol{\xi})|)d\boldsymbol{\eta}\right|^2, \end{aligned} \tag{189}$$

where we used the fact that $0 \leq \omega(x) \leq 1$ and definition of $\bar{\boldsymbol{u}}_{\boldsymbol{\eta}}(\boldsymbol{x}+\epsilon\boldsymbol{\xi})$. We now apply inequality Equation 68 with $C = 1$, $\alpha = 0$ and $p(\boldsymbol{\eta}) = |\boldsymbol{u}(\boldsymbol{x}+\epsilon\boldsymbol{\xi}+\epsilon\boldsymbol{\eta})| + |\boldsymbol{u}(\boldsymbol{x}+\epsilon\boldsymbol{\xi})|$ to obtain

$$\begin{aligned}|a(\boldsymbol{x},\boldsymbol{\xi})|^2 &\leq \frac{\bar{J}_0}{\omega_d}\int_{H_1(\mathbf{0})} J(|\boldsymbol{\eta}|)(|\boldsymbol{u}(\boldsymbol{x}+\epsilon\boldsymbol{\xi}+\epsilon\boldsymbol{\eta})|+|\boldsymbol{u}(\boldsymbol{x}+\epsilon\boldsymbol{\xi})|)^2 d\boldsymbol{\eta} \\ &\leq \frac{2\bar{J}_0}{\omega_d}\int_{H_1(\mathbf{0})} J(|\boldsymbol{\eta}|)(|\boldsymbol{u}(\boldsymbol{x}+\epsilon\boldsymbol{\xi}+\epsilon\boldsymbol{\eta})|^2+|\boldsymbol{u}(\boldsymbol{x}+\epsilon\boldsymbol{\xi})|^2)d\boldsymbol{\eta}, \end{aligned} \tag{190}$$

where we have also used the inequality $(a+b)^2 \leq 2a^2 + 2b^2$. This inequality holds for all $\boldsymbol{x}$ and $\boldsymbol{\xi}$ which includes $\boldsymbol{x} = \boldsymbol{x}_i$ and $\boldsymbol{\xi} = \mathbf{0}$.

With estimate on $|a(\boldsymbol{x},\boldsymbol{\xi})|^2$ and the fact that $\boldsymbol{u}$ is a piecewise constant function defined over unit cells U_i, we immediately have

$$\sum_{i,\boldsymbol{x}_i\in D}\int_{U_i}|a(\boldsymbol{x},\boldsymbol{\xi})|^2 d\boldsymbol{x} \leq 4\bar{J}_0^2||\boldsymbol{u}||_{L^2}^2 = 4\bar{J}_0^2||\hat{\boldsymbol{u}}(t)||_{L^2}^2, \tag{191}$$

where we substituted $\hat{\boldsymbol{u}}(t)$ for $\boldsymbol{u}$. Combining above estimate with Equation 188 we get

$$I \leq 64\bar{J}_0^2||\hat{\boldsymbol{u}}(t)||_{L^2}^2. \tag{192}$$

Finally, we use the bound on I and substitute it into Equation 187 to show

$$\begin{aligned}||\sigma_D(t)||_{L^2}^2 &\leq \left(\frac{g''(0)}{\epsilon^2}\right)^2 \frac{\bar{J}_0}{\omega_d}\int_{H_1(\mathbf{0})} J(|\boldsymbol{\xi}|)64\bar{J}_0^2||\hat{\boldsymbol{u}}(t)||_{L^2}^2 d\boldsymbol{\xi} \\ \Rightarrow ||\sigma_D(t)||_{L^2} &\leq \frac{8g''(0)\bar{J}_0^2}{\epsilon^2}||\hat{\boldsymbol{u}}(t)||_{L^2}. \end{aligned} \tag{193}$$

On renaming the constants the bound on $\sigma(t)$ can be summarized as

$$\begin{aligned}&||\sigma(t)||_{L^2} \\ &\leq \begin{cases} \frac{4C_1^f\bar{J}_{1/2}\sqrt{|D|}}{\epsilon^{3/2}} + \frac{4C_1^g\bar{J}_0\sqrt{|D|}}{\epsilon^2} \leq \frac{C}{\epsilon^2} & \text{for convex-concave } g, \\ \frac{4C_1^f\bar{J}_{1/2}\sqrt{|D|}}{\epsilon^{3/2}} + \frac{8g''(0)\bar{J}_0^2}{\epsilon^2}||\hat{\boldsymbol{u}}(t)||_{L^2} \leq \frac{C_1+C_2||\hat{\boldsymbol{u}}(t)||_{L^2}}{\epsilon^2} & \text{for quadratic } g\,. \end{cases} \end{aligned} \tag{194}$$

B.2 Energy inequality

From Equation 179 and noting the identity

$$\frac{d}{dt}\mathcal{E}^\epsilon(\hat{\boldsymbol{u}})(t) = (\ddot{\hat{\boldsymbol{u}}}(t),\dot{\hat{\boldsymbol{u}}}(t)) - (\mathcal{L}^\epsilon(\hat{\boldsymbol{u}}(t)),\dot{\hat{\boldsymbol{u}}}(t)) \tag{195}$$

we have

$$\begin{aligned}\frac{d\mathcal{E}^\epsilon(\hat{\boldsymbol{u}})(t)}{dt} &= (\hat{\boldsymbol{b}}(t),\dot{\hat{\boldsymbol{u}}}(t)) + (\sigma(t),\dot{\hat{\boldsymbol{u}}}(t)) \\ &\leq (||\hat{\boldsymbol{b}}(t)||_{L^2} + ||\sigma(t)||_{L^2})\,||\dot{\hat{\boldsymbol{u}}}(t)||_{L^2}. \end{aligned} \tag{196}$$

When g is convex-concave we can apply identical steps as in the proof of Theorem 5 of Jha and Lipton (2018a) together with the estimate Equation 194 to obtain

$$\sqrt{\mathcal{E}^\epsilon(\hat{\boldsymbol{u}})(t)} \leq \sqrt{\mathcal{E}^\epsilon(\hat{\boldsymbol{u}})(0)} + \frac{tC}{\epsilon^2} + \int_0^t ||\hat{\boldsymbol{b}}(s)||_{L^2} ds \tag{197}$$

for all $t \in [0, T]$. This completes the proof of energy stability for convex-concave potential functions g.

We now address the case of quadratic potential functions g. We introduce the energy $\bar{\mathcal{E}}^\epsilon(\hat{\boldsymbol{u}})(t)$ given by

$$\bar{\mathcal{E}}^\epsilon(\boldsymbol{u})(t) := \mathcal{E}^\epsilon(\boldsymbol{u})(t) + \frac{1}{2}||\boldsymbol{u}(t)||^2_{L^2}.$$

Differentiation shows that

$$\frac{d\mathcal{E}^\epsilon(\hat{\boldsymbol{u}})(t)}{dt} = \frac{d\bar{\mathcal{E}}^\epsilon(\hat{\boldsymbol{u}})(t)}{dt} - (\hat{\boldsymbol{u}}(t), \dot{\hat{\boldsymbol{u}}}(t)).$$

Thus from Equation 196 we get

$$\begin{aligned}\frac{d\bar{\mathcal{E}}^\epsilon(\hat{\boldsymbol{u}})(t)}{dt} &\leq (||\hat{\boldsymbol{b}}(t)||_{L^2} + ||\sigma(t)||_{L^2})\, ||\dot{\hat{\boldsymbol{u}}}(t)||_{L^2} + (\hat{\boldsymbol{u}}(t), \dot{\hat{\boldsymbol{u}}}(t)) \\ &\leq (||\hat{\boldsymbol{b}}(t)||_{L^2} + C_1/\epsilon^2)\, ||\dot{\hat{\boldsymbol{u}}}(t)||_{L^2} + (C_2/\epsilon^2 + 1)||\hat{\boldsymbol{u}}(t)||_{L^2}\ ||\dot{\hat{\boldsymbol{u}}}(t)||_{L^2}. \end{aligned} \tag{198}$$

From the definition of energy $\bar{\mathcal{E}}^\epsilon$ we have

$$||\hat{\boldsymbol{u}}(t)||_{L^2} \leq \sqrt{2\bar{\mathcal{E}}^\epsilon(\hat{\boldsymbol{u}})(t)} \qquad \text{and} \qquad ||\dot{\hat{\boldsymbol{u}}}(t)||_{L^2} \leq \sqrt{2\bar{\mathcal{E}}^\epsilon(\hat{\boldsymbol{u}})(t)}. \tag{199}$$

Using the above inequalities in Equation 198 along with Cauchy's inequality gives

$$\frac{d\bar{\mathcal{E}}^\epsilon(\hat{\boldsymbol{u}})(t)}{dt} \leq ||\hat{\boldsymbol{b}}(t)||^2_{L^2} + \frac{C_1^2}{\epsilon^4} + 3(\frac{C_2}{\epsilon^2} + 1)\bar{\mathcal{E}}^\epsilon(\hat{\boldsymbol{u}})(t). \tag{200}$$

Using the integrating factor $\exp[-3(C_2/\epsilon^2 + 1)t]$ we recover the inequality

$$\begin{aligned}\bar{\mathcal{E}}^\epsilon(\hat{\boldsymbol{u}})(t) \leq \exp[3(C_2/\epsilon^2 + 1)t]\Bigg(&\bar{\mathcal{E}}^\epsilon(\hat{\boldsymbol{u}})(0) \\ &+ \int_0^t (\frac{C_1^2}{\epsilon^4} + ||\hat{\boldsymbol{b}}(s)||^2_{L^2}) \exp[-3(C_2/\epsilon^2 + 1)s] ds\Bigg). \end{aligned} \tag{201}$$

This completes the proof of Theorem 2.